修 士 学 位 論 文

三周波数によるアンビギュイティ測定に関する研究

THE BENEFIT OF TRIPLE FREQUENCIES SYSTEM IN AMBIGUITY RESOLUTION

BY

YUN ZHANG

INFORMATION ENGINEERING AND LOGISTICS
GRADUATE SCHOOL OF MERCANTILE MARINE SCIENCE AND TECHNOLOGY
TOKYO UNIVERSITY OF MARINE SCIENCE AND TECHNOLOGY
TOKYO, JAPAN

SEPTEMBER 2004

Deeply thanks for my parents

修 士 学 位 論 文

三周波数によるアンビギュイティ測定に関する研究

THE BENEFIT OF TRIPLE FREQUENCIES SYSTEM IN AMBIGUITY RESOLUTION

BY

YUN ZHANG

INFORMATION ENGINEERING AND LOGISTICS
GRADUATE SCHOOL OF MERCANTILE MARINE SCIENCE AND TECHNOLOGY
TOKYO UNIVERSITY OF MARINE SCIENCE AND TECHNOLOGY
TOKYO, JAPAN

SEPTEMBER 2004

LIST OF CONTENTS

LIST OF TABLES

LIST OF FIGURES

ABSTRACT

The Benefit of Triple Frequencies in Ambiguity Resolution

2002215 Yun Zhang
Laboratory of Communication Engineering,
Tokyo University of Marine Science and Technology

As part of the modernization of GPS, a third civil frequency at 1176.45 MHz will be added to the GPS system. This new frequency will bring a number of benefits. The carrier-phase differential user will be a prime beneficiary because the extra-wide-lane combination L2 -L5 has long wavelength. In addition, by various linear combinations, more ambiguity resolution methods can be used. The users can get more benefit from the triple frequencies.

Both in the dual and triple frequencies, the wide-lane combination will be used to resolve the ambiguities, and HMW（Hatch-Melbourne-Wübbena）combination is used to estimate the ambiguity of wide-lane signal.

On short baselines, there are two methods to resolve the ambiguities in the triple frequencies. The first method for the ambiguity resolution is to use wide-lane (L1-L5) signal (called as widelane method) instead of substituting wide-lane (L1-L2) signal. Because the ranging accuracy will improve because of the larger bandwidth (24 MHz) of the L5 signal, there will be less code noise and multipath error on L5 frequency signal than on L2 frequency signal. The second method (called as extra-widelane method) is to use the extra-wide-lane L2-L5 signal to perform the ambiguity resolution by three steps. In short base line, the phase observation noise will be the important error source in triple frequencies system if multipath is small. From the results of ambiguity success rate (ASR) of the simulation, on short baselines, the ambiguity resolution will be faster and more accurate in triple frequencies than in double frequency system.

On medium and long baselines, the ionosphere influence becomes more serious. In the middle baseline (about 10-30 km), the extra-wide-lane (L2-L5) signal is used to improve the AR for the primary frequency, but the longer distance user will get limited gains from the new frequency because of ionosphere delay. However, in triple frequencies, the ambiguity of wide-lane signal can be estimated easily, and two independent Geometry-Free combinations are obtained. This makes it possible to determine the primary ambiguity and ionosphere influence at the same time only by using carrier-phase observation. This method (called as geometry-free method) can be used in long baseline, because the ambiguity resolution is not influenced by ionosphere delay. The amplified phase observation noise in wide-lane signal (about 7 times as L1 phase observation noise) and extra-wide-lane signal (about 34 times as L1 phase observation noise) will affect the accuracy of the ambiguity resolution. By reducing this noise, we can improve the primary frequency ambiguity resolution.

In order to test the impact of the GPS modernization on ambiguity resolution performance, three-frequency GPS data are required. In this article, the triple frequencies simulation is also introduced. In the simulation, GPS satellite orbit is from YUMA files. By using narrow correlator tracking theory, the code tracking noise and carrier phase tracking noise can be generated. Ionosphere error is simulated using Klobuchar Model;

troposphere error is simulated by using Saastamoinen Model; ephemeris error is simulated likely as navigation message ephemeris error with standard deviation 2.1m. Multipath error is also generated on narrow correlator. The code differential positioning results in different baseline length are estimated to evaluate the triple frequencies simulation.

From the results using data from triple frequencies simulation, the benefits from the triple frequencies can be confirmed. Influence of ionosphere error in ambiguity resolution can be estimated. Effect of code and phase noises in ambiguity resolution can be determined. We can also see that ambiguity resolution is a function of numbers of visible satellites in both in the dual and triple frequencies. At the end of this article, multipath error influence in the short baseline in dual and triple frequencies is discussed.

ACKNOWLEDGEMENTS

I wish to show deep gratitude to Prof. Dr. Akio Yasuda, the author's supervisor, for his encouragement, guidance, and financial support during my graduate studies.

Special thanks also goes to Mr. Nobuaki Kubo, the assistant in Yasuda Laboratory. The author has gained a lot from his teachings in GPS theory and C programming. It also goes to Mr. Falin Wu, the doctor student in Yasuda Laboratory, for his teaching in RTK GPS theory.

I would also specially acknowledge Mr. Hiroshi Isshiki, in Institute of Mathematical Analysis (IMA), for teaching me the mathematical theory in GPS system.

Thanks also goes to Mr. Kentaro Kondo, the doctor student in our laboratory, for his teaching the theory of ambiguity resolution, and to Mr. Sounosuke Fukushima, the doctor student in our laboratory, for his teaching the theory of the satellite orbit calculation.

I would like to appreciate Takaki Tominaga, Takashi Suzuki and other numbers in the research group in Yasuda Laboratory. Our close collaboration during the past years has made the work a pleasure. Thanks are also extends to Mr. Masashi Kawamura for his assistance in the experiment.

Finally, I would thank my fellow graduate students in this Laboratory: Shinya Okamoto, Shinji Tanaka, and others who have given me much help in my study, and also in my life.

CHAPTER 1
INTRODUCTION

1.1 BACKGROUND

In Washington D.C., on 25 January 1999, Vice President Al Gore announced a new civil frequency would be broadcast on future Block IIF Global Positioning System (GPS) satellites, called L5, in the Aeronautical Radio Navigation System band at 1176.45 MHz [Mohinder S. Grewal, Lawrence R. Weill Angus P. Andrews.].

A new L5 frequency signal was modulated by a new code structure. To gain maximum performance, the L5 spread spectrum codes will have a higher chipping rate and longer period than the C/A codes (Coarse/Acquisition Code). Proposed codes have a 10.23-megachip/s chipping rate and period of 10230 chips. Additionally the plan is to transmit two signals phase quadrature, one of which will not carry modulation.

The L5 signal will provide the following system improvements:

First: a third frequency for GPS will be applicable for the carrier-phase differential users. Triple frequencies system could make it much easier and reliable to resolve the whole-cycle ambiguities than dual frequencies system. This will be pointed in the present research.

Second: the aviation user will also be one of the prime beneficiaries because the new frequency is in a protected aviation band (1164MHz—1215MHz)、and the signal will be protected. Thus the system will be more robust against interference and jamming, there are more details of the “protected aviation band” in: (http://www.aea.be/AEAWebsite/datafiles/ceptworkshopaea.ppt.)

Third: ranging accuracy will improve because of the larger bandwidth of the proposed codes. As a consequence, both code-base positioning accuracy and phase ambiguity resolution performance will improve.

Forth: Multipath error will reduce because the larger bandwidth of the new codes will sharpen the peak of the code autocorrelation function.

There are more other benefits from the third new frequency, for example carrier phase tracking will improve due to the “data-free” quadrature component of L5 signal and the codes will be better isolated from each other due to the longer length of L5 codes, and so on.

From the above discussion, it is expected that the planned GPS Modernization, when completed in about 2015, would make determining precise position as easy as determining precise time today, and knowledge of position would come to occupy the same important place in our daily lives as time does today [Pratap Misra, Per Enge, 2001].

1.2 PURPOSE OF RESEARCH

In the present research, the ambiguity resolution (AR) improvement in triple frequencies system will be focused; the ambiguity success rate (ASR) will be estimated to evaluate the performance of AR method. The higher this probability, the better the performance of this estimator.

Precise positioning with GPS is possible with reliable fixing of the signal phase ambiguities. The success in real time positioning is dependent on the fast ambiguity fixing. Various methods have been developed for fast and reliable ambiguity estimation over short baselines.

On the other hand, for long baselines, time to fix ambiguities increases drastically due to the influence of

various system effects, in particular the ionosphere bias. However, one well-known exception is the wide-lane ambiguity, which can be quickly determined also for long baseline from a linear combination of phase and code data. But mainly the ionosphere effect restricts success of position estimation for long baselines.

In order to compare the difference between AR methods in the dual and triple frequencies systems, the triple frequencies signal simulation is conducted in the present research. GPS satellite orbit information by using GPS YUMA Almanacs file and error models (for example Klobuchar Model in ionosphere error simulation, Saastamoinen Model in troposphere error simulation and so on) generate three frequencies signals.

Various methods for AR are developed in short length and long length baseline. In the case of short baseline (about 10 km, or shorter), the first method (called as widelane method) is using widelane (L1-L5) signal to instead of using widelane (L1-L2); the second method (called as extra-widelane method) is to use extre-widelane (L2-L5) signal through three steps. In the case of long baseline, extra-widelane (L2-L5) method can be used in the middle distance (about 10-30km), and two independent Geometry-Free combination signals (called as geometry-free method) can be used to estimate the primary ambiguity in the long or extra long distance.

According to the ASR results of the simulation in triple frequencies system using carrier-phase data only, differential carrier-phase users will be able to resolve the whole-cycle ambiguities much more quickly, often in a single epoch when employed over short distances. On the medium length baseline the ASR is also increased. The longer distance user of carrier-phase differential measurement will see limited gains from the new frequency by widelane signal alone. If geometry-free combination is used, AR will be improved by reducing carrier noise, since AR becomes independent on the ionosphere delay in this case and influenced only by amplified phase observation noise in widelane signal.

1.3 OUTLINE

The thesis is composed of 8 chapters. Background and purpose of research are introduced in chapter 1.

In Chapter 2, current and modernization GPS signal structure and character are discussed, and GPS satellite constellation is introduced. The advantage of the L5 signal is also introduced in this chapter.

In Chapter 3, code and carrier phase measurements are discussed. Single and double difference code and carrier phase measurements are introduced. The advantage of the double difference carrier phase measurement is presented in this chapter.

Chapter 4 presents the theory that estimating the ambiguity of carrier phase liner combination signal is faster and more accurate than estimating ambiguity of primary signal. HMW method is introduced, and widelane, ionosphere-free and geometry-free combinations are also discussed in this chapter.

In Chapter 5, dual and triple frequencies ambiguity resolution methods under various scenarios are introduced, and Geometry-free method is proposed in long baseline length. The benefit of triple frequencies is presented in this chapter.

Chapter 6 describes the error parameters in the triple frequencies signal simulation. Different error models used in the simulation are introduced in details. The positioning results of code differential measurement under the cases of different baselines are also estimated in this chapter.

In Chapter 7, using data from triple frequencies signal simulation, ASR under the cases of different baselines is estimated. From the results by numerical calculation, it can be confirmed of the benefit from the triple frequencies. Ionosphere error, code and carrier phase noise, and multipath error influence in the ambiguity estimation are discussed in this chapter.

Chapter 8 summarizes the whole research works with conclusions and recommendations.

CHAPTER 2
GPS SIGNAL

2.1 CURRENT GPS SIGNAL

Currently, each GPS satellite transmits continuously using two radio frequencies in the L-band referred to as L1 and L2. The center frequencies of L1 and L2 are as below:

$$L1:\ f_{L1} = 1575.42MHz \qquad L2:\ f_{L2} = 1227.60MHz\,.$$

Two signals are transmitted on L1, one for civil users, and other for DoD-authorized users. The signal on L2 is intended for the Do-D-authorized user only.

2.1.1 GPS Signal Structure

All GPS satellites emit signals on 2 frequencies: L1 (1575.42 MHz) and L2 (1227.6 MHz). Two pseudo random noise (PRN) ranging codes are in use:

The coarse/acquisition (C/A) code modulates the L1 carrier and has a 1.023 MHz chip rate and a period of 1 ms

The precision (P) code modulates L1 and L2 carriers (P1, P2) and has a 10.23 MHz chip rate and a period of 7 days .

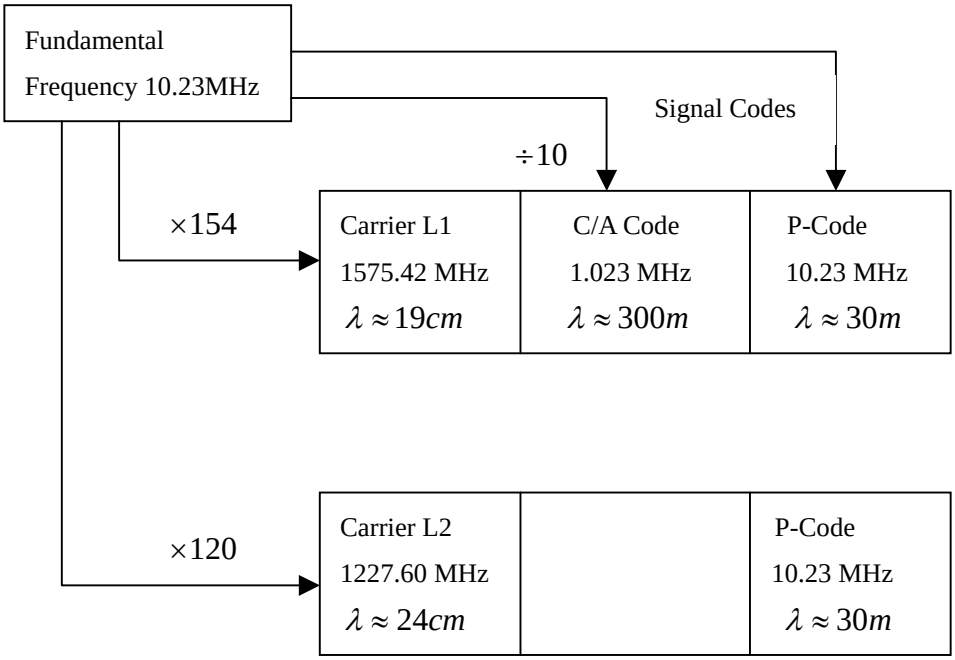

Figure 2.1: GPS Current Signal

(From http://www.gps.oma.be/common/mordern.html)

2.1.2 GPS Satellite Constellation

There are four generations of the GPS satellite: the Block I, Block II/IIA, Block IIR and Block IIF. The first Block I GPS satellite was launched in 1978. The first 10 satellites were developmental satellites. They were used to test the principles of the system, and lessons learned from those satellites were incorporated into later

blocks.

From 1989 to 1990, 23 so-called operational satellites were launched. The first 8 were Block II satellites. The Block IIA (Advanced Block II) satellites are the second series of operational satellites. They were launched November 1990 through November 1997. The launch of the 24th satellite, in 1994, completed the system.

The Block IIR satellites are the operational replenishment satellites. Launching of the Block IIRs began in January 1997.

28 Block II/IIA/IIR satellites make up the current constellation. It consists of 2 Block II , 16 Block IIA and 10 Block IIR satellites. Figure 2.2 shows GPS satellite Block II, IIA and IIR.

Upcoming-launch of the GPS satellites is IIR-12 F4 PRN23 Jun 24 2004; IIR-13 A2 PRN 02 Sep. 22 2004; IIR-14 M-1 Feb. 1 2005; IIR-15 M-2 Apr. 20 2005; IIR-16 M-3 Jun 24 2005. (From http://earth-info.nga.mil/GandG/sathtml/satinfo.html)

Each satellite transmits a navigation message containing: orbital elements, clock behavior, system time and status messages. An almanac is also provided which gives the approximate data for each active satellite.

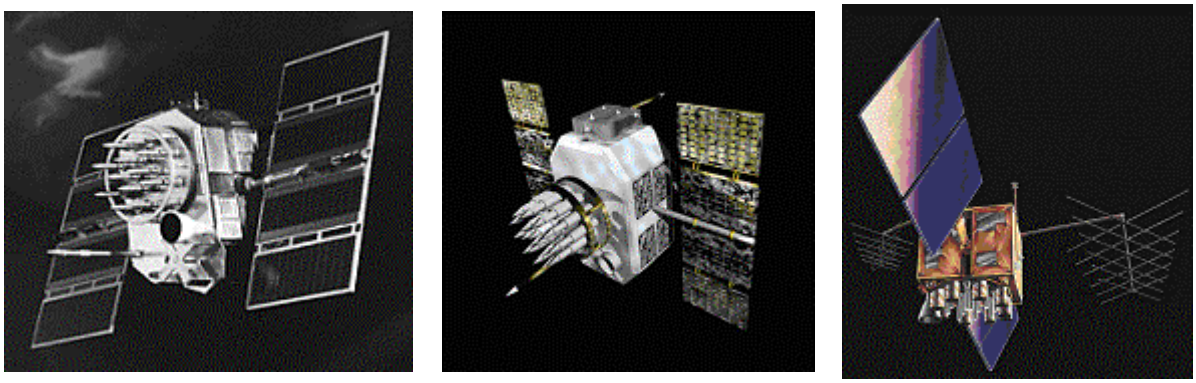

Figure 2.2 Block II (left), Block IIA (Middle) and Block IIR (Right) GPS Satellite
(From http://www.gps.oma.be/common/modern.html)

2.2 GPS MODERNIZATION

The specific objectives of the Modernization are to make Standard Position Service (SPS) more accurate and robust. It is to provide two additional signals to civil users:

a C/A-coded signal on L2;

a stronger, wide-band (bandwidth>20 MHz) signals at a newly defined frequency band to be called L5 centered at 1176.45 MHz.

2.2.1 GPS Block IIR-M and Block IIF Satellite

Block IIF satellites will be the fourth generation of satellites and will continue with the L2C signal on L2 and the M code on the L1 and L2 frequencies, but will add a new civil code at the L5 frequency (for safety of life). The first launch of a IIR-M satellite is planned for 2003, The new civil signal at L5 will not be available until the first block IIF is launch in 2005 [Pratap Misra, Per Enge, 2001], and the full operational availability around 2012 [Lioneal Ries, 2002]. It is shown that the imaging of the Block IIR-M and Block IIF GPS

satellites in Figure 2.3. In the Table 2.1, the new signal will be availability in the GPS satellites.

Signal/SV	IIR	IIR-M	IIF
L1 C/A code	X	X	X
L1 P (Y) code	X	X	X
L1 M code		X	X
L2 Civil		X	X
L2 P code	X	X	X
L2 M code		X	X
L5 Civil			X
	1996	2003	2005

Table 2.1: New Signal Availability

(From http://www.hr-tews.de/GPS/modernesierung_gps.htm)

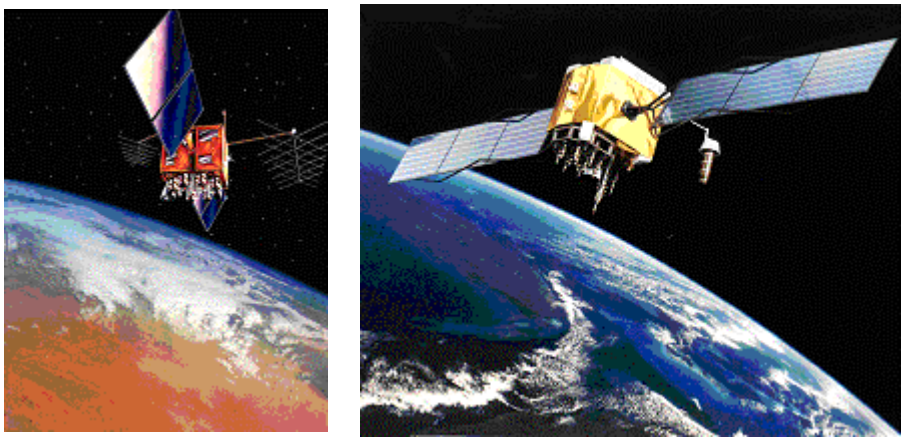

Figure 2.3: Block IIR-M (left) and Block IIF (Right) GPS Satellite

(From http://www.gps.oma.be/common/modern.html)

2.2.2 L5 Signal Character

The new L5 signal will have the following Characteristics:

1) QPSK-modulated
2) Signal is centered on 1176.45 MHz., and bandwidth is 24 MHz
3) Two components have each a different spreading code clocked at 10.23 MHz.
4) The In-phase component, also called the data channel, carries the navigation message, at 100 symbols per second (50 bits per second with a convolutional encoder)
5) The Quadrature component, also called the pilot channel, carriers no message at all.
6) The data and pilot L5 spreading codes are each modulated with a distinct Neumann-Hoffman code clocked at 1 kHz.
7) The specified power is such that the receiver levels on the ground should be –154.9 dBW (i.e. –157.9 dbW for each component)

8) Codes with 2 - 13 stage shift registers

–Length of one (XA code) = 8190 chips

–Length of second (XB code) = 8191 chips

–Exclusive-Or'd together to generate longer code

2.2.3 L5 Signal Structure

The L5 signal radiated by satellite I is a QPSK modulated of the L5 carrier with a data and a pilot channel that can be modeled as 2.1 [Lioneal Ries, 2002]:

$$S_{L5}^{i}(t) = \sqrt{P}d^{i}(t)d^{i}(t)NH_{10}(t)XI^{i}(t)\cos(2\pi f_s t) + \sqrt{P}NH_{20}(t)XQ^{i}(t)\cos(2\pi f_s t) \ldots (2.1)$$

where

P is such that the minimum total power of the L5 signal is –154.9 dbW, or –157.9 dbW for each one of the data and pilot component [RTCA C-159].

d is the L5 navigation message encoded with a convolution FEC (rate 1/2). The original L5 navigation message has a 50 bps rate, while *d* has a final 100 sps rate after encoding. Thus the duration of one final symbol in d is 10 ms.

NH_{10} and NH_{20} are respectively the 10 bits and 20 bits Neuman-Hoffman code. These codes are clocked at a rate of 1 kHz, thus the duration of one bit is 1ms.

XI and *XQ* are respectively the data and pilot component PRN codes. Those codes are clocked at a rate of 10.23MHz and have a period of 1ms.

2.3 GPS III

GPS III is the GPS system of the future. The goal of the GPS III program is to deliver best-value acquisition and architectural solutions that will satisfy the currently defined, yet evolving, military and civilian needs for a space-based positioning, navigation and timing system through 2030. Figure 7.4 shows the conceptual drawing of GPS III satellites created by Aerospace's Concept Design Center.

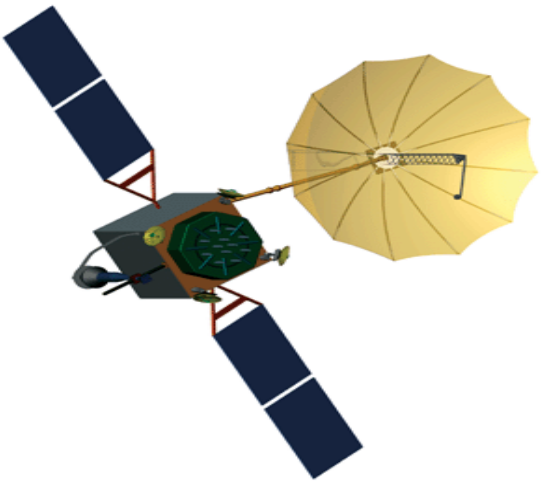

Figure 2.4: A conceptual drawing of a GPS III satellite.

(From: http://www.aero.org/publications/crosslink/summer2002/07.html)

The USAF (US Air Force) wants GPS III to deliver better anti-jam capability, by providing two new high-power spot beams for the M-code signals to the L1 and L2 channels that service military users (+20dB in power over earlier M-code signal). Furthermore, it will have two other channels that provide navigation signals for civilian use in local, regional and national safety-of-life applications for improved position, navigation and timing knowledge. One of the new civil signals (S-Band 2227.5 MHz) [Royal Observatory of Belgium] is expected to transmit higher power than the other two signals for improved reception worldwide. The first of the new satellites is to be launched in 2010.

SUMMARY

From the above introduction, the Comparisons of the three civil signals will be shown in Table 2.2. Table 2.2 indicates the basics, like the center frequency, the length of the code or codes, the overall code clock rate, and whether the signal consists of one bi-phase component or two components in phase quadrature. It also shows the data bit rate for each signal and whether the data has forward error correction (FEC) or not. That the signals have rather different characteristics can be seen.

The last column shows one effect of the different frequencies. Because ionospheric refraction error is inversely proportional to frequency squared, ionospheric error at L2 is 65% larger than at L1, and at L5 it's 79% larger. If a local differential GPS correction signal (DGPS) is available, that's not too much of a problem. However, partly because satellite orbit and clock accuracy have improved so much, the ionosphere is the largest source of single-frequency navigation error. Therefore, L1 will be maybe continued to use for all applications where single-frequency in the future. If GPS III carries a better L1 signal, then a dozen years or so from now we won't have that problem either."

Civil Signal	Carrier frequency	Code Length (chips)	Code Clock (MHz)	FEC function	Phase	Fully Available	Ionosphere Error Ratio
L1	1575.42	1,023	1.023	No	Bi-phase	Now	1.00
L2	1227.60	10,230(CM) 767,250(CL)	1.023	Yes	Bi-phase	--2011	1.65
L5	1176.45	10,230	10.23	Yes	Quad-Phase	--2015	1.79

Table 2.2: Comparison in three civil frequency signals

Figure 2.5 overviews the present and modernized GPS signals in the frequency spectrum. . The actual GPS band is 24MHz wide so the satellite should attenuate the tails transmit filter. The center frequency may also differ by up to 5kHz due to Doppler shift from the motion of the satellite.

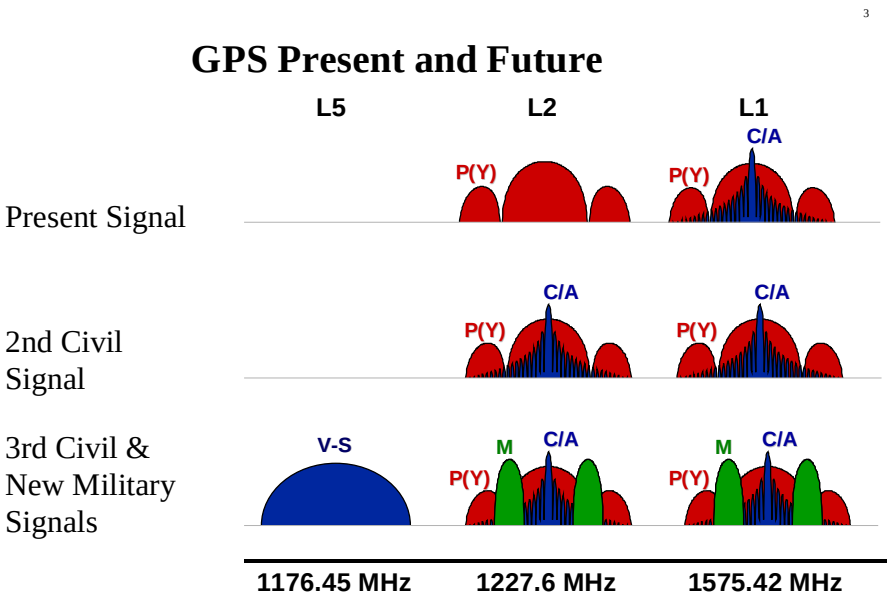

Figure 2.5: GPS signal frequency spectrum in present and future

(From: Satellite Navigation (SATNAV) September 1999)

CHAPTER 3
GPS OBSERVABLE MODELING

3.1 MEASUREMENT MODEL

There are two range-type measurements that can be made on the GPS signals: pseudo-range and carrier-phase observations. Code tracking provides estimates of instantaneous ranges to the satellites. The code phase measurements at an instant from different satellites have a common bias and are, therefore, called pseudo-ranges. Carrier phase tracking provides measurements of the received carrier phase relative to the phase of a sinusoidal signal generated-user pseudo-range over a time interval, and estimate of its instantaneous [Pratap Misra, Per Enge, 2001].

3.1.1 Code Phase Measurement

A basic measurement made by a GPS receiver is code phase measurement. It is measured as the amount of time shift required to aligning the C/A-code replica generated at the receiver with the signal received from the satellite.

The code observation equation for the measured pseudo-range can be written as [Pratap Misra, Per Enge, 2001]:

$$\rho = r + c[\delta t_u - \delta t^s] + I_\rho + T_\rho + \varepsilon_\rho \quad \text{.....m.....(3.1)}$$

where

r is the true range from the receiver to GPS satellite,

ρ is pseudo-range, a biased and noisy measurement of r,

I_ρ and T_ρ are the delays associated with the transmission of the signal through the ionosphere and the troposphere, respectively,

δt_u and δt^s are the amounts by which the satellite and receiver clocks are advanced in relation to GPST.

The satellite clock bias (δt^s) is estimated by the Control Segment and specified in terms of the coefficients of a quadratic polynomial in time. The values of these coefficients are broadcast in the navigation message.

ε_ρ is to denote modeling error, and measurement error in code phase measurement.

As a "rule-of-thumb": the alignment of the incoming and receiver generated codes is generally possible to within about 1-2% of the chipping rate, hence the measurement precision of C/A code ranging is of the order of 3-5m, and for P code ranging it is of the order of 0.3-0.5m. (Modern "narrow correlate" technology has demonstrated 10 times better correlation performance for the C/A code than that above.)

3.1.2 Carrier Phase Measurement

A measurement much more precise than that of code phase is the phase of the carrier received from a satellite. The carrier phase measurement is the difference between the phase of the receiver-generated carrier signal and the carrier receiver from satellite at the instant of the measurement.

The carrier-phase observation equation for the measurement pseudo-range can be written as:

$$\phi = \lambda^{-1}[r - I_\phi + T_\phi] + \frac{c}{\lambda}(\delta t_u - \delta t^s) + N + \varepsilon_\phi, \text{ ……cycles……(3.2)}$$

$$\Phi = r - I_\phi + T_\phi + c(\delta t_u - \delta t^s) + \lambda N + \varepsilon_\Phi, \text{……m……(3.3)}$$

where:

ϕ is pseudo-range, a biased and noisy measurement of r,

I_ϕ and T_ϕ are the ionosphere and troposphere propagation delay in meters, respectively,

δt_u and δt^s are the amounts by which the satellite and receiver clocks are advanced in relation to GPST.

The satellite clock bias (δt^s) is estimated by the Control Segment and specified in terms of the coefficients of a quadratic polynomial in time. The values of these coefficients are broadcast in the navigation message.

N is the inter ambiguity. Estimating of N is referred to as inter ambiguity resolution (AR) or initialization.

c is the speed of light in a vacuum,

ε_ϕ is to denote modeling error, and measurement error in carrier phase measurement.

Note that the equation (3.2) is in units of cycles, and equation (3.3) is in unit of meters.

3.1.3 Multiple Frequency Measurement

By the first refraction index of the ionosphere, rewriting equation (3.1) and (3.3), the pseudo-ranges between satellite "*i*" and receiver "*a*" are measured by multiple frequency f_{LK} code and carrier phase measurements, the ionosphere delay at L1 is denoted as I_a^i.

$$\rho_{Ka}^i = r_a^i + c[\delta t_u - \delta t^s] + \frac{(f_{L1})^2}{(f_{LK})^2} I_a^i + T_a^i + \varepsilon_{K\rho}, \text{……m……(3.4)}$$

$$\Phi_{Ka}^i = r_a^i + c(\delta t_a - \delta t^i) - \frac{(f_{L1})^2}{(f_{LK})^2} I_a^i + T_a^i + \lambda_K N_{Ka}^i + \varepsilon_{K\Phi} \text{……m……(3.5)}$$

3.2 Phase Differencing Techniques

The carrier phase measurement is very precise and is used for sub-cent-meter GPS positioning. Many of the errors associated with GPS must be eliminated, reduced, or modeled within software. In order to do this, and to compute the ambiguities a number of processing strategies have been adopted.

3.2.1 Between Satellites Difference

Receiver clock bias errors may be eliminated by forming the difference between simultaneous observations by one GPS receiver to two satellites (see Figure 3.1 below).

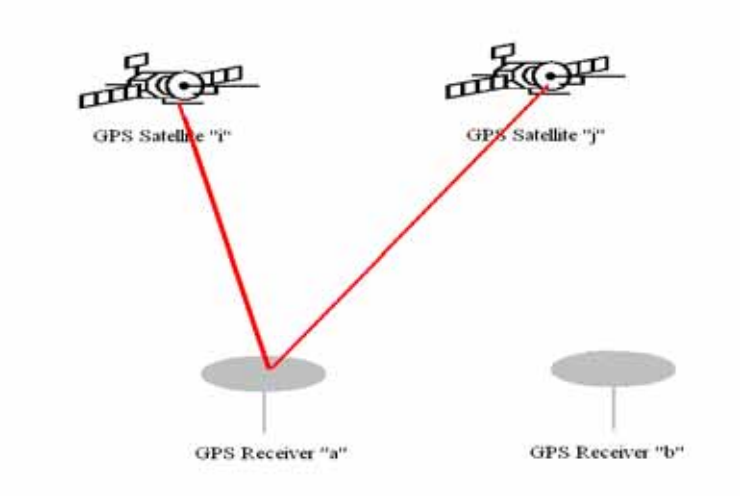

Figure 3.1: Single difference between satellites

The operator "∇" indicates a between satellite difference. Using equation (3.6), the differenced observable of signal "κ"can be written as:

$$\nabla\Phi_{\kappa a}^{ij} = \Phi_{\kappa a}^{i} - \Phi_{\kappa a}^{j} \quad \text{.....m.....(3.6)}$$

$$\nabla\Phi_{\kappa a}^{ij} = \nabla r_a^{ij} - c \times \nabla \delta t^{ij} - \frac{(f_{L1})^2}{(f_{L\kappa})^2}\nabla I_a^{ij} + \nabla T_a^{ij} + \lambda_\kappa \nabla N_{\kappa a}^{ij} + \nabla \varepsilon_{\kappa\Phi} \quad \text{.....m.....(3.7)}$$

3.2.2 Between Receivers Difference

The satellite clock phase errors may be (almost) eliminated by forming the difference between observations with two GPS receivers to one satellite at the same time (see Figure 3.2 below).

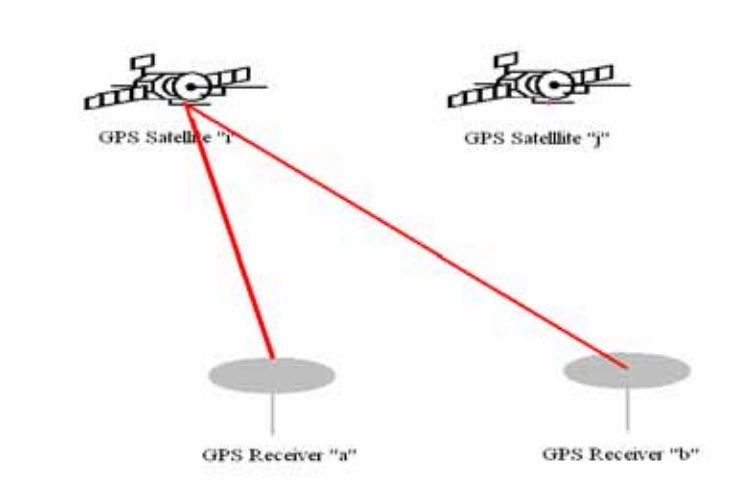

Figure 3.2: Single difference between Receivers

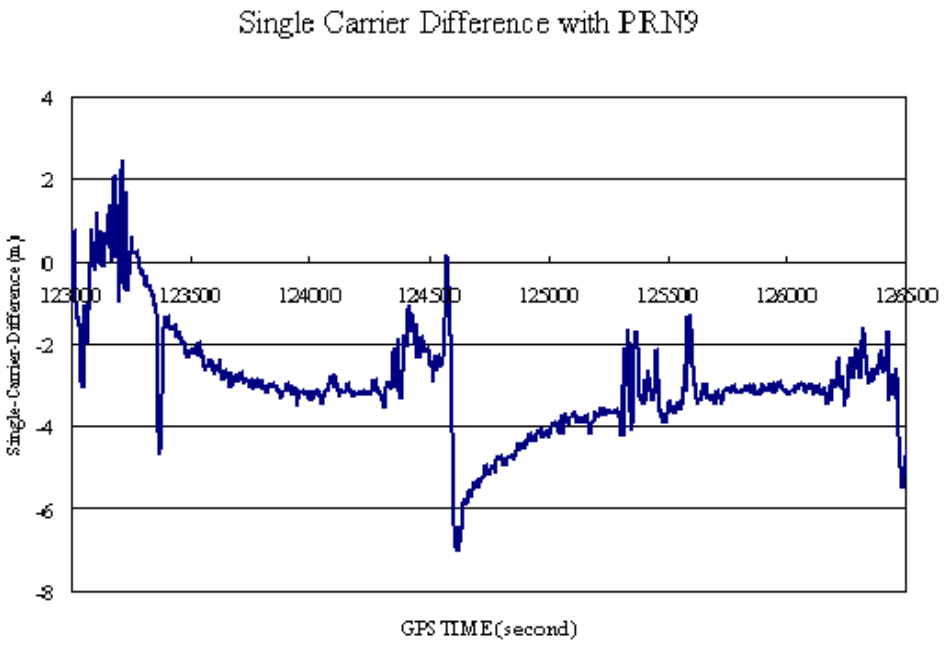

Figure 3.3: Carrier phase single difference between receivers by PRN 9 with two OEM4 receivers under the case of zero baselines

The operator "Δ" indicates a between-station difference, also sometimes referred to confusingly as a single-difference. Although the nominal observation or reception times of the two measurements may be the same, the actual time of measurement may differ between one receiver and another because of receiver time-tag errors (or satellite Ephemeris Error) [Rizos, 1990]. The differenced observation can be constructed from:

$$\Delta\Phi^{i}_{\kappa ab} = \Phi^{i}_{\kappa a} - \Phi^{i}_{\kappa b} \text{ ……..m……(3.8)}$$

$$\Delta\Phi^{i}_{\kappa ab} = \Delta r^{i}_{ab} + c\Delta\delta t_{ab} - \frac{(f_{L1})^2}{(f_{L\kappa})^2}\Delta I^{i}_{ab} + \Delta T^{i}_{ab} + \lambda_{\kappa}\Delta N^{i}_{\mathrm{K}ab} + \Delta\varepsilon_{\kappa\Phi} \text{ ……m……(3.9)}$$

Figure 3.3 shows carrier phase single-difference between two OEM4 receivers by PRN9 under the case of zero baselines. Because the multipath and other error can be neglected in the zero baseline difference, and phase noise is very small, the residual error can be seemed as single difference receiver clock bias only.

3.2.3 Carrier Phase Double Differences (DD)

The "double-difference" will refer to the observation that has been formed by differencing between satellites and between stations (see Figure 3.4 below). The operator "$\Delta\nabla$" indicates DDs between stations and receivers. Assuming that the satellite clock phase errors cancel in a between-station difference, forming the between-satellite (i,j) difference phase and then differencing between stations (a,b), which may create this receiver-satellite double-differenced phase:

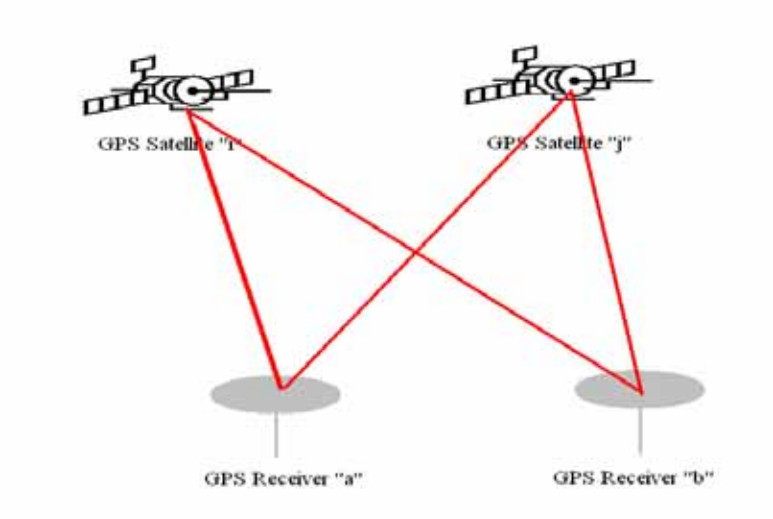

Figure 3.4: Double differences between receivers and satellites

$$\Delta\nabla\Phi^{ij}_{\kappa ab} = \nabla\Phi^{ij}_{\kappa a} - \nabla\Phi^{ij}_{\kappa b}, \ldots\ldots\ldots\ldots\ldots\ldots\ldots\ldots\ldots\ldots\ldots\text{m}\ldots\ldots\ldots\ldots\ldots\ldots\ldots\ldots\ldots\ldots(3.10)$$

$$\Delta\nabla\Phi^{ij}_{\kappa ab} = \Delta\nabla r^{ij}_{ab} - \frac{(f_{L1})^2}{(f_{L\kappa})^2}\times\Delta\nabla I^{ij}_{ab} + \Delta\nabla T^{ij}_{ab} + \lambda_{\kappa}\times\Delta\nabla N^{ij}_{\kappa ab} + \Delta\nabla\varepsilon_{\kappa\Phi} \ldots\ldots\ldots\text{m}\ldots\ldots\ldots\ldots\ldots\ldots\ldots(3.11)$$

3.2.4 Pseudorange (Code) Double Differences (DD)

Similar to the case of the carrier phase measurement, the receiver makes a pseudorange measurement each epoch for all satellites being actively tracked. The pseudorange suffers from similar propagation and timing effects, as is the case for the carrier phase. The only basic difference is that where the ionosphere advances the carrier phase, however, the pseudorange information experiences a group delay.

$$\Delta\nabla\rho^{ij}_{\mathrm{K}ab} = \Delta\nabla r^{ij}_{ab} + \frac{(f_{L1})^2}{(f_{L\mathrm{K}})^2}\Delta\nabla I^{ij}_{ab} + \Delta\nabla T^{ij}_{ab} + \Delta\nabla\varepsilon_{\mathrm{K}\rho} \ldots\ldots\ldots\ldots\ldots\ldots\ldots\text{m}\ldots\ldots\ldots\ldots\ldots\ldots\ldots(3.12)$$

As the same as the case of the DD carrier phase, the satellite ephemeris error will be larger by the longer length of the baseline.

Now two distinct sets of DDs have been created. The first is based upon differencing the low noise (less than 1cm) but ambiguity carrier phase measurement; the second set is formed from the unambiguous but noisy (1 to 2 m) pseudorange (code) measurement [Rizos, 1990].

Figure3.5 shows the code double difference and the carrier phase double difference measurements under the case of the zero baselines by two OEM4 receivers. In figure 3.5, the carrier phase double difference is zero-meaning results to compare to code double difference results. The code DD is very noisy and the carrier DD is very precise can be seen.

In the DD measurements, we have to notice the influence of the DD ephemeris error with the length of baseline. The longer the baseline is, the larger the effect of orbital error (difference ephemeris error) becomes.

3.2.5 DD code and carrier phase in short baseline

Equations (3.11) and (3.12) can be rewritten as equation (3.13) and (3.14) in the reasonable short baseline (about 10km, or shorter), because the ionosphere and troposphere error, or the ephemeris error can be neglected in this case.

$$\Delta\nabla\Phi^{ij}_{\kappa ab} = \Delta\nabla r^{ij}_{ab} + \lambda_{\kappa} \times \Delta\nabla N^{ij}_{\kappa ab} + \Delta\nabla \varepsilon_{\kappa\Phi} \text{ .....m.....(3.13)}$$

$$\Delta\nabla\rho^{ij}_{\kappa ab} = \Delta\nabla r^{ij}_{ab} + \Delta\nabla \varepsilon_{\kappa\rho} \text{ .....m.....(3.14)}$$

It is very difficult to determine how long is the exact length of the short baseline in fact, because the ionosphere error is variable in the days, seasons and years. In general, the length of the baseline is assumed as 10km. It means that if the baseline is shorter than 10 km, the ionosphere error and the troposphere, or ephemeris error will be assumed to neglect. This is basic concept in the ambiguity resolution in the short baseline.

SUMMARY

In this chapter, the various GPS observation modeling was discussed. In this thesis, the carrier phase double differential measurement is to be pointed to estimate the precise position. But the ambiguity resolution is the most the problem in the carrier phase positioning. In the next chapter, the concept of widelane combinations will be introduced. It will resolve the ambiguity problem faster and more accurate than directly by primary signals.

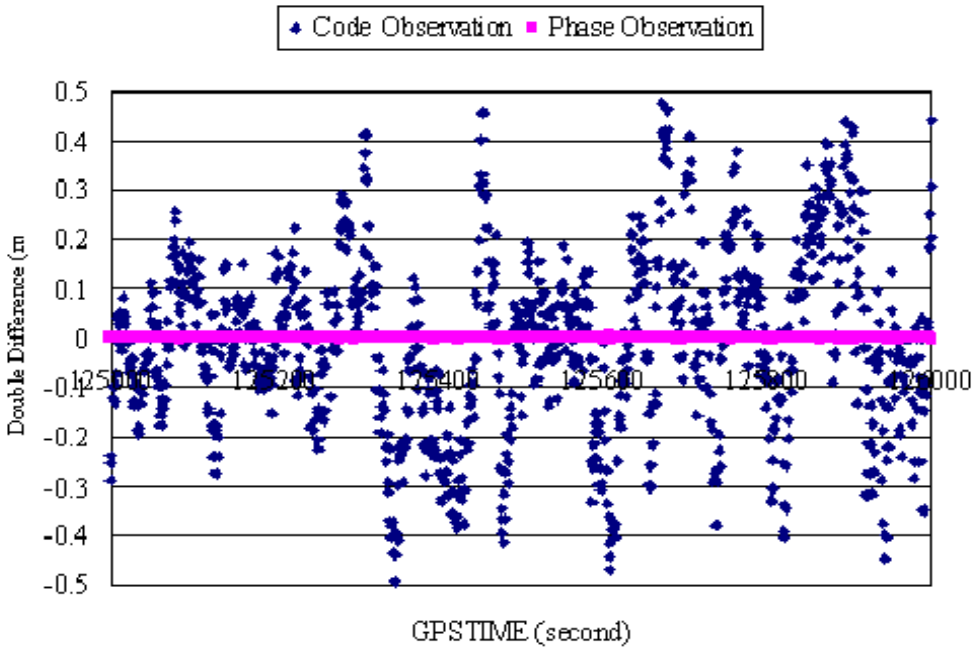

Figure 3.5: Comparisons between code DD and zero-mean carrier phase DD under zero baselines

CHAPTER 4
LINEAR COMINATIONS OF OBSERVATIONS

Because DD ambiguity of primary signal is difficult to be estimated fast in single frequency or by primary frequencies (L1 and L2) directly, the carrier phase linear combination is necessary. In this chapter, the Hatch-Melbourne-Wübbena (HMW) Linear Combinations and various combinations, including widelane, narrow, ionosphere-free and geometry-free combinations, will be discussed. From this chapter, the operator "$\Delta\nabla$", indexes of satellites (*i*,*j*) and receivers (*a*,*b*) will be not written for writing simply.

4.1 SINGLE FREQUENCY COMBINATIONS

An approach to ambiguity resolution in the single frequency is suggested by the equation (3.13) and (3.14) in the last chapter: Use the code measurements, which are unambiguous, to do the AR performance. Here, the success of the approach is depended on the accuracy of the code measurement [Teunissen, 2003]. The DD code and carrier phase measurement at L1 are shown as following:

$$\rho_{L1} = r + \varepsilon_{\rho L1}, \text{.....m.....(4.1)}$$

$$\phi_{L1} = \frac{r}{\lambda_{L1}} + N_{L1} + \varepsilon_{\phi L1}, \text{.....cycles.....(4.2)}$$

where r is the double geometric range from receiver to satellite; ρ_{L1} is the double-differenced precise pseudo-ranges on L1; ϕ_{L1} is the double-differenced carrier phase observations in units of cycles; N_{L1} is the integer cycle ambiguity of the L1 double-differenced carrier observations; $\varepsilon_{\rho L1}$ is the code observation noise and $\varepsilon_{\phi L1}$ is the carrier phase observation noise on L1 double-differenced observations.

The estimation of integer ambiguity of L1 will be as:

$$\hat{N}_{L1} = [(\phi_{L1} - \frac{\rho_{L1}}{\lambda_{L1}})]_{round\,off} \text{ .....cycles.....(4.3)}$$

How good is the estimation? The error model is assumed as $\sigma_{\rho L1} = 0.3m$ and $\sigma_{\phi L1} = 0.01cycle$, the sigma of the ambiguity L1 estimation can be estimated as following:

$$\sigma_{N(L1)} = \sqrt{{\sigma_{\phi L1}}^2 + \left(\frac{\sigma_{\rho L1}}{\lambda_{L1}}\right)^2} \approx 2.5cycles \text{ .....(4.4)}$$

4.2 DUAL FREQUENCIES IN SHORT BASELINE

In the case of short baseline (ionosphere absent), DD code and carrier phase measurements in dual frequencies system (L1 and L2), can be written as equation 4.5. Equation 4.5.1 shows on code observations, and equations (4.5.2)(4.5.3) show on carrier phase observation.

$$\rho_{L1} = r + \varepsilon_{\rho L1}$$
$$\rho_{L2} = r + \varepsilon_{\rho L2} \text{.....m.....(4.5.1)}$$

$$\phi_{L1} = \frac{r}{\lambda_{L1}} + N_{L1} + \varepsilon_{\phi L1}$$

$$\phi_{L2} = \frac{r}{\lambda_{L2}} + N_{L2} + \varepsilon_{\phi L2} \text{.....cycles.....} \quad (4.5.2)$$

$$\Phi_{L1} = r + \lambda_{L1} N_{L1} + \varepsilon_{\Phi L1}$$

$$\Phi_{L2} = r + \lambda_{L2} N_{L2} + \varepsilon_{\Phi L2} \text{.....m.....} \quad (4.5.3)$$

4.2.1 Primary Frequency

The matrix notations of equation (4.5) can be shown as:

$$r = \begin{bmatrix} 0.5 & 0.5 \end{bmatrix} \begin{bmatrix} \rho_{L1} \\ \rho_{L2} \end{bmatrix} \text{……..…….} \quad (4.6)$$

$$\begin{bmatrix} N_{L1} \\ N_{L2} \end{bmatrix} = \begin{bmatrix} \phi_{L1} \\ \phi_{L2} \end{bmatrix} - \begin{bmatrix} 2.6315 & 2.6315 \\ 2.0492 & 2.0492 \end{bmatrix} \begin{bmatrix} \rho_{L1} \\ \rho_{L2} \end{bmatrix} \text{……} \quad (4.7)$$

Measurements at a single epoch give four equations in three unknowns. But the equations are not error-free, especially in the DD code measurements. The error in DD code measurement (including the code observation noise, mulitipath error in the code measurement) will affect the AR performance.

The same error model is used, $\sigma_\rho = 0.3m$ and $\sigma_\phi = 0.01cycle$, the variance-covariance (vc) matrix of real-valued ambiguity can be derived:

$$D_N = \begin{bmatrix} 1 & 0 \\ 0 & 1 \end{bmatrix} \times \sigma_\phi^{\,2} + \begin{bmatrix} 13.8496 & 10.7849 \\ 10.7849 & 8.3984 \end{bmatrix} \times \sigma_\rho^{\,2} \text{……..} \quad (4.8)$$

$$D_N = \begin{bmatrix} 13.8496 + \dfrac{\sigma_\phi^2}{\sigma_\rho^2} & 10.7849 \\ 10.7849 & 8.3984 + \dfrac{\sigma_\phi^2}{\sigma_\rho^2} \end{bmatrix} \times \sigma_\rho^2 = \begin{bmatrix} 1.2466 & 0.9706 \\ 0.9706 & 0.7560 \end{bmatrix} \text{…….……} \quad (4.9)$$

It is very difficult to estimate the primary frequency integer ambiguities because their variances are too big relative to the primary signal wavelength. Therefore, the integer linear combinations should be formed:

$$\overline{N} = Z \times N$$

$$D_{\overline{N}} = Z \times D_N Z^T$$

$$D_{\overline{N}} = \begin{bmatrix} 1 & 0 \\ 0 & 1 \end{bmatrix} \times D_N \times \begin{bmatrix} 1 & 0 \\ 0 & 1 \end{bmatrix}^T = \begin{bmatrix} 1.2466 & 0.9706 \\ 0.9706 & 0.7560 \end{bmatrix} \text{…….} \quad (4.10)$$

when $Z = \begin{bmatrix} 1 & 0 \\ 0 & 1 \end{bmatrix}$, the corresponding optimal linear combinations of the signal carrier phase

measurements are:

$$Z \times \begin{bmatrix} \phi_{L1} \\ \phi_{L2} \end{bmatrix} = \begin{bmatrix} \phi_{L1} \\ \phi_{L2} \end{bmatrix} \quad \text{……..……(4.11)}$$

$$\sigma_{N(L1)} = 1.11 cycle\,,\ \ \sigma_{N(L2)} = 0.87 cycle$$

It can be seen that the ambiguities are very difficult to fixed in one epoch. Because the wavelength of the carrier phase observation is only 19.03cm for L1 signal and 24.42cm for L2 signal.

4.2.2 Hatch-Melbourne-Wübbena (HMW) Linear Combinations

The ambiguity of L1 or L2 is difficult to be estimated by the primary frequency, on the contrary, the widelane ambiguity can be accurately determined because they have relative long wavelength. Using equation (4.5), the ambiguity of L1 and L2 will be estimated as following:

$$N_{L1} = \frac{\Phi_{L1}}{\lambda_{L1}} + \frac{1}{1-\left(\frac{f_{L1}}{f_{L2}}\right)^2}\left\{\left[1+\left(\frac{f_{L1}}{f_{L2}}\right)^2\right]\frac{\rho_{L1}}{\lambda_{L1}} - 2\frac{\rho_{L2}}{\lambda_{L2}}\right\}$$

$$N_{L2} = \frac{\Phi_{L2}}{\lambda_{L2}} + \frac{1}{1-\left(\frac{f_{L1}}{f_{L2}}\right)^2}\left\{2\left(\frac{f_{L1}}{f_{L2}}\right)^2\frac{\rho_{L1}}{\lambda_{L1}} - \left[1+\left(\frac{f_{L1}}{f_{L2}}\right)^2\right]\frac{\rho_{L2}}{\lambda_{L2}}\right\} \quad \text{……..cycles…….……(4.12)}$$

Now the widelane (L1-L2) ambiguity can be calculated as following:

$$\hat{N}_{w12} \equiv (N_1 - N_2)_{round} = (\frac{\Phi_{L1}}{\lambda_{L1}} - \frac{\Phi_{L2}}{\lambda_{L2}} - \frac{f_{L1}-f_{L2}}{f_{L1}+f_{L2}}(\frac{\rho_{L1}}{\lambda_{L1}} + \frac{\rho_{L2}}{\lambda_{L2}}))_{round} \text{ ……..cycles……(4.13)}$$

Meanwhile, the narrowlane (L1+L2) can be measured as following:

$$\hat{N}_{N12} \equiv (N_1 + N_2)_{round} = (\frac{\Phi_{L1}}{\lambda_{L1}} + \frac{\Phi_{L2}}{\lambda_{L2}} - \frac{f_{L1}+f_{L2}}{f_{L1}-f_{L2}}(\frac{\rho_{L1}}{\lambda_{L1}} - \frac{\rho_{L2}}{\lambda_{L2}}))_{round} \text{ ……...cycles……(4.14)}$$

Because $\frac{f_{L1}-f_{L2}}{f_{L1}+f_{L2}} \approx 0.124$, and $\frac{f_{L1}+f_{L2}}{f_{L1}-f_{L2}} \approx 8.06$, so the error due to DD code measurements are reduced to about 1/10 in widelane combination, on the other hand, they will become 10 times bigger in the case of narrowlane combination. So the widelane ambiguity will be more precisely estimated than narrowlane. Subsequently, $\hat{N}_{w12}$ is independent of baseline length, ionosphere bias, and in most cases it can quickly be fixed to its correct integer value.

Equation (4.13) can be rewritten for the multiple frequencies widelane combination as following,

$$\hat{N}_{w\kappa\lambda} \equiv \hat{N}_{\kappa} - \hat{N}_{\lambda} = (\frac{\Phi_{\kappa}}{\lambda_{\kappa}} - \frac{\Phi_{\lambda}}{\lambda_{\lambda}} - \frac{f_{\kappa}-f_{\lambda}}{f_{\kappa}+f_{\lambda}}(\frac{\rho_{\kappa}}{\lambda_{\kappa}} + \frac{\rho_{\lambda}}{\lambda_{\lambda}}))_{round} \text{ ……..cycles……..(4.15)}$$

Equation (4.15) can also be called as **HMW Linear Combination** [Belbourne, 1985]. It is very important in the widelane ambiguity resolution.

The standard error of the widelane ambiguity determined from the signals by the HMW combination can be shown as following:

$$\sigma_{NW\kappa\lambda} = \sqrt{(\sigma_{\phi\kappa})^2 + (\sigma_{\phi\lambda})^2 + \left(\frac{f_\kappa - f_\lambda}{f_\kappa + f_\lambda} \times \frac{\sigma_{\rho\kappa}}{\lambda_\kappa}\right)^2 + \left(\frac{f_\kappa - f_\lambda}{f_\kappa + f_\lambda} \times \frac{\sigma_{\rho\lambda}}{\lambda_\lambda}\right)^2} \quad \text{.....cycles..……..(4.16)}$$

If the error model is assumed as $\sigma_\phi = 0.01 cycles$ and $\sigma_\rho = 0.3m$, the sigma of the widelane L1-L2 AR can be given as $\sigma_{N(wL1L2)} \approx 0.24 cycles$. Using the new signal L5, the sigma of widelane L2-L5 signal AR can be estimated, $\sigma_{N(wL2L5)} \approx 0.03 cycles$, and the wavelength of L2-L5 signal is about 5.8610m. Now we can conclude that the widelane signal ambiguity can be estimated more easily than do primary signal ambiguity. In the widelane signal, because L2-L5 extra-widelane signal has long wavelength, the ambiguity of it can be estimated fastest. More details of the widelane ambiguity resolution method analysis will be discussed in the next chapter.

4.2.3 Widelane Combination Signal

The widelane L1-L2 signal in short baseline (ionopshere absent) is given as following:

$$\Phi_{w12} = r + \lambda_{w12} N_{w12} + \varepsilon_{w12} \text{ ……..m}$$

$$\phi_{w12} = \frac{r}{\lambda_{w12}} + N_{w12} + \varepsilon_{w12} \text{ ……cycles……..……(4.17)}$$

where, $\phi_{w12} = \phi_{L1} - \phi_{L2}$, λ_{w12} is the wave length of widelane L1L2 signal,

Using equation (4.7) (4.8) and (4.11), the standard deviation of the estimation by widelane signal can be given as:

When $Z = \begin{bmatrix} 1 & -1 \\ 0 & 1 \end{bmatrix}$,

$$Z \times \begin{bmatrix} \phi_{L1} \\ \phi_{L2} \end{bmatrix} = \begin{bmatrix} \phi_{L1} - \phi_{L2} \\ \phi_{L2} \end{bmatrix} \text{ ……(4.18)}$$

$$D_{\bar{N}} = \begin{bmatrix} 1 & -1 \\ 0 & 1 \end{bmatrix} \times D_N \times \begin{bmatrix} 1 & -1 \\ 0 & 1 \end{bmatrix}^T = \begin{bmatrix} 0.0610 & 0.2147 \\ 0.2147 & 0.7560 \end{bmatrix} \text{ ……..……..(4.19)}$$

where D_N has been calculated in equation (4.9).

We can see that the widelane signal ambiguity can be estimated easily because $\sigma_{W(NL1-L2)} = 0.24 cycles$, but signal L2 ambiguity is also difficult to be estimated fast because $\sigma_{N(L2)} = 0.87 cycles$.

4.3 DUAL FREQUENCIES OBSERVATIONS IN LONG BASELINE

The observation equations in long baseline (ionosphere present) can be written as following:

$$\begin{aligned} \rho_{L1} &= r + I_{L1} + \varepsilon_{\rho L1} \\ \rho_{L2} &= r + \frac{f_{L1}^2}{f_{L2}^2} I_{L1} + \varepsilon_{\rho L2} \text{.....(m)} \end{aligned} \quad \text{……(4.20.1)}$$

$$\phi_{L1} = \frac{r}{\lambda_{L1}} - \frac{I_{L1}}{\lambda_{L1}} + N_{L1} + \varepsilon_{\phi L1}$$
$$\phi_{L2} = \frac{r}{\lambda_{L2}} - \frac{1}{\lambda_{L2}} \frac{f_{L1}^2}{f_{L2}^2} I_{L1} + N_{L2} + \varepsilon_{\phi L2} .....(cycle) \quad \text{……..……(4.20.2)}$$

where I_{L1} is the ionosphere effect on L1 signal. Equation (4.20.1) shows on the code observation and equation (4.20.2) shows on carrier phase observation.

$$\begin{bmatrix} r \\ I_{L1} \end{bmatrix} = \begin{bmatrix} 2.5456 & -1.5456 \\ -1.5456 & 1.5456 \end{bmatrix} \times \begin{bmatrix} \rho_{L1} \\ \rho_{L2} \end{bmatrix} \text{……..….(4.21)}$$

$$\begin{bmatrix} N_{L1} \\ N_{L2} \end{bmatrix} = \begin{bmatrix} \phi_{L1} \\ \phi_{L2} \end{bmatrix} - \begin{bmatrix} 21.5326 & -16.2694 \\ 20.8656 & -16.7672 \end{bmatrix} \begin{bmatrix} \rho_{L1} \\ \rho_{L2} \end{bmatrix} \text{……(4.22)}$$

$$D_N = \begin{bmatrix} 1 & 0 \\ 0 & 1 \end{bmatrix} \times \sigma_\phi^{\,2} + \begin{bmatrix} 728.3462 & 722.0829 \\ 722.0829 & 716.5123 \end{bmatrix} \times \sigma_\rho^{\,2} \text{……(4.23)}$$

Using the same error model, the variance-covariance matrix can be given:

$$D_N = \begin{bmatrix} 65.5513 & 64.9875 \\ 64.9875 & 64.4862 \end{bmatrix} \text{……..……(4.24)}$$

AR is estimated by primary frequency,

$$Z = \begin{bmatrix} 1 & 0 \\ 0 & 1 \end{bmatrix}, D_{\bar{N}} = \begin{bmatrix} 65.5513 & 64.9875 \\ 64.9875 & 64.4862 \end{bmatrix} \text{……..……(4.25)}$$

AR is estimated by widelane signal method,

$$Z = \begin{bmatrix} 1 & -1 \\ 0 & 1 \end{bmatrix}, D_{\bar{N}} = \begin{bmatrix} 0.0625 & 0.5014 \\ 0.5014 & 64.4862 \end{bmatrix} \text{……..……(4.26)}$$

From the results of the equation (4.26), the sigma of widelane signal AR is about 0.25cycles, the value is about as the same as the case of the short baseline. But the ambiguity of L2 primary signal in long baseline is estimated worse than in the case of short baseline, because sigma of L2 signal is about 8.03cycles.

4.4 COMPARISON BETWEEN WIDELANE & PRIMARY SIGNAL

The effect of the widelane signal transformation can be seen best if the ambiguity search space, represented by the standard ellipse (which is centered around the corresponding ambiguities), is considered [B.Horfmann-Wellenhof, H. Lichtenegger, and J. Collins]. Now the case of long baseline is discussed, recalling the standard variance of the observation matrix (4.25) and (4.26), hence, the standard deviation can be estimated, if the origin primary signal ambiguity is assumed as: $\hat{N}_{L1} = 1.30$, $\hat{N}_{L2} = 1.05$. The parameters of the standard ellipse can be calculated:

$D_{\hat{N}}$: $a = 4.0156, \mathrm{b} = 0.0425, \alpha = 44.8826^{\circ}$, when $Z = \begin{bmatrix} 1 & 0 \\ 0 & 1 \end{bmatrix}$

$D_{\hat{N}'}$: $a = 2.8450, \mathrm{b} = 0.4314, \alpha = 84.8424^{\circ}$, when $Z = \begin{bmatrix} 1 & -1 \\ 0 & 1 \end{bmatrix}$

where, a, b are two semi axes of the ellipse, and α is the direction of the semi major axis.

Graphically, the standard ellipses are shown in Fig 4.1. The standard ellipse for $D_{\hat{N}}$ is centered on the ambiguities $\hat{N}$; here the origin is at $\hat{N}_{L1} = 1.30$, $\hat{N}_{L2} = 1.05$. The standard ellipse for $D_{\hat{N}'}$, is centered on the ambiguities $\hat{N}'$, here amounts to $\hat{N}'_{L1} = \hat{N}_{L1} - \hat{N}_{L2} = 0.25$, $\hat{N}'_{L2} = \hat{N}_{L2} = 1.05$.
Figure 4.1 shows search windows with sides parallel to the two axes of the two-dimensional integer search space, i.e., two ellipses horizontal and two vertical tangents of the ellipse. **It is noted that the "volumes" of the two ellipses are the same because the transformation is volume preserving, but the shape and the orientation of the ellipse has changed.** The distance between the two horizontal tangents has not changed be**cause** these two tangents bound the search range for the N_2 ambiguity that remained unaltered by the transformation. However, the distance of the two vertical tangents has changed.

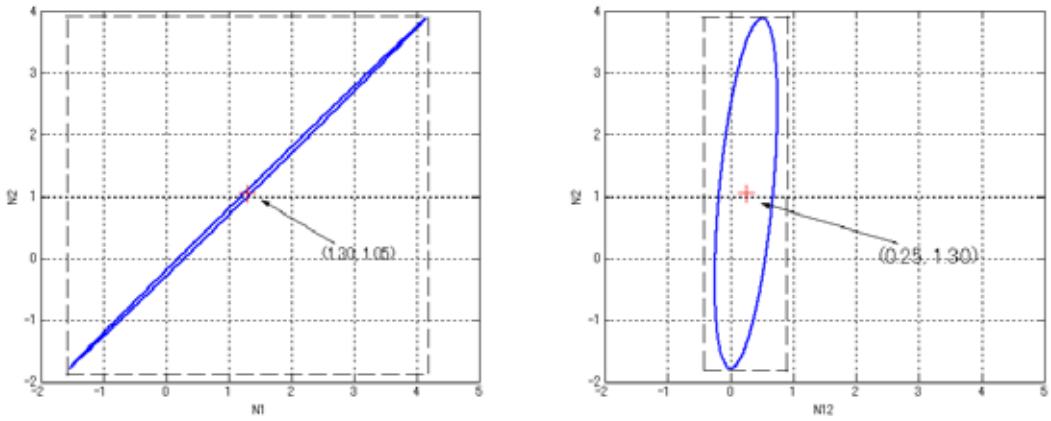

Figure 4.1: Ambiguity search space for $D_{\hat{N}}$ (left) and transformed ambiguity (widelane) search spaces for $D_{\hat{N}'}$ (right)

In figure 4.1, each grid point represents one pair of ambiguities. Under the assumption that each grid point of the search window must be regarded as a possible candidate to be investigated for a research solution, the advantage of the widelane transformed search space becomes obvious. In the other word, from comparing the off-diagonal elements of $D_{\hat{N}}$ and widelane $D_{\hat{N}'}$, the decrease of correlation is evident.

4.5 TRIPLE FREQUENCIES IN SHORT BASELINE

Similar to the investigation of the case in dual frequencies, widelane combination is also used in triple frequencies. The fundamental measurements from modernized GPS will be three pseudo-ranges and three carrier phase measurements including L1, L2 and L5 signals. The new signal (L5) observation equation in

short baseline (ionosphere absent) can be written as:

$$\rho_5 = r + \varepsilon_{\rho L5} \text{.....} m$$

$$\phi_{L5} = \frac{r}{\lambda_{L5}} + N_{L5} + \varepsilon_{\phi L5} \text{.....} cycle \quad \text{……(4.27)}$$

where $\varepsilon_{\rho L5}$ is code noise on signal L5, $\varepsilon_{\phi L5}$ is the carrier phase observation noise on L5, N_{L5} is the integer ambiguity on signal L5.

Using equation (4.5) and (4.27),

$$[r] = \begin{bmatrix} \frac{1}{3} & \frac{1}{3} & \frac{1}{3} \end{bmatrix} \begin{bmatrix} \rho_{L1} \\ \rho_{L2} \\ \rho_{L5} \end{bmatrix} \text{……..(4.28)}$$

$$\begin{bmatrix} N_{L1} \\ N_{L2} \\ N_{L5} \end{bmatrix} = \begin{bmatrix} \phi_{L1} \\ \phi_{L2} \\ \phi_{L5} \end{bmatrix} - \begin{bmatrix} 1.7543 & 1.7543 & 1.7543 \\ 1.3661 & 1.3661 & 1.3661 \\ 1.3046 & 1.3046 & 1.3046 \end{bmatrix} \begin{bmatrix} \rho_{L1} \\ \rho_{L2} \\ \rho_{L5} \end{bmatrix} \text{……..….(4.29)}$$

Assuming that the standard deviation of L1 L2 and L5 carrier phase measurements are the same, the variance-covariance matrix can be derived:

$$D_N = \begin{bmatrix} 1 & 0 & 0 \\ 0 & 1 & 0 \\ 0 & 0 & 1 \end{bmatrix} \times \sigma_\phi^{\,2} + \begin{bmatrix} 9.2327 & 7.1896 & 6.8660 \\ 7.1896 & 5.5987 & 5.3466 \\ 6.8660 & 5.3466 & 5.1059 \end{bmatrix} \times \sigma_\rho^{\,2} \quad \text{……..(4.30)}$$

Using the same error model as same as in case of the dual frequencies, the variance-covariance matrix can be estimated:

$$D_N = \begin{bmatrix} 0.8310 & 0.6471 & 0.6179 \\ 0.6471 & 0.5040 & 0.4812 \\ 0.6179 & 0.4812 & 0.4596 \end{bmatrix} \text{……..(4.31)}$$

If ambiguity is estimated by primary signal (L1, L2 and L5) directly, for this case variance-covariance matrix can be estimated:

$$D_{\bar{N}} = Z \times D_N \times Z^T = \begin{bmatrix} 1 & 0 & 0 \\ 0 & 1 & 0 \\ 0 & 0 & 1 \end{bmatrix} \times D_N \times \begin{bmatrix} 1 & 0 & 0 \\ 0 & 1 & 0 \\ 0 & 0 & 1 \end{bmatrix}^T = \begin{bmatrix} 0.8310 & 0.6471 & 0.6179 \\ 0.6471 & 0.5040 & 0.4812 \\ 0.6179 & 0.4812 & 0.4596 \end{bmatrix} \text{……(4.32)}$$

If ambiguity is estimated by extra-widelane signal (L2-L5), widelane (L1-L2) and primary signal L5, for this case variance-covariance matrix can be estimated:

$$D_{\bar{N}} = Z \times D_N \times Z^T = \begin{bmatrix} 0 & 1 & -1 \\ 1 & -1 & 0 \\ 0 & 0 & 1 \end{bmatrix} \times D_N \times \begin{bmatrix} 0 & 1 & -1 \\ 1 & -1 & 0 \\ 0 & 0 & 1 \end{bmatrix}^T = \begin{bmatrix} 0.0012 & 0.0063 & 0.0216 \\ 0.0063 & 0.0409 & 0.1367 \\ 0.0216 & 0.1367 & 0.4596 \end{bmatrix} \text{(4.33)}$$

The corresponding linear combinations of the L1, L2 and L5 carrier phase measurements in two cases are:

$$Z \times \begin{bmatrix} \phi_{L1} \\ \phi_{L2} \\ \phi_{L5} \end{bmatrix} = \begin{bmatrix} \phi_{L1} \\ \phi_{L2} \\ \phi_{L5} \end{bmatrix} \text{ in the first case and } Z \times \begin{bmatrix} \phi_{L1} \\ \phi_{L2} \\ \phi_{L5} \end{bmatrix} = \begin{bmatrix} \phi_{L2} - \phi_{L5} \\ \phi_{L1} - \phi_{L2} \\ \phi_{L5} \end{bmatrix} \text{ in the second case.}$$

From the results, the sigma of the extra-widelane signal ambiguity estimation is only 0.03 cycles. Float number will be fixed easily to the nearest integer cycle value because its standard deviation is very small. and the sigma of widelane signal and L5 signal ambiguity estimation are about 0.2 cycle and 0.68 cycles, the values are smaller than the case of the dual frequencies in short line. The ambiguity can be fixed in the triple frequencies faster and more accurate than the case in dual frequencies system.

4.6 LONGBASELINE COMBINATIONS IN TRIPLE FREQUENCIES

The third observation equations in long baseline (considering ionosphere effect) can be given as:

$$\begin{aligned} \rho_5 &= r + \frac{f_{L1}^2}{f_{L5}^2} I_{L1} + \varepsilon_{\rho 5} \text{.....} m \\ \phi_{L5} &= \frac{r}{\lambda_{L5}} - \frac{f_{L1}^2}{f_{L5}^2} \frac{I_{L1}}{\lambda_{L5}} + N_{L5} + \varepsilon_{\phi L5} \text{.....} cycle \end{aligned} \quad \text{……..…….(4.34)}$$

where, $\varepsilon_{\rho 5}$ and $\varepsilon_{\phi L5}$ is the observation noise in DD code measurements and carrier measurements.

$$\begin{bmatrix} r \\ I_{L1} \end{bmatrix} = \begin{bmatrix} 2.32694 & -0.35965 & -0.96730 \\ -1.34697 & 0.46821 & 0.87876 \end{bmatrix} \begin{bmatrix} \rho_{L1} \\ \rho_{L2} \\ \rho_{L5} \end{bmatrix} \text{……..(4.35)}$$

$$\begin{bmatrix} N_{L1} \\ N_{L2} \\ N_{L5} \end{bmatrix} = \begin{bmatrix} \phi_{L1} \\ \phi_{L2} \\ \phi_{L5} \end{bmatrix} - \begin{bmatrix} 19.30654 & -4.35039 & -9.70112 \\ 18.61236 & -4.63026 & -9.88727 \\ 18.61029 & -4.70618 & -9.97990 \end{bmatrix} \begin{bmatrix} \rho_{L1} \\ \rho_{L2} \\ \rho_{L5} \end{bmatrix} \text{……(4.36)}$$

$$D_N = \begin{bmatrix} 1 & 0 & 0 \\ 0 & 1 & 0 \\ 0 & 0 & 1 \end{bmatrix} \times \sigma_\phi^{\,2} + \begin{bmatrix} 485.7830 & 475.40131 & 476.59032 \\ 475.40131 & 465.61720 & 466.84613 \\ 476.59032 & 466.84613 & 468.08641 \end{bmatrix} \times \sigma_\rho^{\,2} \text{……..(4.37)}$$

Using the same error model, $D_N = \begin{bmatrix} 43.7206 & 42.7861 & 42.8931 \\ 42.7861 & 41.9056 & 42.0162 \\ 42.8931 & 42.0162 & 42.1279 \end{bmatrix}$ ……..…….(4.38)

When $Z = \begin{bmatrix} 1 & 0 & 0 \\ 0 & 1 & 0 \\ 0 & 0 & 1 \end{bmatrix}$, $D_{\bar{N}} = \begin{bmatrix} 43.7206 & 42.7861 & 42.8931 \\ 42.7861 & 41.9056 & 42.0162 \\ 42.8931 & 42.0162 & 42.1279 \end{bmatrix}$ ……..(4.39)

When $Z=\begin{bmatrix}0 & 1 & -1\\ 1 & -1 & 0\\ 0 & 0 & 1\end{bmatrix}$, $D_{\bar{N}}=\begin{bmatrix}0.0012 & 0.0035 & -0.1120\\ 0.0035 & 0.0540 & 0.8770\\ -0.1120 & 0.8770 & 42.1279\end{bmatrix}$ ……..…..(4.40)

Comparing the cases of the short baseline in triple frequencies, the sigma of extra-widelane and widelane signal AR in long baseline is about 0.03cycles and 0.23 cycles, the values are almost same as the case of the short baseline. But the ambiguity of L5 primary signal in long baseline will be estimated worse than in the case of short baseline.

4.7 VARIOUS LINEAR COMBINATIONS

4.7.1 Widelane Linear Combination

From the above calculation results, the widelane and extra-widelane signal ambiguity can be estimated faster and more accurate in single epoch than estimating the primary signal ambiguity. The widelane and extra-widelane signal is introduced here.

The widelane linear combination can be given as following:

$$\Phi_{w\kappa\lambda}=\frac{\lambda_{w\kappa\lambda}}{\lambda_\kappa}\Phi_\kappa-\frac{\lambda_{w\kappa\lambda}}{\lambda_\lambda}\Phi_\lambda=r+\frac{f_{L1}^{\ 2}}{f_\kappa f_\lambda}I_{L1}+\lambda_{w\kappa\lambda}N_{w\kappa\lambda}+\varepsilon_{w\kappa\lambda}\ \text{……..….m……..(4.41)}$$

where $f_{w\kappa\lambda}=f_\kappa-f_\lambda,\lambda_{w\kappa\lambda}=\frac{c}{f_\kappa-f_\lambda}=1/\left(\frac{1}{\lambda_\kappa}-\frac{1}{\lambda_\lambda}\right)$ ……(4.42)

$\varepsilon_{w\kappa\lambda\Phi}$ is the noise in the widelane signal, if assuming no correlation between the primary signals, it can be estimated as:

$$\varepsilon_{w\kappa\lambda}=\sqrt{\left(\frac{\lambda_{w\kappa\lambda}}{\lambda_\kappa}\right)^2\sigma_{\Phi\kappa}^{\ 2}+\left(\frac{\lambda_{w\kappa\lambda}}{\lambda_\lambda}\right)^2\sigma_{\Phi\lambda}^{\ 2}}\qquad\text{……m……..……..(4.43)}$$

L1-L2 widelane combination:

$$\Phi_{wL1L2}=\frac{\lambda_{wL1L2}}{\lambda_{L1}}\Phi_\kappa-\frac{\lambda_{wL1L2}}{\lambda_{L2}}\Phi_\lambda=r+\frac{f_{L1}^{\ 2}}{f_{L1}f_{L2}}I_{L1}+\lambda_{wL1L2}N_{wL1L2}+\varepsilon_{wL1L2}\ \text{…m……..……(4.44)}$$

In the widelane signal, the ionosphere effect will be about –1.2833 times relative to L1 signal.

If the error model assumed that $\sigma_\Phi=0.003m$ and $\sigma_\rho=0.3m$, the noise in the widelane carrier phase measurement can be estimated by (4.43), the results as 0.00172m, it is about 5.7 times as big as the carrier phase observation noise in the primary signal.

In the widelane signal, the ambiguity can be estimated easily, but will be noisier with the amplified the noise by widelane combination.

L2-L5 extra-widelane combination:

$$\Phi_{wL2L5}=\frac{\lambda_{wL2L5}}{\lambda_{L2}}\Phi_\kappa-\frac{\lambda_{wL2L5}}{\lambda_{L5}}\Phi_\lambda=r+\frac{f_{L1}^{\ 2}}{f_{L2}f_{L5}}I_{L1}+\lambda_{wL2L5}N_{wL2L5}+\varepsilon_{wL2L5}\ \text{….m……..…(4.45)}$$

In the extra-widelane combination, the ionosphere effect is about –1.7185 times relative to the L1 signal. Using the same error model as widelane signal, the sigma of the noise in the extra-widelane carrier phase measurement can be estimated as 0.0998m, it is about 33.27 times as big as the DD carrier phase observation noise in the primary signal.

In the extra-widelane signal, the ambiguity can be estimated much easily because of the long wavelength, but there is much noise in the extra-widelane signal, it will be affected in the ambiguity estimation.

4.7.2 Ionosphere-Free Combination

Ionosphere-Free combination can be shown as following:

$$\Phi_{I\kappa\lambda} = f_\kappa \Phi_\kappa - f_\lambda \Phi_\lambda = r + \frac{c}{f_\kappa^{\,2} - f_\lambda^{\,2}}(f_\kappa N_\kappa - f_\lambda N_\lambda) + \varepsilon_{I\kappa\lambda} \text{ …….m……..……..(4.46)}$$

where $\varepsilon_{I\kappa\lambda}$ is observation noise in Ionosphere-Free signal

Constructing a combined ionosphere-free phase or pseudo-range observable from the multiple frequencies data can eliminate the ionospheric refraction bias.

4.7.3 Geometry-Free Combination

Geometry-Free combination can be shown as following:

$$\Phi_{G\kappa\lambda} = \Phi_\kappa - \Phi_\lambda = \left(-\frac{f_{L1}^{\,2}}{f_\kappa^{\,2}} + \frac{f_{L1}^{\,2}}{f_\lambda^{\,2}} \right) I_{L1} + (\lambda_\kappa N_\kappa - \lambda_\lambda N_\lambda) + \varepsilon_{G\kappa\lambda} \text{ ……..m…….(4.47)}$$

where $\varepsilon_{G\kappa\lambda}$ is the observation noise in Geometry-Free signal.

Equation (4.47) can be rewritten in the short baseline; the ionosphere error can be neglected,

$$\Phi_{G\kappa\lambda} = \Phi_\kappa - \Phi_\lambda = (\lambda_\kappa N_\kappa - \lambda_\lambda N_\lambda) + \varepsilon_{G\kappa\lambda} \text{ ……m……..…….(4.48)}$$

SUMMARY

In this chapter, the ambiguity of widelane combination signal can be determined more easily and accurately than primary signal ambiguity directly. Using this theory, before the primary signal ambiguity (for example L1) is estimated, the widelane or extra-widelane signal ambiguities are estimated in the first. This is the basic concept in the next chapter. However with the widelane combination, the carrier observation noise will be bigger than the primary signal. About the noise in the modernization signal will be introduced in the section 5.4 in the next chapter.

Table 4.1 shows the comparison of the sigma of the primary signal, widelane and extra-widelane signal AR in dual or triple frequencies when short baseline and long baseline. It has to be noted that in Table 4.1, the error model is assumed that the standard error is same in the DD code and carrier phase measurements, $\sigma_\rho = 0.3m$ and $\sigma_\phi = 0.01cycles$. From the equation variance-covariance matrix estimation (4.8), it can be seen that the standard error of the estimated ambiguity of the primary or the widelane signal is affected by the standard deviation of L1, L2 and L5 DD code or carrier phase measurements.

Sigma of Signal Ambiguity Resolution (cycles)				
	Short Baseline		Long Baseline	
	Dual frequencies	Triple frequencies	Dual frequencies	Triple frequencies
Primary	0.87	0.68	8.03	6.49
Wideline	0.24	0.2	0.25	0.22
Extra-widelane		0.03		0.03

Table 4.1: Comparison of standard deviation of ambiguity resolution using primary and widelane signal in dual or triple frequencies in single epoch.

From the Table 4.1, the standard deviations of the estimated widelane signal ambiguity are almost same between the case of the long and short baseline. It means that they are nearly no affected by the ionosphere effect.

In this chapter, HMW combination is also introduced. This equation can be used to estimate the widelane ambiguity of the pair of the satellites and receivers. Geometry-free combination and ionosphere-free combination are introduced in this chapter. These two combinations can be used for the different application.

In the triple frequencies, more linear combinations (including widelane, ionosphere-free, geometry-free combination, and so on) can be created than in the dual frequencies. This is the most important concept in this thesis. And then in the next chapter, with more linear combinations in triple frequencies, more AR methods can be performed. For the user, there is more choice to select which method is the best to use.

CHAPTER 5
AMBIGUITY RESOLUTION

5.1 INTRODUCTION

Determining the value of the unknown initial (integer) ambiguity for a GPS double-differenced phase solution is an important task of GPS phase reduction software. Ambiguity resolution is probably the most uniquely identifiable characteristic of high precision GPS positioning.

In this thesis, the ambiguity of primary signal will be estimated by OTF (on the fly) method and wide lane combination. The concept of widelane combination has been introduced in last chapter. In dual frequencies, widelane L1L2 signal is used (called as widelaneL1L2 method). In triple frequencies, two methods, including using widelane L1L5 signal (called as widelaneL1L5 method) and using widelaneL2L5 signal (called as extra-widelane method), are proposed. Figure 5.1 shows that widelane ambiguity method procedure. In the end of this chapter, geometry-free method will be introduced to use in long baseline in triple frequencies. Relative to the widelane method, geometry-free method is no affected by the baseline influence.

At the first, the widelane method is introduced as following:

(1) The initial estimate of widelane ambiguities are determined by HMW combination using the position of the receiver, which is calculated using the double differences of carrier, smoothed L1 pseudoranges. Here, four satellites that have the minimum RDOP (Relative Dilution of Precision) as primary satellites among all the satellites, shown as following:

$$RDOP = \sqrt{trace(H^T H)^{-1}}$$

$$H = \left(\frac{\partial DD_1}{\partial r} \cdots \frac{\partial DD_{1\backslash nsv-1}}{\partial r} \right)^T \quad \cdots\cdots(5.1)$$

$$= \begin{pmatrix} \frac{r^T - r_{SV1}^{*T}}{\rho_u^{*1}} - \frac{r^T - r_{SV2}^{*T}}{\rho_u^{*2}} \\ \vdots \\ \frac{r^T - r_{SV1}^{*T}}{\rho_u^{*1}} - \frac{r^T - r_{SVnsv}^{*T}}{\rho_u^{*nsv}} \end{pmatrix}$$

where H is the measurement matrix, ρ_u^{*1} is the distance from user receiver to i-th satellite. DD_i is the double differenced observable between the first and i+1-th satellite, in which the smoothed pseudorange.

(2) Receiver position is computed with each ambiguity candidate, and the statistical tests are performed in the measurement domain and position domain.

(3) If one ambiguity candidate set is retained, that is considered as the solution. And if more than one candidate are retained, similar statistical tests will be performed at the next epoch.

(4) Procedure (2) and (3) are repeated until only one candidate is retained. If the number of total epochs exceed a threshold number, the process is back to (1)

(5) The initial values of L1 ambiguity are calculated from Geometry-Free method

(6) Procedures similar to (2) and (3) are repeated until one candidates is retained. If the number of total epochs exceeds a thread number, the process is back to (5).

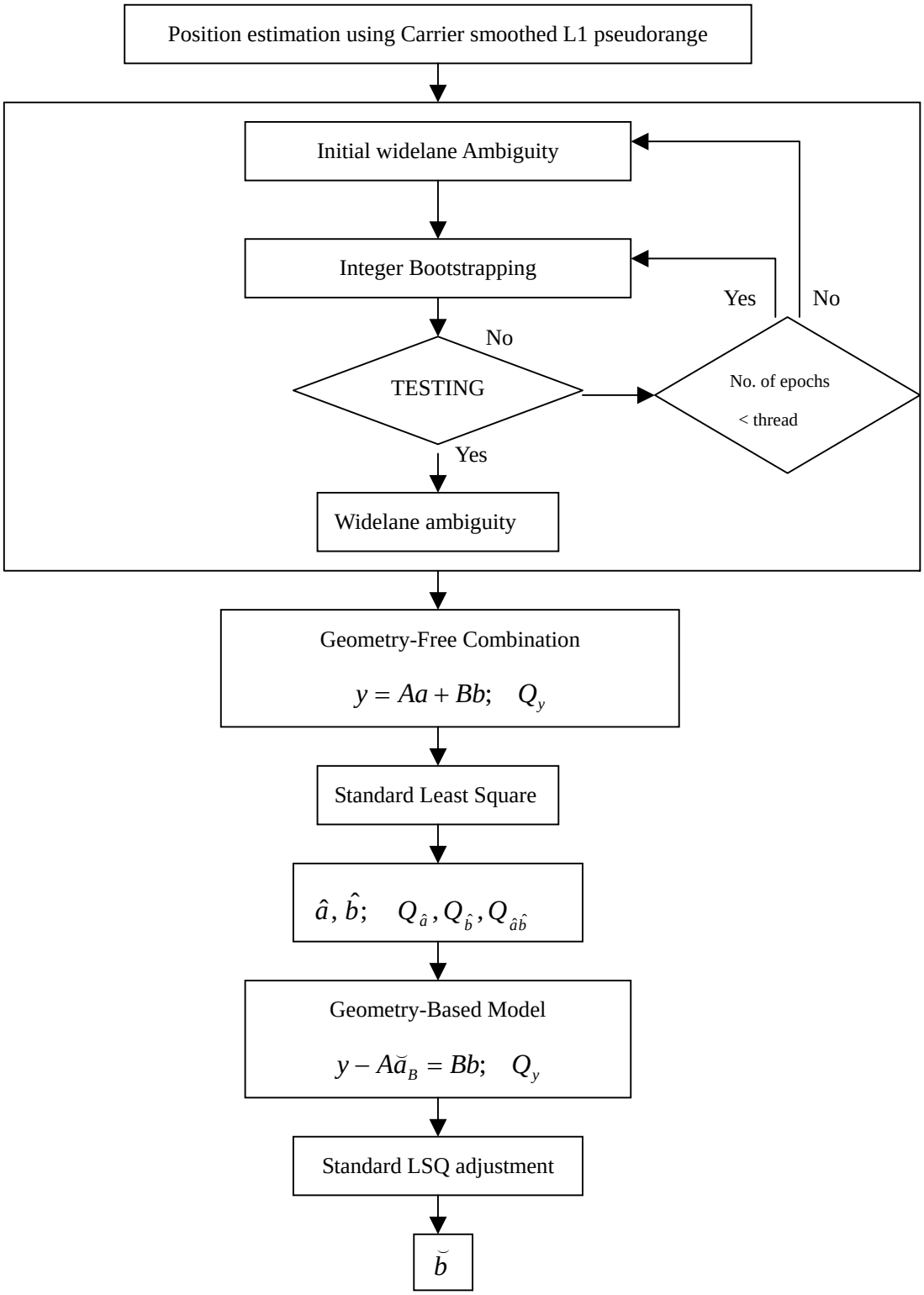

Figure 5.1: Example of ambiguity resolution using widelane combination method

In Figure 5.1, $y = Aa + Bb + e$, y is the given m-dimensional Global Navigation Satellite System (GNSS) data vector, "a" and "b" are the unknown parameter vectors respectively of order n and p, where e is the noise vector. The entries of vector a are then the DD carrier phase ambiguities, expressed in units of cycles rather than range. They are known to be integers. The entries of vector b will consist of the remaining unknown

parameters, such as DD ranges in case of the geometry-free model or baseline components (coordinates) in case of the geometry-based model, possibly together with atmospheric delay parameters (troposphere, ionosphere) and/or other parameters of interest.

In the triple frequencies, one start with the extra widelane carrier phase combination of L2 and L5, This combination has a wavelength of 5.86m and the ambiguity is resolved by rounding its 'float' solution to the nearest integer. With this information the widelane combination of L1 and L2, with wavelength of 0.86m, is resolved in the second step through rounding. Using the information of the first two steps, the third and last step amounts resolving the ambiguity on any one frequency (usually L5 signal) through rounding.

5.2 INTEGER BOOTSTRAPPING

Carrier phase ambiguity resolution is the key to fast and high precision GPS positioning. Critical in the application of ambiguity resolution is the quality of the computed integer ambiguity resolution is the quality of the computed integer ambiguity. The success or failure of carrier phase ambiguity resolution can be predicted by means of the probability of correct integer estimation, also referred to as the ambiguity success-rate (ASR). The higher this probability, the better the performance of the AR performance. In the recent research, the upperbound for the bootstrapped success-rate is to be computed.

5.2.1 Definition

There are very ways of computing an integer ambiguity vector $\breve{a} \in Z^n$ from its real-valued counterpart $\hat{a} \in R^n$, also referred to as 'float' solution. To each such method belongs a mapping $S : R^n \mapsto Z^n$, the map *S* will not be one-to-one, but instead a many-to-one map. This implies that different real-valued ambiguity vectors will be mapped to the same integer vector. One can therefore assign a subset $S_Z \subset R^n$ to each integer vector $z \in Z^n$:

$$S_z = \{x \in R^n \mid z = S(x)\}, \quad z \in Z^n \qquad \text{.....(5.2)}$$

The subset S_z contains all real-valued ambiguity vectors that will be mapped by S to the same integer vector $z \in Z^n$. This subset is referred to as the *pull-in region* of *z*. It is the region in which all ambiguity 'float' solutions are pulled to the same 'fixed' ambiguity vector *z*. Using the pull-in regions, one can give an explicit expression for the corresponding integer ambiguity estimator. It reads $\breve{a} = \sum_{z \in Z^n} z s_z(\hat{a})$ with the indicator function $s_z(\hat{a})$ equal to one if $\hat{a} \in S_z$ and zero otherwise.

With the division of R^n into mutually exclusive pull-in regions, we are in the position to consider the distribution of $\breve{a}$. This distribution is of the discrete type and it will be denoted as $P(\breve{a} = z)$. It is a probability mass function, having zero masses at nongrid points and nonzero masses at some or all grid points. If we denote the *continuous* probability density function $\hat{a}$ as $p_{\hat{a}}(x)$, the distribution of $\breve{a}$ follows as [Teunissen, 2003]:

$$P(\breve{a} = z) = \int_{S_z} p_{\hat{a}}(x)dx, \quad z \in Z^n \qquad \text{.....(5.3)}$$

Note that the dependence on the chosen integer estimation principle enters through the pull-in regions S_z. The above expression holds for any distribution the "float" ambiguities $\hat{a}$ might have. In most GNSS applications however, one assumed the vector of observable to be normally distributed. The estimator $\hat{a}$ is then normally distributed too, with mean $a \in Z^n$ and vc-matrix $Q_{\hat{a}}$. Its probability density function (pdf) reads

$$p_{\hat{a}}(x) = \frac{1}{\sqrt{\det(Q_{\hat{a}})(2\pi)^{\frac{1}{2}n}}} \exp\left\{-\frac{1}{2}\|x-a\|^2_{Q_{\hat{a}}}\right\} \quad \text{.....(5.4)}$$

with the squared weighted norm $\|\bullet\|^2_{Q_{\hat{a}}} = (\bullet)^T Q_{\hat{a}}^{-1}(\bullet)$.

The probability $P(\breve{a} = a)$ equals the probability of *correct* integer ambiguity estimation, the ambiguity success-rate.

5.2.2 Integer Bootstrapping

If *n* ambiguities are available, one starts with the first ambiguity $\hat{a}_1$, and rounds its value to the nearest integer. Having obtained the integer value of this first ambiguity, the real-valued estimates of all remaining ambiguities are then corrected by virtue of their correlation with the first ambiguity, Then the second, but now corrected, real-valued ambiguity estimate is rounded to its nearest integer. Having obtained the integer value of the second ambiguity, the real-valued estimates of all remaining *n-2* ambiguities are then again corrected, but now by virtue of their correlation with the second ambiguity. This process is continued until all ambiguities are considered. The components of the bootstrapped estimator $\breve{a}_B$ are given as:

$$\begin{aligned}
\breve{a}_{B,1} &= \left[\hat{a}_1\right] \\
\breve{a}_{B,2} &= \left[\hat{a}_{2|1}\right] = \left[\hat{a}_2 - \sigma_{21}\sigma_1^{-2}\left(\hat{a}_1 - \breve{a}_{B,1}\right)\right] \\
&\vdots \\
\breve{a}_{B,n} &= \left[\hat{a}_{n|N}\right] = \left[\hat{a}_n - \sum_{j=1}^{n-1} \sigma_{n,j|J}\sigma_{j|J}^{-2}\left(\hat{a}_{j|J} - \breve{a}_{B,j}\right)\right]
\end{aligned} \quad \text{,.....(5.5)}$$

where the short notation $\hat{a}_{i|I}$ stands for the i-th least-squares ambiguity obtained through a conditioning on the previous $I = \{i, \ldots, (i-1)\}$ sequentially rounded ambiguities, $[\bullet]$ denotes the operation of integer rounding, $\sigma_{i,j|J}$ denotes the covariance between $\hat{a}_i$ and $\hat{a}_{j|J}$, and $\sigma^2_{j|J}$ denotes variance of $\hat{\sigma}_{j|J}$. For a review of the theory of integer bootstrapping we refer to [Teunissen, 2001].

The first two conditions of the definition are satisfied, since any 'float' solution gets mapped to an unique integer ambiguity vector. Also the third condition of the definition applies. To see this, let $\breve{a}'_B$ be the bootstrapped estimator that corresponds with $a' = \hat{a} - z$. It follows then from (5.5) that $\breve{a}_B = \breve{a}'_B + z$.

The real-valued sequential conditional least-squares solution can be obtained by means of the triangular decomposition of the ambiguity variance-covariance matrix. When using the bootstrapped pull-in region for the probability mass function (5.2) with pdf (5.3), the success-rate of integer bootstrapping can be shown to follow as:

$$P(\breve{a}_B = a) = \prod_{i=1}^{n} (2\Phi(\frac{1}{2\sigma_{i|I}}) - 1), \quad \text{.....(5.6)}$$

where the function Φ is defined as $\Phi(x) = \int_{-\infty}^{x} \frac{1}{2\pi} \exp\{-\frac{1}{2}v^2\}dv$. This shows that the bootstrapped success-rate is determined by the conditional variances $\sigma_{i|I}^2, i = 1,...., n.$

The outcome of integer bootstrapping and its success-rate depends on the chosen ambiguity parameterization. For instance, a simple recording of the ambiguities will already affect the success-rate. The fact that the bootstrapped success-rate will not remain invariant when an arbitrary ambiguity transformation is applied is a consequence of the uniqueness of the triangular decomposition. Using two methods to check the accuracy of the estimated ambiguity in the recent research.

5.3 TESTING

5.3.1 Test in the Measurement Domain

χ^2 test is performed using the sum of measurement residuals. The candidates satisfying the following condition are rejected: [Toshiaki, 1998]

$$\frac{v^T C_w^{-1} v}{df} > \frac{\chi^2_{df,1-a}}{df} k_1^w, \quad \text{.....(5.7)}$$

where, v, a and df denote the residual vector, the significant level of the χ^2 test, and the degree of freedom (= nsv-4), respectively, k_1^w is an empirical parameter of tolerance, which is set to 1-2 in our study.

5.3.2 Test in the Position Domain

Taking the differences between the horizontal computed using smoothed pseudorange and those using each ambiguity candidate, the candidate satisfy the following condition are rejected:

$$\left| r^{PR} - r^W \right|_H > k_2^w \sigma_H^{PR-W}, \quad \text{.....(5.8)}$$

where r^{PR} and r^W denote the position vectors of antenna calculated using smoothing pseudorange and widelane, respectively, and $|\bullet|_H$ means to take the horizontal norm. σ_H^{PR-W} shows the standard deviation of the difference between the pseudorange-position and the widelane-position in the horizontal direction. k_2^W is an empirical parameter of tolerance, which is set to 2 or 3 in our study.

The standard deviation of position error when the pseudoranges are used is written as follows

$$\sigma_p^{PR} = RDOP \times \sigma_m^{PR}, \quad \text{.....(5.9)}$$

where σ_m^{PR} is the standard deviation of pseudorange measurement error, and then it can be divided into the following:

$$\sigma_H^{PR-W} = RHDOP\sqrt{\left(\sigma_m^{PR}\right)^2 + \left(\sigma_m^W\right)^2}, \quad \text{.....(5.10)}$$

where, $RHDOP$ indicate the dilution of relative position precision in the horizontal direction.

5.4 MODERNIZATION GPS SIGNAL NOISE

From the discussion of the last chapter, the widelane signal ambiguity estimated by HMW combination can be estimated more precisely than by primary frequency directly, and is nearly no affected by atmosphere and ephemeris error. However, it will be influenced by code and phase observation noise and multipath error. In the chapter 2, the L5 signal structure has been introduced, and comparison with three GPS frequencies was shown in Table 2.2. Now the code and phase noise in DD measurements in modernization GNSS will be discussed in details here.

With the modernization of the GNSS, there will be low-noise code ranges with small multipath sensitivity in GPS L5 signal. For the minimum received power we assumed the values listed in Table 5.1 [Eissfeller, 2002]. For L1 we assumed that only C/A code is tracked. On L2 the whole civil signal (medium and long code) is tracked. On L5 it is necessary to track the data-free Q-channel to achieve a better carrier phase tracking threshold and to track the I-channel to recover the navigation data message. The relation of the typical carrier-to-noise ratio C/N_0 to the minimum received power can be determined by looking at a L1 C/A-code receiver, which shows maximum C/N_0 values typically in the range of 45-50 dBHz. Taking 47.3 dBHz yields a difference of –205 dBW, if a minimum received power of –157.7 dBW is assumed for the C/A code signal (about C/N_0 will be discussed in the next chapter). It can also be seen that the various data rate is employed and the use of data free (DF) channel is planned.

Acronym	L1	L2	L5
Power Level [dbW]	-157.7	-160	-154
Typical C/N [dBHz]	47.3	45	51
Data Rate	50bps	50bps	I: 100bps Q: DF

Table 5.1: GPS signal parameters

From the simulation of a GPS receiver-tracking channel described in [Pany, 2002], typical (undifferenced) code measurement accuracy values due to thermal noise are determined and listed in Table 5.2. In addition to the signal parameters the accuracy is determined by the bandwidth of signal at the intermediate frequency level *Bw* and the predetection integration time *Td*. The code standard deviation can be estimated by equation (5.11), and the carrier phase standard deviation can be estimated by equation (5.12) as following. The value refers to a tracking channel with a non-coherent early-power minus late-power discriminator, a discriminator spacing *d* (in chips). From Table 5.2, it should be noted that the accuracy changes significantly if one of the parameters (especially DLL and PLL bandwidth or signal-to-noise ratio) changes. Although not considered here, the error due to multipath will in most cases be much larger than those due to thermal noise. In the following, to reflect these aspects, slightly larger and round standard deviation values are used for the analyses on ambiguity resolution.

$$\sigma_{DLL} = \lambda_c \times \sqrt{\frac{\alpha \times d \times B_{DLL}}{C/N_0}\left[1+\frac{2}{T_d \times C/N_0}\right]}\text{,……(m)……..(5.11)}$$

$$\sigma_{PLL} = \sqrt{\frac{B_{PLL}}{C/N_0}\left(1+\frac{1}{2T_d \times C/N_0}\right)}, \text{..(cycles)..(5.12)}$$

where, $\alpha = 0.5$ shows early/late correlator in equation (5.11),;

λ_c shows GPS propagation constant/PRN code chipping rate (m/sec)/(chip/sec).

These two equations will be also used in the next chapter to generate the code and phase tracking noise in code and carrier measurements.

Acronym	L1	L2	L5
d	0.1	0.1	1
Bw [MHz]	32	24	24
Td [ms]	20	20	10
DLL bandwidth (Hz)	1	1	1
PLL bandwidth (Hz)	10	10	10
Sigma of code noise (m)	0.2833	0.3696	0.0584
Sigma of phase noise (cycles)	0.0136	0.0178	0.0089

Table 5.2: Receiver parameters for a modernized GPS receiver

By considering the multipath error influence, the standard error of code and phase noise in triple frequencies (L1 L2 L5) code and carrier phase observation measurements will be assumed as Table 5.3

Acronym	L1	L2	L5
Sigma of code noise (m)	0.30	0.38	0.06
Sigma of phase noise (cycles)	0.014	0.018	0.009

Table 5.3: Error model in GPS modernization

5.5AR IN DUAL FREQUENCIES

5.5.1 Long Baseline (Ionosphere Present)

If we only considered the carrier phase measurements, the observation equations in dual frequencies can be shown as following:

$$\Phi_{L1} = r - I_{L1} + Trop + \lambda_{L1}N_{L1} + \varepsilon_{L1\Phi} \text{ ..m..(5.13)}$$

$$\Phi_{L2} = r - \frac{f_{L1}^{\ 2}}{f_{L2}^{\ 2}} I_{L1} + Trop + \lambda_{L2}N_{L2} + \varepsilon_{L2\Phi} \text{ ..m..(5.14)}$$

$$\Phi_{w12} = r + \frac{f_{L1}^{\ 2}}{f_{L1}f_{L2}} I_{L1} + Trop + \lambda_{wL1L2}N_{wL1L2} + \varepsilon_{wL1L2\Phi} \text{ ..m..(5.15)}$$

where, *Trop* means the troposphere error in DD measurement.

From last chapter, we can see that $\hat{N}_{wL1L2}$ can be estimated by HMW combination easily, it can be fixed

easily by integer estimation. So the widelane signal ambiguity can be treated as known value. Here the resolution of N_{wL1L2} will be affected by L1 and L2 code observation noise, and then, only one Geometry-Free combination can be used.

If the carrier measurements are only considered, the matrix notation can be measured as:

$$\begin{bmatrix} 1 & -1 & 1 \\ 1 & -\frac{f_{L1}^{\ 2}}{f_{L2}^{\ 2}} & \frac{f_{L1}}{f_{L2}} \end{bmatrix} \begin{bmatrix} r+Trop \\ I_{L1} \\ \lambda_{L1}N_{L1} \end{bmatrix} = \begin{bmatrix} \Phi_{L1} - \varepsilon_{\Phi L1} \\ \Phi_{L2} + \lambda_{L2}N_{wL1L2} - \varepsilon_{\Phi L2} \end{bmatrix} \text{……..(5.16)}$$

Standard error of the primary ambiguity N_{L1} resolution can be estimated as following:

$$\sigma_{NL1} = \sigma_{\phi L1} \times (A^T \times W \times A)_{33}^{-\frac{1}{2}} \approx 1.97 \times 10^5 \ cycles$$

where $\sigma_{\phi L1}$ is the sigma of L1 phase noise; $A = \begin{bmatrix} 1 & -1 & 1 \\ 1 & -\frac{f_{L1}^{\ 2}}{f_{L2}^{\ 2}} & \frac{f_{L1}}{f_{L2}} \end{bmatrix}$;

W is the weighting matrix calculated by error model.

The result means that primary ambiguity cannot be estimated only by the carrier phase measurements (including widelane signal). Then the code measurements are used to estimate primary frequency, the widelane signal ambiguity is also used here. AR can be shown as matrix notation as following:

$$\begin{bmatrix} 1 & 1 & 0 \\ 1 & \frac{f_{L1}^{\ 2}}{f_{L2}^{\ 2}} & 0 \\ 1 & -1 & 1 \\ 1 & -\frac{f_{L1}^{\ 2}}{f_{L2}^{\ 2}} & \frac{f_{L1}}{f_{L2}} \end{bmatrix} \begin{bmatrix} r+Trop \\ I_{L1} \\ \lambda_{L1}N_{L1} \end{bmatrix} = \begin{bmatrix} \rho_{L1} - \varepsilon_{\rho_{L1}} \\ \rho_{L2} - \varepsilon_{\rho L2} \\ \Phi_{L1} - \varepsilon_{\Phi L1} \\ \Phi_{L2} + \lambda_{L2}N_{wL1L2} - \varepsilon_{\Phi L2} \end{bmatrix} \text{……..m…..……..(5.17)}$$

Using the error model in the Table 5.3, the standard error of the primary ambiguity N_{L1} resolution can be estimated as following:

$$\sigma_{NL1} = (A^T \times W \times A)_{33}^{-\frac{1}{2}} \approx 10.45 \ cycles \text{ ……..(5.18)}$$

where, $\sigma_{\phi L1}$ is the sigma of L1 phase noise; $A = \begin{bmatrix} 1 & 1 & 0 \\ 1 & -\frac{f_{L1}^{\ 2}}{f_{L2}^{\ 2}} & 0 \\ 1 & -1 & 1 \\ 1 & -\frac{f_{L1}^{\ 2}}{f_{L2}^{\ 2}} & \frac{f_{L1}}{f_{L2}} \end{bmatrix}$;

W is the weighting matrix calculated by error model.

The result shows that it is also difficult to estimate the primary signal ambiguity by code measurement in short session because there is noisy in the code measurements.

In the long baseline, not only the ionosphere will be more serious, but also the troposphere and satellite ephemeris error will be larger, the errors will affect the AR performance in the dual

frequencies system.

Because widelane ambiguity can be fixed easily for most time by HMW combinations, it can be treated as known. There are four unknowns in the equation (5.16). The troposphere can almost be estimated by troposphere model, so the ionosphere error will be the most influence in AR performance. To resolve equation (5.16), the following method may be considered:

(1) Neglected the ionosphere error in short baseline;

(2) Estimating the ionosphere delay by using the external source (for example as Global Ionosphere Model (GIM) by the Center for Orbit Determination in Europe (CODE) http://www.aiub.unibe.ch/ionosphere/).

(3) Estimating the ionosphere error by the Local TEC maps (for example using the receivers in GEONET (GPS Earth Observation Network) in Japan).

The item (1) is only effective in the short baseline. In item (2), the AR performance is depending on the precise of the extern source. In Item (3) the multiple receivers are needed in the local area to estimate the Local TEC, and are difficult to estimate the real-time ionosphere error.

5.5.2 Short Baseline (Ionosphere Absent)

The case of short baseline is discussed. Ionosphere, troposphere, and satellite ephemeris error can be neglected. The residual error is only multipath error, and the carrier phase observation noise in the widelane signal and in the primary signal. Multipath is receiver-satellite geometry dependent, and the causes of multipath tend to be horizontal, vertical, or oblique planes/objects (such as metallic fences, buildings, chimneys, superstructure, water surfaces, etc.). In a “clean” environment, multipath error is about 0.5cm-1.0cm in the carrier phase measurement [Pratap Misra, Per Enge, 2001]. Here, the multipath error will be neglected in our discussing. The AR in short baseline can be rewritten as following:

$$\begin{bmatrix} 1 & 1 \\ 1 & \frac{f_{L1}}{f_{L2}} \end{bmatrix} \begin{bmatrix} r \\ \lambda_{L1} N_{L1} \end{bmatrix} = \begin{bmatrix} \Phi_{L1} - \varepsilon_{\Phi L1} \\ \Phi_{L2} + \lambda_{L2} N_{wL1L2} - \varepsilon_{\Phi L2} \end{bmatrix} \quad \text{.....(5.19)}$$

There are only two unknowns in equation (5.19), so ambiguity can be estimated. The standard error of the estimated primary ambiguity N_{L1} in short baseline can be calculated as following:

$$\sigma_{NL1} = \sigma_{\phi L1} \times (A^T \times W \times A)_{22}^{-\frac{1}{2}} \approx 0.106\, cycles \quad \text{.....(5.20)}$$

where, $A = \begin{bmatrix} 1 & 1 \\ 1 & \frac{f_{L1}}{f_{L2}} \end{bmatrix}$; W is the weighting matrix calculated by error model.

Using the equation (4.19) introduced in the last chapter, the standard error of estimated widelane signal ambiguity can be calculated as: $\sigma_{N(wL1L2)} = 0.2761\, cycles$

Now we can see that in the short baseline, by using widelane method, the primary signal ambiguity can be estimated faster in short session. However, it can also be difficult to estimate in long baseline.

5.6 AR IN TRIPLE FREQUENCIES

Similar to the case of the dual frequencies, we only consider the carrier phase measurements in the triple frequencies system, and ambiguity of the widelane signals will be estimated by HMW combination at the first. The carrier phase observations in triple frequencies will be shown as following:

$$\Phi_{L1} = r - I_{L1} + Trop + \lambda_{L1} N_{L1} + \varepsilon_{L1\Phi}$$

$$\Phi_{L2} = r - \frac{f_{L1}^{\ 2}}{f_{L2}^{\ 2}} I_{L1} + Trop + \lambda_{L2} N_{L2} + \varepsilon_{L2\Phi}$$

$$\Phi_{L5} = r - \frac{f_{L1}^{\ 2}}{f_{L5}^{\ 2}} I_{L1} + Trop + \lambda_{L5} N_{L5} + \varepsilon_{L5\Phi} \quad \text{……m……..(5.21)}$$

The widelane signals are shown as following:

$$\Phi_{w12} = r + \frac{f_{L1}^{\ 2}}{f_{L1} f_{L2}} I_{L1} + Trop + \lambda_{wL1L2} N_{wL1L2} + \varepsilon_{wL1L2\Phi}$$

$$\Phi_{w15} = r + \frac{f_{L1}^{\ 2}}{f_{L1} f_{L5}} I_{L1} + Trop + \lambda_{wL1L5} N_{wL1L5} + \varepsilon_{wL1L5\Phi}$$

$$\Phi_{w25} = r + \frac{f_{L1}^{\ 2}}{f_{L2} f_{L5}} I_{L1} + Trop + \lambda_{wL2L5} N_{wL2L5} + \varepsilon_{wL2L5\Phi} \quad \text{…….m…….(5.22)}$$

Signal	Frequency (MHz)	Wavelength (m)	Ionosphere Error Relative to L1 (m)	Carrier Noise (m)
L1	1575.42	0.1903	1.0	0.00266
L2	1227.60	0.2442	1.6469	0.00440
L5	1176.45	0.2548	1.7932	0.00230
widelane (L1-L2)	347.82	0.8619	-1.2833	0.0197
widelane (L1-L5)	398.97	0.7514	-1.3391	0.0125
widelane (L2-L5)	51.15	5.8610	-1.7185	0.118

Table 5.4: The Characters in primary signals and combination signals in triple frequencies

Table 5.4 lists the most significant signal and signal-combination characteristics, which are of interest. The results of the last item in Table 5.4 are assumed that carrier noise is estimated as values of PLL (Phase Lock Loop) tracking noise from Table 5.3. Because multipath error is present, so the results in the fact should be larger than the numbers of the last item in Table 5.4. From table 5.4, we can see that extra-widelane has the longest wavelength, but is the noisiest.

5.6.1 Short Baseline (Ionosphere Absent)

In reasonable short baseline, the ionosphere, troposphere and satellite ephemeris error can be neglected. The multipath error is also neglected here.

The first method is to use the low-noise L5 code in the AR processing.

The widelane (L1-L5) signal ambiguity will be calculated, instead of the ambiguity of the widelane (L1-L2) signal.

The matrix is shown as:

$$\begin{bmatrix} 1 & 1 \\ 1 & \frac{f_{L1}}{f_{L5}} \end{bmatrix} \begin{bmatrix} r \\ \lambda_{L1} N_{L1} \end{bmatrix} = \begin{bmatrix} \Phi_{L1} - \varepsilon_{\Phi L1} \\ \Phi_{L5} + \lambda_{L5} N_{wL1L5} - \varepsilon_{\Phi L5} \end{bmatrix}, \text{.....m.....} \quad (5.23)$$

where $\hat{N}_{wL1L5} \equiv \hat{N}_1 - \hat{N}_5 = (\frac{\Phi_{L1}}{\lambda_{L1}} - \frac{\Phi_{L5}}{\lambda_{L5}} - \frac{f_{L1} - f_{L5}}{f_{L1} + f_{L5}} (\frac{\rho_{L1}}{\lambda_{L1}} + \frac{\rho_{L5}}{\lambda_{L5}}))_{round} (cycles)$

The standard error of the estimated primary ambiguity N_{L1} here can be calculated as following:

$$\sigma_{NL1} = \sigma_{\phi L1} \times (A^T \times W \times A)_{22}^{-\frac{1}{2}} \approx 0.055\, cycles, \text{.....} \quad (5.24)$$

where, $A = \begin{bmatrix} 1 & 1 \\ 1 & \frac{f_{L1}}{f_{L5}} \end{bmatrix}$

Using the acknowledge introduced in the last chapter, the standard error of estimated widelane signal (L1-L5) ambiguity can be calculated as: $\sigma_{N(wL1L5)} = 0.232\, cycles$

The result shows that σ_{NL1} estimated by widelane L1-L5 is smaller than estimated by widelane signal L1-L2. It is because that the code noise in L5 code is smaller than in the L2 code measurement. In the other hand, the N_{wL1L5} will be fixed more accurately than N_{wL1L2} by HMW combinations.

In this method, the AR of widelane (L1-L5) signal will be affected by the noise in the L1 and L5 code measurements. AR of the primary signal will be affected by the carrier noise in the widelane (L1-L2) signal.

If we do not consider the effect of the low-noise in the L5 signal, the second method is to propose the widelane (L2-L5) signal in the AR performance. It includes three steps:

(1) Estimating the ambiguity of the widelane (L2-L5) signal by HMW combination.

$$\hat{N}_{wL2L5} \equiv (N_2 - N_5)_{round} = (\frac{\Phi_{L2}}{\lambda_{L2}} - \frac{\Phi_{L5}}{\lambda_{L5}} - \frac{f_{L2} - f_{L5}}{f_{L2} + f_{L5}} (\frac{\rho_{L2}}{\lambda_{L2}} + \frac{\rho_{L5}}{\lambda_{L5}}))_{round} \text{.....(cycles).....} \quad (5.25)$$

Because the widelane (L2-L5) (also be called extra-widelane) has longer wavelength than the other signals (seeing Table 5.1), N_{wL2L5} can be fixed easily and feasibly.

As same as estimating $\sigma_{N_{wL2L5}}$ and $\sigma_{N_{wL2L5}}$, the standard error of estimated N_{wL2L5} can be calculated as: $\sigma_{N(wL2L5)} = 0.0391\, cycles$

(2) Estimating the ambiguity of the widelane (L1-L2) by Geometry-Free combination;

$$\begin{aligned} \Phi_{GL1L2-L2L5} &= \Phi_{wL1L2} - \Phi_{wL25} \\ &= \left(\frac{f_{L1}^{\ 2}}{f_{L1} f_{L2}} - \frac{f_{L1}^{\ 2}}{f_{L2L5}^{\ 2}} \right) I_{L1} + (\lambda_{wL1L2} N_{wL1L2} - \lambda_{wL2L5} N_{wL2L5}) + \varepsilon_{GL1L2-L2L5} \end{aligned} \quad (5.26)$$

where f_{wL1L2} and f_{wL1L5} can be calculated by equation (4.42) in the last chapter, N_{wL2L5} is as known by estimated in the first step, and I_{L1} will be neglected in the short baseline, so N_{wL1L2} will be estimated

Standard error of the estimated N_{wL1L2} can be calculated as: $\sigma_{N(wL1L2)} = 0.1388\, cycles$

(3) Estimating the primary frequency, with estimated ambiguity of widelane (L1-L2) signal in the second step.

$$\begin{bmatrix} 1 & 1 \\ 1 & \frac{f_{L5}}{f_{L1}} \\ 1 & \frac{f_{L5}}{f_{L2}} \end{bmatrix} \begin{bmatrix} r + Trop \\ \lambda_{L5} N_{L5} \end{bmatrix} = \begin{bmatrix} \Phi_{L5} - \varepsilon_{\Phi L5} \\ \Phi_{L1} - \lambda_1 N_{w15} - \varepsilon_{\Phi L1} \\ \Phi_{L2} - \lambda_2 N_{w25} - \varepsilon_{\Phi L2} \end{bmatrix} \text{……..……..(5.27)}$$

$$\sigma_{NL5} = \sigma_{\phi L5} \times (A^T \times W \times A)_{22}^{-\frac{1}{2}} \approx 0.0695\, cycles \text{ ……..……(5.28)}$$

The results show that both two methods can estimate the primary ambiguity in short session, especially in single epoch.

5.6.2 Long Baseline (Ionosphere Present)

The ionosphere, troposphere and satellite ephemeris error will be serious in the long baseline, they cannot be neglected. In the long baseline, the standard deviations of the DD ionosphere and troposphere errors are assumed as: $\sigma_{I_{L1}} = 0.4\, m \quad \sigma_{Trop} = 0.1 m$.

In Dual Frequencies:

Standard error of AR can be calculated as $\sigma_{NL1} = 3.68\, cycles$

In Triple Frequencies:

In the widelaneL1L5 method, standard error of AR can be calculated as $\sigma_{NL1} = 3.23\, cycles$.

In the extra-widelane method, standard error of AR can be calculated as $\sigma_{NL1} = 3.25\, cycles$

We can conclude that AR of primary signal in triple frequencies on long baseline is affected by baseline influence (including DD ionopshere and troposphere error, and so on), and cannot be determined in short session similar to dual frequencies.

5.6.3 Improved Medium Baseline

Now the case of middle baseline is discussed. In the middle baseline, the standard deviations of the DD ionosphere and troposphere errors are assumed as: $\sigma_{I_{L1}} = 0.02\, m \quad \sigma_{Trop} = 0.01 m$.

In Dual Frequencies:

Standard error of AR can be calculated as $\sigma_{NL1} = 0.2674\, cycles$

In Triple Frequencies:

In the wideline L1L5 method, standard error of the AR can be calculated as $\sigma_{NL1} = 0.2606\, cycles$.

In the extra-widelane L2L5 method, standard error of AR can be calculated as $\sigma_{NL1} = 0.1801\, cycles$

We can see the standard errors of estimated primary ambiguity by both two methods in triple frequencies are smaller than in the dual frequencies.

5.6.4 Geometry –Free Method

Under the case of the long baseline, one more method is proposed. The observation matrix of the triple carrier observations is shown as following:

$$\begin{bmatrix} 1 & -\frac{f_{L1}^2}{f_{L5}^2} & 1 \\ 1 & -1 & \frac{f_{L5}}{f_{L1}} \\ 1 & -\frac{f_{L1}^2}{f_{L2}^2} & \frac{f_{L5}}{f_{L2}} \end{bmatrix} \begin{bmatrix} r + Trop \\ I_{L1} \\ \lambda_{L5} N_{L5} \end{bmatrix} = \begin{bmatrix} \Phi_{L5} - \varepsilon_{\Phi L5} \\ \Phi_{L1} - \lambda_1 N_{w15} - \varepsilon_{\Phi L1} \\ \Phi_{L2} - \lambda_2 N_{w25} - \varepsilon_{\Phi L2} \end{bmatrix} \quad \text{.....(5.29)}$$

The standard error of the estimated primary ambiguity N_{L1} here can be calculated as following:

$$\sigma_{NL5} = \sigma_{\phi L5} \times (A^T \times W \times A)_{33}^{-\frac{1}{2}} \approx 3.44\, cycles \quad \text{.....(5.30)}$$

where $A = \begin{bmatrix} 1 & -\frac{f_{L1}^2}{f_{L5}^2} & 1 \\ 1 & -1 & \frac{f_{L5}}{f_{L1}} \\ 1 & -\frac{f_{L1}^2}{f_{L2}^2} & \frac{f_{L5}}{f_{L2}} \end{bmatrix}$; $\sigma_{\phi L5} = 0.009\, cycles$

This method is also called Geometry-Free method. Because in this method, there are two different Geometry-Free combinations in the carrier phase measurements. It is the most difference from the dual frequencies because there is only one Geometry-free combination in the carrier phase measurements.

$$\begin{aligned} \Phi_{GL5-L2L5} &= \Phi_{L5} - \Phi_{wL25} \\ &= \left(-\frac{{f_{L1}}^2}{{f_{L5}}^2} - \frac{{f_{L1}}^2}{f_{L2} f_{L5}} \right) I_{L1} + (\lambda_{L5} N_{L5} - \lambda_{wL2L5} N_{wL2L5}) + \varepsilon_{GL5-L2L5} \\ &= -\frac{f_1}{f_5} \left(\frac{f_1}{f_5} + \frac{f_1}{f_2} \right) I_{L1} + \lambda_{L5} N_{L5} - \lambda_{wL2L5} N_{wL2L5} + \varepsilon_{GL5-L2L5} \end{aligned} \quad \text{.....m.....(5.31)}$$

$$\begin{aligned} \Phi_{GL5-L1L5} &= \Phi_{L5} - \Phi_{wL15} \\ &= \left(-\frac{{f_{L1}}^2}{{f_{L5}}^2} - \frac{{f_{L1}}^2}{f_{L1} f_{L5}} \right) I_{L1} + (\lambda_{L5} N_{L5} - \lambda_{wL1L5} N_{wL1L5}) + \varepsilon_{GL5-L1L5} \\ &= -\frac{f_1}{f_5} \left(\frac{f_1}{f_5} + 1 \right) I_{L1} + \lambda_{L5} N_{L5} - \lambda_{wL1L5} N_{wL1L5} + \varepsilon_{GL5-L1L5} \end{aligned} \quad \text{.....m.....(5.32)}$$

The advantage of Geometry-Free method is that ambiguity resolution is not affected by the ionosphere influence. In this method, the troposphere and satellite ephemeris error will be canceled in Geometry-Free combinations; the ionosphere error will be canceled in combinations between equations (5.31) and (5.32), However, the problem is the amplified carrier noise in the carrier phase combinations, especially in the extra-widelane (L2-L5) signal. They will be influenced in the AR performance. By time average processing for long sessions or other methods, the carrier noise will be reduced, and AR will be improved. After

combining (5.31) and (5.32), the time average of L5 signal ambiguity can be given as:

$$N_{L5} = time\ average\left\{1\Big/\left[\lambda_5\left(-\frac{f_1}{f_5}\right)\right]\cdot\left[\left(\frac{f_1}{f_2}+\frac{f_1}{f_5}\right)\left(\Phi_{L5}(t)-\Phi_{wL2L5}(t)+\lambda_{wL2L5}N_{wL2L5}\right)\right.\right.$$

$$\left.\left.-\left(1+\frac{f_1}{f_5}\right)\left(\Phi_{L5}(t)-\Phi_{wL1L5}(t)+\lambda_{wL1L5}N_{wL1L5}\right)\right]\right\}\quad (cycles) \quad (5.33)$$

5.7 COMPARISON AR METHODS IN DUAL & TRIPLE FREQUENCIES

5.7.1 Comparing Short Baseline AR in Dual and Triple frequencies

Short baseline AR methods in the dual and triple frequencies are described as Table 5.5. In triple frequencies, extra-widelane method and widelane (L1L5) method are proposed under the case of short baseline (or medium baseline).

The most errors that affect the AR performance in various steps will be shown as Table 5.6, the multipath error is neglected here.

	Dual frequencies	Triple frequencies	
		WidelaneL1L5 method	Extra-widelane method
First Step	N_{wL1L2} estimated by HMW combination	N_{wL1L5} estimated by HMW combination	N_{wL2L5} estimated by HMW combination
Second Step	N_{L1} estimated by signal L1 & widelane(L1-L2)	N_{L1} estimated by signal L1 & widelane(L1-L5)	N_{wL1L2} estimated by widelane(L1-L5)&(L2-L5)
Third Step			N_{L1} estimated by signal L1 & widelane(L1-L2)

Table 5.5: Short Baseline AR Methods in Dual and Triple frequencies System

	Dual frequencies	Triple frequencies	
		WidelaneL1L5 method	Extra-widelane method
First Step	code noise in signal L1&L2	code noise in signal L1 & L5	code noise in signal L2 & L5
Second Step	carrier noise in signal widelane (L1-L2)	carrier noise in signal widelane(L1-L5)	carrier noise in widelane(L1-L2)&(L2-L5)
Third Step			carrier noise in widelane (L1-L2)

Table 5.6: Errors in Short Baseline AR Methods in Dual and Triple frequencies

From Table 5.6, two methods in triple frequencies can both improve the AR performance. The first method is using the low-noise L5 signal instead of L2 signal in the first step, N_{wL1L5} will be estimated more accurate

than N_{wL1L2}. In the second method, long wavelength widelane (L2-L5) is using to estimate N_{wL1L2}, so N_{wL1L2} will not be affected by the code noise in primary signals, it is more useful in the case of the large signal code noise.

5.7.2 Comparing Long Baseline AR in Dual and Triple frequencies

Long baseline AR methods in the dual and triple frequencies are described as Table 5.7. In triple frequencies, extra-widelane method and geometry-free method are proposed, and the most errors that affect the long baseline AR performance in various steps will be shown as Table 5.8, the multipath error is neglected here.

	Dual frequencies	Triple frequencies	
		Extra-widelane method	Geometry-free method
First Step	N_{wL1L2} estimated by HMW combination	N_{wL2L5} estimated by HMW combination	N_{wL2L5} & N_{wL1L5} estimated by HMW combinations
Second Step	N_{L1} estimated by signal L1 & widelane(L1-L2)	N_{wL1L2} estimated by widelane(L1-L5)&(L2-L5)	N_{L5} estimated by two Geometry-Free combination
Third Step		N_{L1} estimated by signal L1 & widelane(L1-L2)	

Table 5.7: Long Baseline AR Methods in Dual and Triple frequencies System

	Dual frequencies	Triple frequencies	
		Extra-widelane method	Geometry-free method
First Step	code noise in signal L1&L2	code noise in signal L2 & L5	code noise in signal L1& L2&L5
Second Step	carrier noise in signal widelane(L1-L2) ionosphere error	carrier noise in signal widelane(L1-L5)&(L2-L5) ionosphere error	carrier noise in two Geometry-Free combination signals
Third Step		carrier noise in signal L1 & widelane(L1-L2) ionosphere error	

Table 5.8: Errors in Long Baseline AR Methods in Dual and Triple frequencies

SUMMARY

In this chapter, the ambiguity resolution was discussed in dual and triple frequencies. Using the error model listed in table 5.2, the standard deviation of primary signal ambiguity estimation was calculated as Table 5.9. From the table 5.9, we can see that in the short baseline, the ambiguity resolution in triple frequencies clearly

prevails over present dual frequencies GPS operation. In short baseline, the standard error is only 0.055 cycles, it means that in triple frequencies, the primary ambiguity can be estimated especially in single epoch. Also in middle baseline, the standard error is 0.1801 cycles. But in long baseline, it was difficult to estimate the primary ambiguity in triple frequencies, too. And in the geometry-free method, the amplified widelane signal noise will affect ambiguity resolution, but AR is not influenced by baseline influence in this method. So it is proposed to use in long and extra-long baseline for long session observation, for example long baseline static positioning. In the next chapter, in order to estimate the ASR in the triple frequencies, the triple signal simulation will be discussed.

Sigma of primary ambiguity resolution (N_{L1} or N_{L5}) (cycles)			
	Dual frequencies (L1 L2)	Triple frequencies (L1 L2 L5)	Geometry-Free method
Short baseline $\sigma_I = 0 \quad \sigma_T = 0$	0.106	0.055	
Middle baseline $\sigma_I = 0.02 \quad \sigma_T = 0.01$	0.2674	0.1801	
Long baseline $\sigma_I = 0.4 \quad \sigma_T = 0.1$	3.68	3.23	3.44

Table 5.9: Comparison of the standard error of primary ambiguity between dual and triple frequencies

CHAPTER 6
TRIPLE FREQUENCIES SIMULATION

Prior to testing the impact of the GPS modernization on ambiguity resolution performance, three-frequency GPS data are required. However, as GPS modernized and new signals are not yet available, a GNSS data simulation has developed to generate the triple signal for this investigation. The simulation will generate signal data with biases and error models such as ionosphere effect, multipath error, and so on. In this simulation, the satellite and clock biases will not be generated because they need not be considered in DD measurements. The triple frequencies simulation is introduced in figure 6.1.

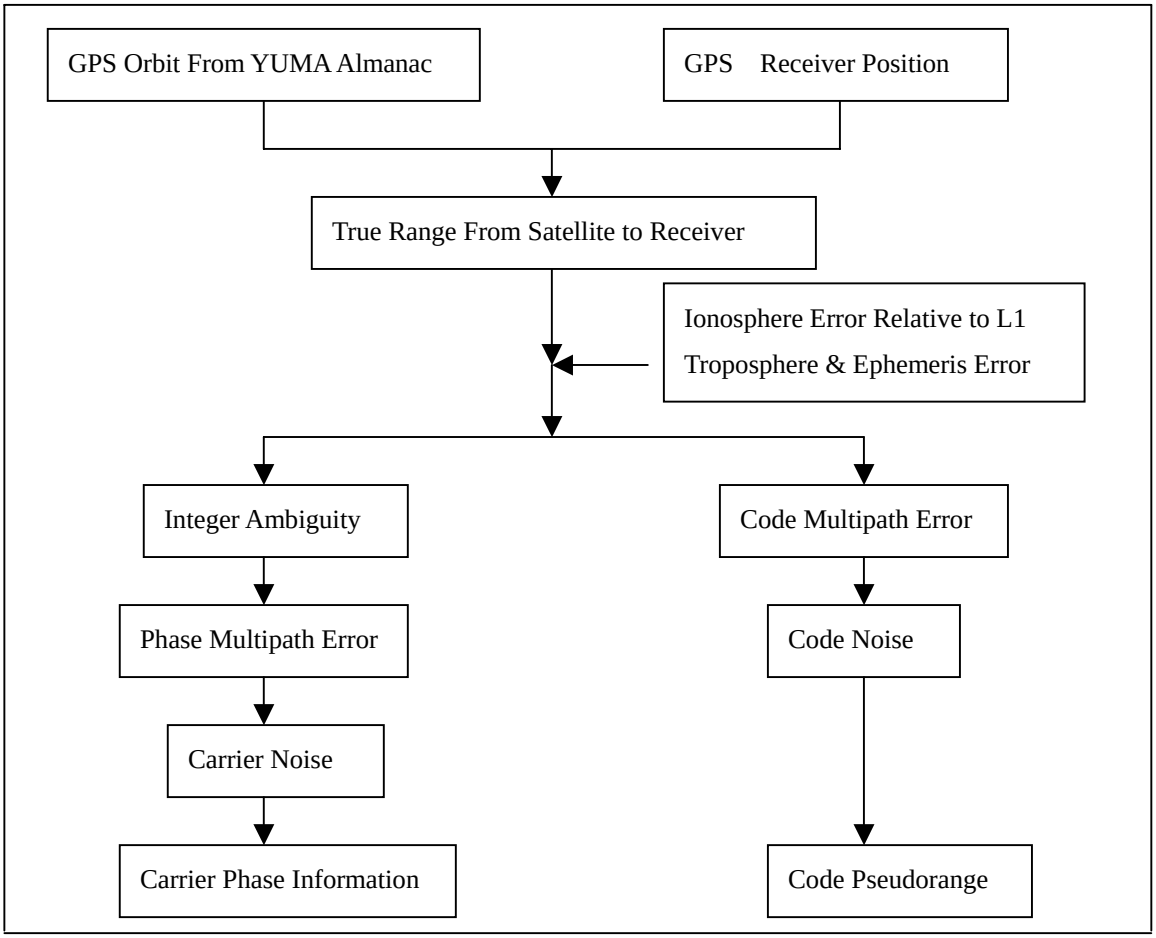

Figure 6.1: Triple frequencies data simulation

6.1 RECEIVER NOISE IN SIMULATION

From the discussion in the last chapter, the receiver noise (including carrier noise and code noise) will be the most influence in the short baseline AR performance, if multipath is neglected.

Code and carrier measurements are affected by random measurements, called receiver noise, which is broad term covering the RF radiation sensed by the antenna in the band of interest unrelated to the signal to the signal; noise introduced by the antenna, amplifiers, cables, and the receiver; multi-access noise; and signal quantizaiton noise. [Pratap Misra, Per Enge, 2001]

6.1.1 Estimating Receiver Noise in Zero-Baseline DD Measurement

In order to estimate the code noise in the receiver, the zero-baseline experiments was done. Two same type receivers were connected to one antenna (see Figure 6.2), hence, the carrier phase DD measurements were done.

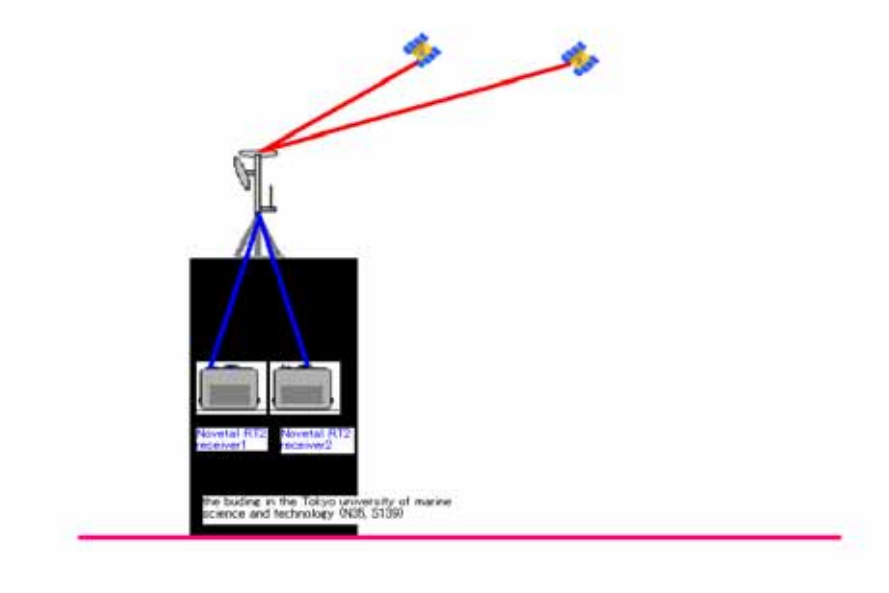

Figure 6.2: Zero baseline experiment

Forming zero baseline double differences (DD's) removes common errors such as satellite clock error, satellite ephemeris error, ionosphere error, troposphere error, receiver multipath error and receiver clock error. Remaining errors are the DD receiver noise, and, in case of the carrier phase, the DD cycle ambiguity. However, the noise level on a DD is higher than the noise level on an undifferenced observation (one pair of receiver and satellite).

If one assumes that the noise between satellites and between receivers is uncorrelated and Gaussian (a reasonable assumption), the noise of a Double Differenced (DD) observation of two high satellites can be determined with the propagation law: $S_{DD} = \sqrt{S^2 + S^2 + S^2 + S^2} = 2 \times S$ or: $S = \frac{S_{DD}}{2}$ Here, the S_{DD} is the DD receiver noise; S is the undifferenced observation noise.

Figure 6.3(1) shows the DD code noise and carrier noise figure 6.3(2) measured by zero-baseline DD measurements by two NOVATEL OEM3 receivers on the roof of the library in the Tokyo University of marine science and technology. Figure 6.4(1) shows the DD code and carrier noise figure 6.4(2) measured by two NOVATEL OEM4 receivers. The yellow line indicates the elevation angle of the satellite. From two figures, we can see the SV elevation is the function of the observation noise. With lowing the elevation angle, the observation noise will be larger. In additional, that both of code and phase noises in L1 signal are smaller than in L2 signal can be seen, especially in case of the NOVATEL OEM3 receiver. The reason is that the minimum power of the near-ground user-receiver L1 and L2 signal is as the function of SV elevation angle [ICD-GPS-200C], and the power level of L1 signal (157.5dBW) is higher than L2 signal (160dbW). (See Table 5.1)

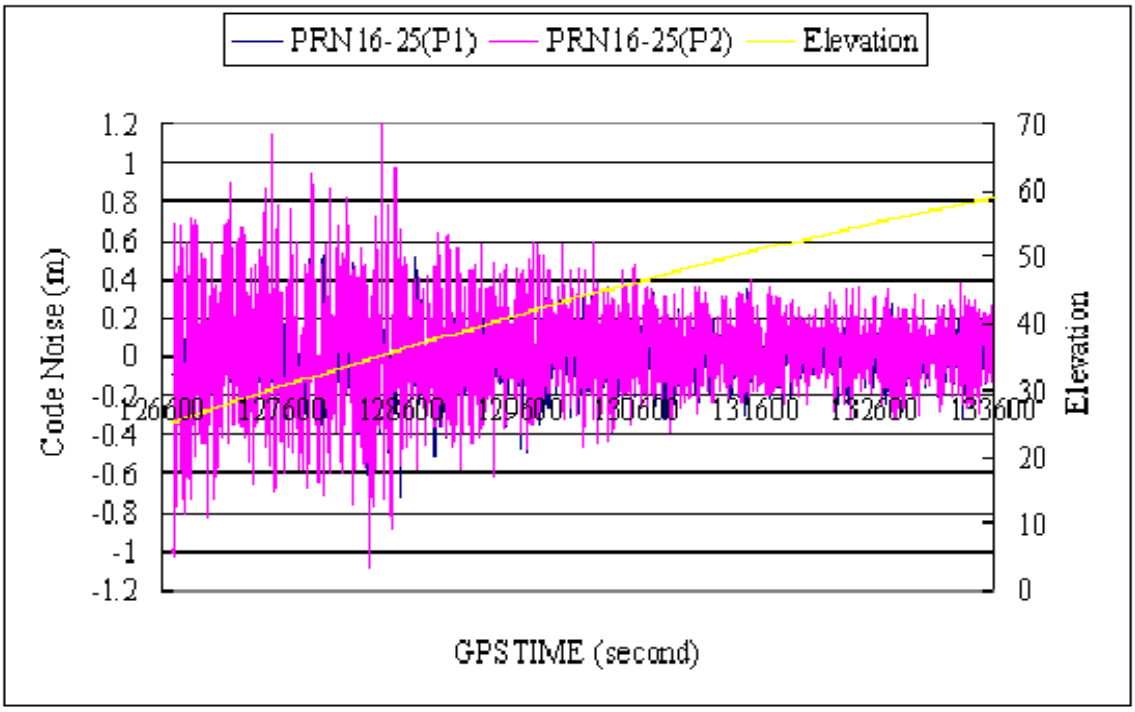

Figure 6.3(1): DD code observation noise of PRN16-25 measured by zero-baseline DD measurements by NOVATEL OEM3 receivers

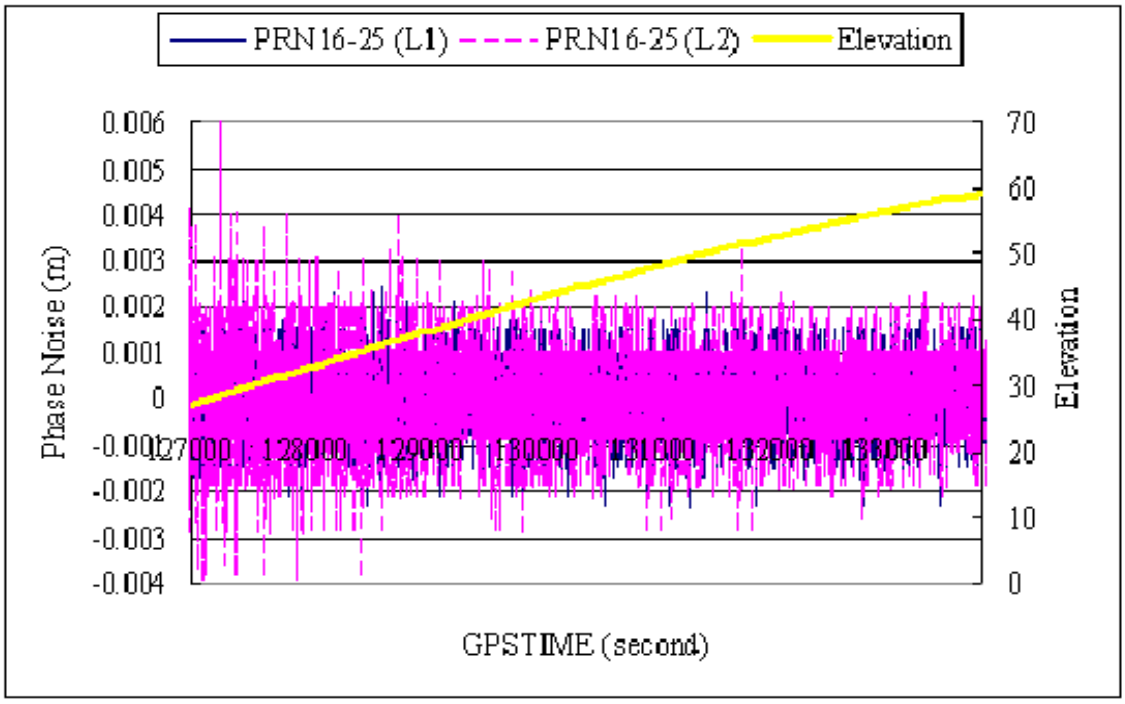

Figure 6.3(2): DD phase observation noise of PRN16-25 measured by zero-baseline DD measurements by NOVATEL OEM3 receivers

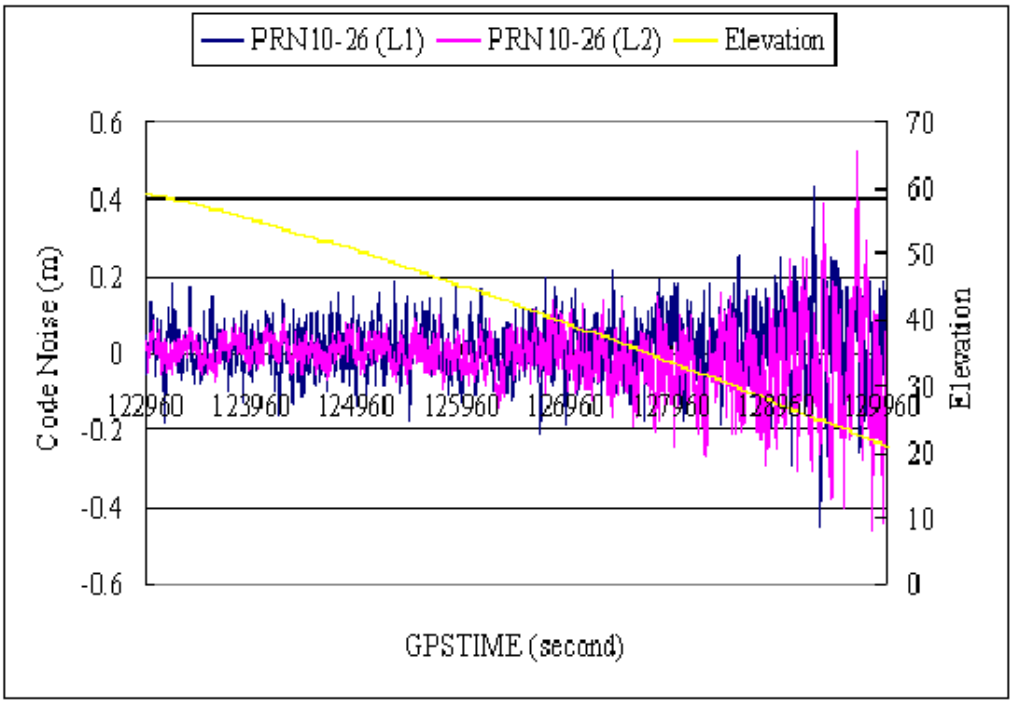

Figure 6.4(1): DD code observation noise of PRN10-26 measured by zero-baseline DD measurement by NOVATEL OEM4 receivers

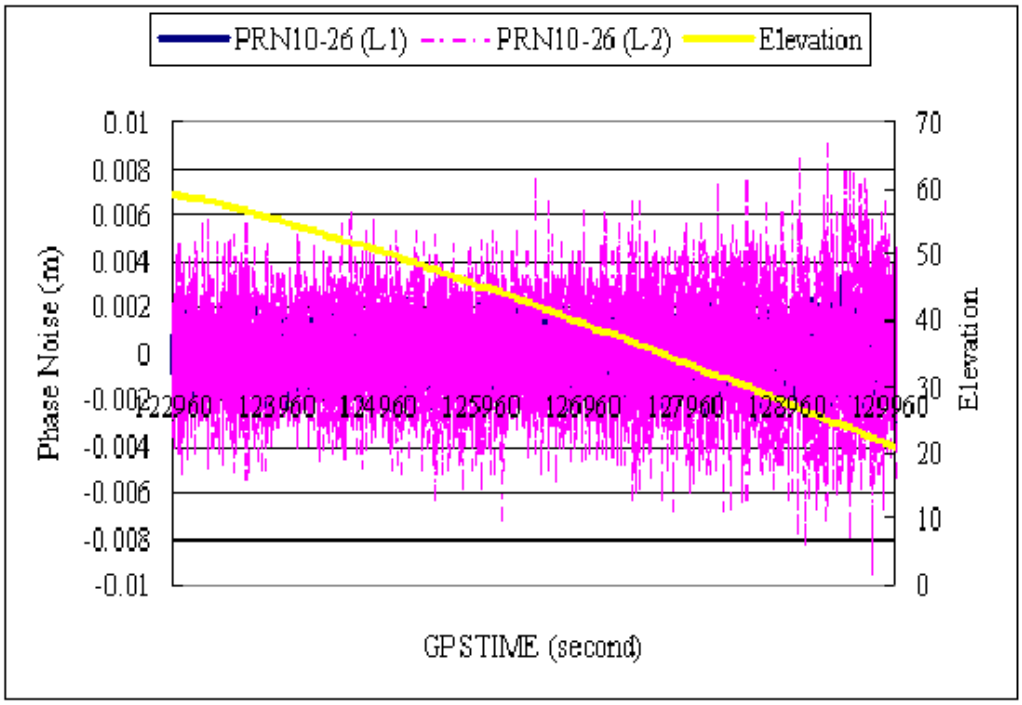

Figure 6.4(2): DD phase observation noise of PRN10-26 measured by zero-baseline DD measurement by NOVATEL OEM4 receivers

6.1.2 Code Tracking Noise

From figure 6.3 and figure 6.4, that the elevation is the function in the observation noise can be known. In the simulation, the code observation noise in L1, L2, and L5 will be generated as narrow correlator DLL (Delay Lock Loop) thermal noise. Recalling equation (5.11), the DLL thermal noise code tracking is shown as following [Kaplan, 1996]:

$$\sigma_{DLL} = \lambda_c \sqrt{\frac{\alpha \times d \times B_{DLL}}{c/n_0}\left[1 + \frac{2}{T_d \times c/n_0}\right]} \text{ ,……m……..……..(6.1)}$$

where, λ_c = GPS propagation constant/PRN code chipping rate (m/sec)/(chip/sec)

= 293.05m/chip for C/A-code

= 29.305 m/chip for P(Y)-code or in L5 frequency signal

α = DLL discriminator correlate factor (dimensionless)

= 1 for time shared tau-dirthered early-late correlator

= 0.5 for dedicated early and late correlator

d = correlator spacing between early, prompt, and late (dimensionless)

B_{DLL} = code loop noise bandwidth (Hz)

c/n_0 = carrier to noise power expressed in dB-Hz

T_d = predetection integration time (sec), it is permitted to increase beyond the 20-msec limitation imposed by the 50-Hz navigation data

As seen in equation (6.1), the DLL jetter is directly proportional to the square root of the filter noise bandwidth (lower B_n results in a lower jetter which, in turn, results in a low c/n_0 threshold). The thermal noise is ten times larger for the C/A code than P(Y) code because the chip wavelength of the C/A code is tem times longer than P(Y) code.

6.1.3 Phase Tracking Noise

Similar to code noise generation, the phase observation noise in L1, L2 and L5 signals will be generated as PLL (Phase Lock Loop) thermal noise. Recalling the equation (5.12), it is given as following:

$$\sigma_{PLL} = \frac{\lambda_L}{2\pi} \sqrt{\frac{B_L}{c/n_0}\left(1 + \frac{1}{2 \times T_d \times c/n_0}\right)} \text{ ,……m……..(6.2)}$$

where, λ_L = GPS propagation constant/L-band carrier frequency (m/sec)/(cycles/sec)

= 0.1903 m/cycles for L1, or = 0.224m/cycle for L2, or =0.2548m/cycle

B_L = carrier loop noise bandwidth

c/n_0 = carrier to noise power expressed as a ratio

T_d = predetection integration time (second).

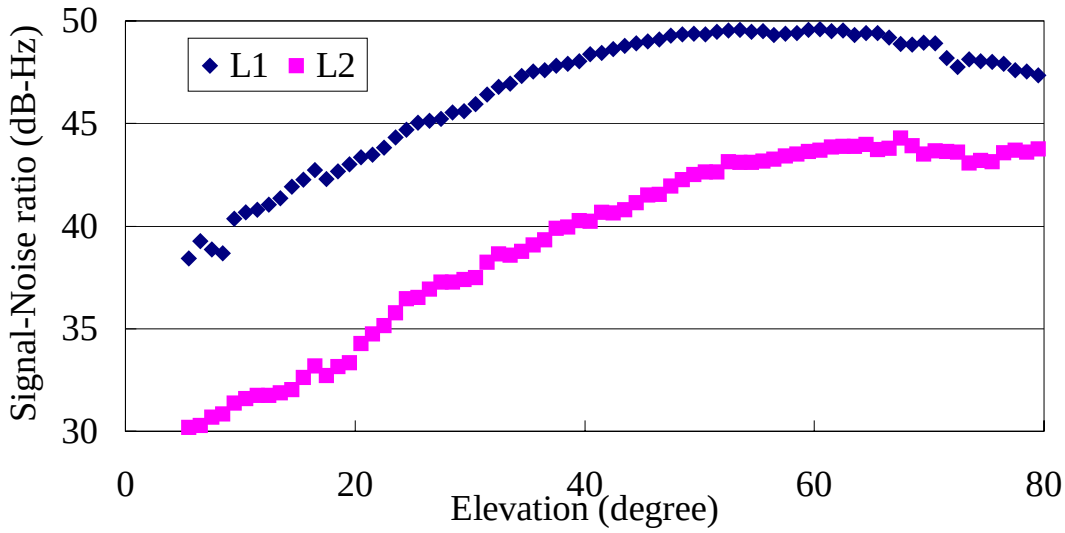

Figure 6.5: c/n_0 results estimated by the NOVETAL 702 antenna and NOVETAL OEM3 receiver

From the equations (6.1) and (6.2), in both of the code noise and phase noise simulation, c/n_0 is necessary to estimate.

6.1.4 Signal-to-Noise Ratio

In order to generate the code and phase noise in the simulation, the signal-noise ratio (c/n_0) of the receiver has to be estimated. The experiments were done to prove that c/n_0 is the function of the elevation of GPS satellites and to determine the value of c/n_0. The experiment was done on the roof of the building in the Tokyo University of marine science and technology. The environment can be seen as "clean". c/n_0 is considered to be only affected with receiver noise. The antenna is NOVATEL 702 choke-ring antenna. The receiver is NOVETAL OEM3 receiver、mask angle is 5-degree. Figure 6.5 shows, the SV elevation is the function of c/n_0, and c/n_0 in L1 signal is higher than in L2. This result is the same as the analysis of the noise in section (6.1.1).

6.2 IONOSPHERE DELAY

The ionosphere is that band of atmosphere extending from about 50 to 1000 kilometers above the earth's surface. In this layer the sun's ultraviolet radiation ionises gas molecules, which then lose an electron. These free electrons in the ionosphere influence the propagation of microwave signals (speed, direction and polarization) as they pass through the layer. The largest effect is on the speed of the signal, and hence the ionosphere primarily affects the measured range.

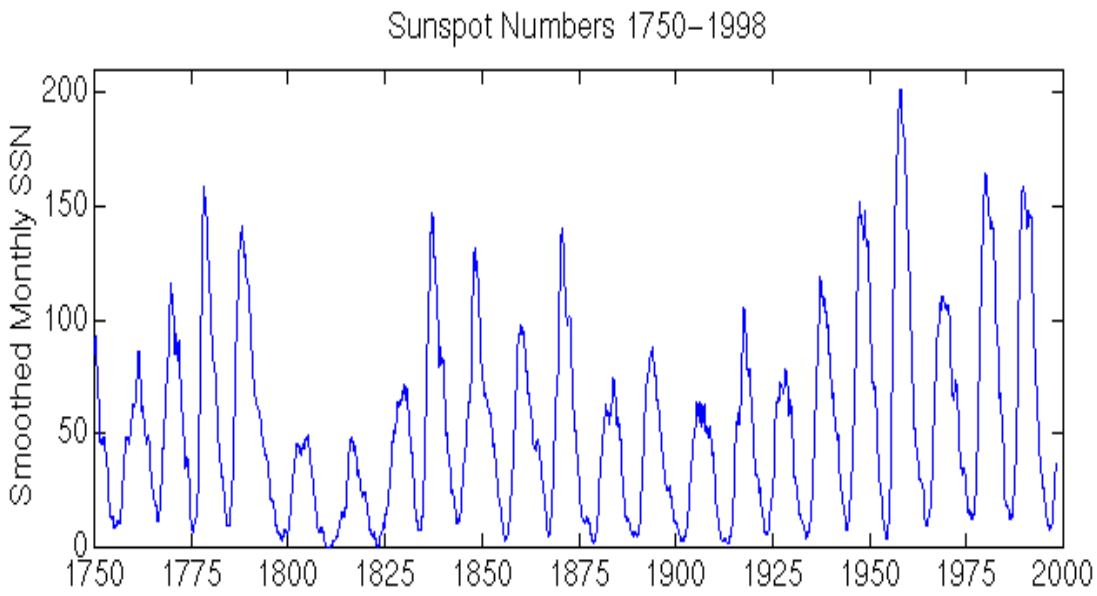

Figure 6.6: Sun spots numbers and periodic behaviors

(From: http://www.oulu.fi/~spaceweb/textbook/cycle.html)

6.2.1 Sun Spots

The activity of the ionosphere is strongly affected by the number of the sunspots. The sunspots are dark patches on the Sun and they always seen in pairs or in groups of pairs. Here the magnetic fields, as strong as those of a horseshoe magnet (which is about 1000 times stronger than the Earth's surface magnetic field), keep heat from flowing up to the surface, thus making the sunspots the coolest places on the sun and accounts for its dark appearance. The Sun's differential rotation, faster at lower than higher latitudes, is critical in producing sunspots. Solar flares (enormous explosive releases of energy from the Sun) are most likely to occur in sunspot groups when they are growing rapidly and rotating, much like a hurricane.

The 11-year periodicity in the Sun's activity was first observed in the sunspot number (see the Figure 6.6) [Bugoslavskaya, 1962]. Figure 6.6 shows the sunspot numbers in the history of 1975—1998. Constantly monitoring the development of sunspot groups is one important job of space weather forecast, especially when the ionosphere activities are reaching the maximum in the middle 2000.

6.2.2 Ionospheric Refraction Index

To quantify the propagation effects on a radio wave traveling through the ionosphere, the refractive index of the medium must be specified, the refractive index of the ionosphere, n, has been derived by Appleton and Hartree [Davies, 1989]. Because we are concerned here only with radio-wave propagation at two GPS current frequencies (L1=1575MHz, L2=1227MHz), and one new frequency (L5=1176.45 MHz), the refractive index of the ionosphere at GPS frequencies given by Brunner and Gu [Brunner, 1991], can be expressed as

$$n = 1 - (\frac{X}{2}) \pm (\frac{1}{f^3}) - (\frac{1}{f^4}) \quad \text{.....(6.3)}$$

where f is system operation frequency,

$X = f_n^2 / f^2$, f_n is the ionospheric plasma frequency.

As equation (6.3) illustrates, the terms contributing to the refractive index of the ionosphere are the

free-space velocity, the first-order term (as often used in GPS TEC measurement), the second-order term and the third order term. The refractive index of the first order in the ionosphere is given by the following:

$$n = 1 - (\frac{X}{2}) \quad \text{……..……..(6.4)}$$

By equations (6.3) and (6.4), the high-order terms are much less than 1% of the first-order terms at GPS frequencies, so with better than 0.1% accuracy, even during worst case ionosphere conditions when f_n =25MHz [Hatch, 2000], so the ionospheric refractive index at GPS frequency can be expressed simply as first-order term. Now using Eq.(6.4) the first-order refractive index, the refraction index for a radio wave of frequency is:

$$n \approx 1 - \frac{40.3N}{f^2} \quad \text{……..……..(6.5)}$$

where, N is local ions density, f is system operation frequency.

The ionosphere is an important source of range and range-rate errors for GPS users, and the variability of the ionosphere is much larger than troposphere. Fortunately, ionized gas is a *dispersive* medium for radio waves. The refraction index is a function of the operating frequency. The group delay of the ionosphere produces range errors, which can be expressed into the units of distance from satellites to GPS users. The ionospheric group delay is shown as following:

$$\Delta r = \frac{40.3}{f^2}\int Ndl = \frac{40.3}{f^2} TEC \quad \text{……..……..(6.6)}$$

So it can be calculated that TEC (Total Electron Content) is effected range delay into meters at f_{L1} of the GPS: 1TECU=0.163m, and effected on f_{L2} : 1TECU=0.267m. Here a value of TEC equal to $1\times10^{16} electrons/m^2$ is called one TEC unit (TECU).

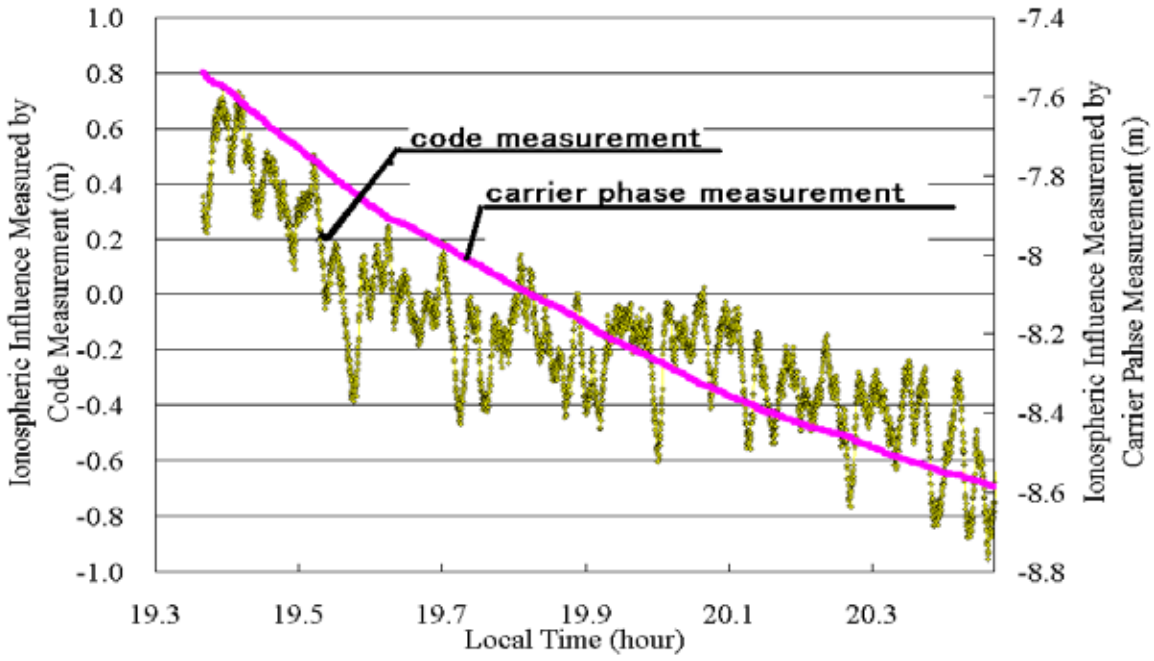

Figure 6.7: Ionospheric influence measured by raw code and carrier phase measurement

6.2.3 Ionosphere Delay

Using the theory of the phase advance and the group delay in the GPS signal, combining code and carrier measurement in two GPS frequencies, we could measure the ionospheric delay. The ionosphere delay measured by code measurement I_ρ and measured by carrier phase measurement I_ϕ can be shown as following:

$$I_\rho = \frac{{f_{L2}}^2}{{f_{L2}}^2 - {f_{L1}}^2}(\rho_{L1} - \rho_{L2})$$
$$I_\phi = \frac{{f_{L2}}^2}{{f_{L2}}^2 - {f_{L1}}^2}(\Phi_{L1} - \Phi_{L2} - \lambda_{L1}N_{L1} - \lambda_{L2}N_{L2}) \quad \text{……..……..(6.7)}$$

Figure 6.7 shows the results of ionospheric influence measured by raw code measurement and carrier phase measurement from dual frequencies GPS receiver. Here it is noted that the different unite of the left and right. It is shown that the code measurement is noisy but absolute, and the carrier is very precise but including the cycle ambiguity would be seen. Using the post-processing methods or real-time carrier smoothing method, the phase-level ionosphere delay can be measured, however, the results are including *IFB* (inter-frequency bias), and the *IFB* can be estimated by SLM (single lay model) assumption and the least squares, the details of the IFB estimation are introduced in the [Zhang, 2003].

The real-time carrier smoothing is used to measure changes in the ionospheric delay correctly and can estimate the ionosphere delay at real-time (*t*). ${I^t}_s$ is determined as following:

$${I^t}_s = {w^t}_m(I_\rho)^t + {w^t}_n({I^{t-1}}_s + ({I_\phi}^t - {I_\phi}^{t-1})) \quad \text{……..……(6.8)}$$

where t is the epoch time, w_m and w_n are the weighting functions, thus $w_m + w_n = 1$,we set ${w^t}_m = {w^{t-1}}_m + 0.001$ and ${I^0}_s = {I^0}_\rho$.

The post-processing measurement is achieved as following:

$${I_{post}}^t = {I_\phi}^t - \frac{1}{K}\sum_{k=0}^{K}({I_\phi}^k - {I_\rho}^k) \quad \text{……..……(6.9)}$$

where t is the epoch time, I_{post} is the result estimated by the post-processed measurement; K is the continuous time for one satellite in visible, we set K=2 hours.

Figure 6.8 shows three GPS ionosphere measurements from a single GPS dual frequencies receiver for one hour: the raw pseudorange difference, carrier-smoothing (step=0.001) and post-processing measurement. From figure 6.8, it could be seen that the carrier ambiguity could be resolved by post-processed measurement and the "phase leveling" result of the past time could be estimated. However, It is impossible that the ionosphere delay is minus in fact, so the results by post-processing measurement were including IFB could be known.

Figure 6.9 shows vertical TECs (VTEC) measured by GPS receiver and from International Reference Ionosphere Model (IRI-95 model) from 00:00 July 7 to 24:00 July 7 2003 for 24 hours. The peak altitude of F2 region in IRI-95 model was chosen. It would be seen that both the GPS and IRI-95 VTECs reach a minimum about 3-4 o'clock, and reach a maximum about 15-16 o'clock in one day.

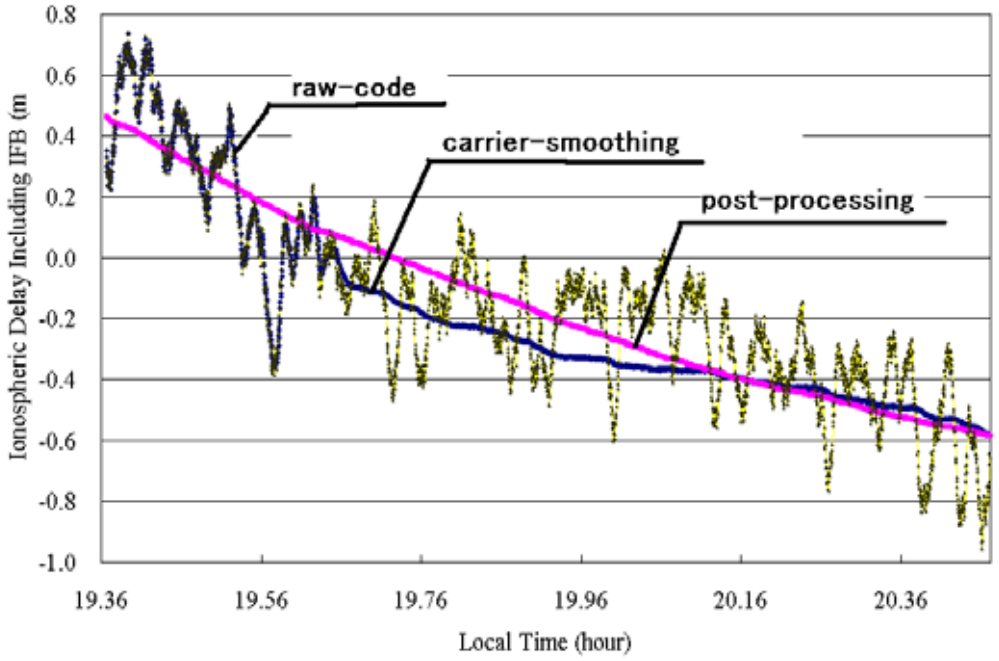

Figure 6.8: Ionosphere delay measured by three GPS ionosphere measurement

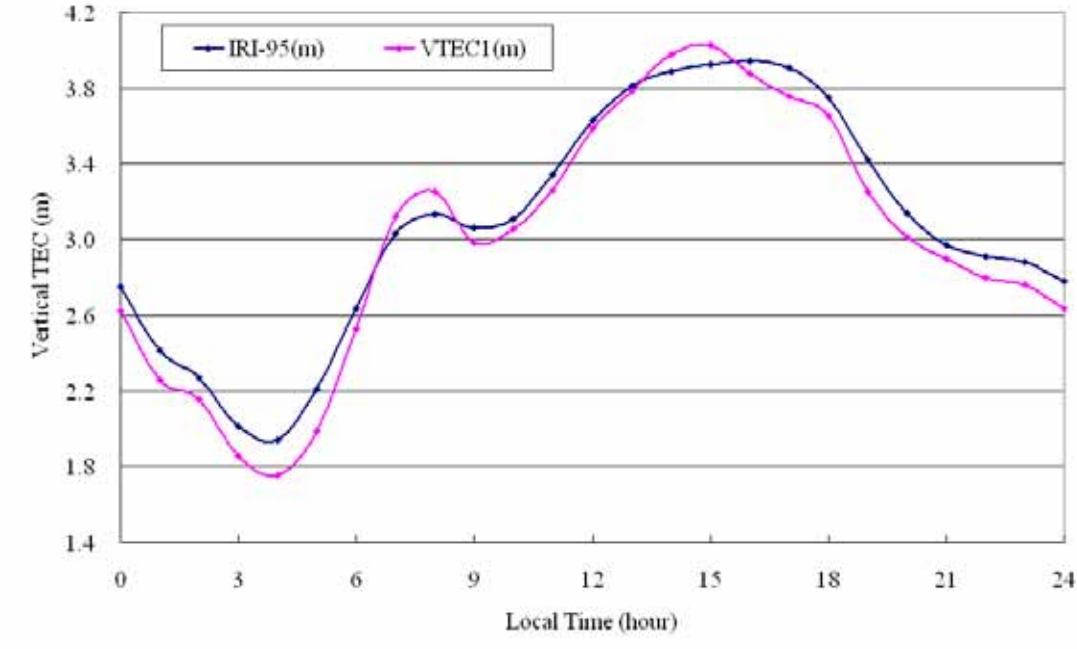

Figure 6.9: Comparison of the local time variations of the one-hour average VTEC measured by GPS receiver and IRI-95 model.

6.2.4 Klobuchar Model

Receiver limits to L1 measurements have recourse to an empirical model whose parameter values are broadcasted by the satellites. This model often referred to as the Klobuchar Model in honor of its developer [Klobuchar, 1996], represents the zenith delay as a constant value at nighttime and a half-cosine function in

daytime. The ionosphere delay time T_{iono} estimate at local time t is given as following (Here Φ_u is approximate geodetic latitude, λ_u is geodetic longitude, E is elevation angle and A is azimuth for every satellites):

1) Calculate the Earth-centered angle, ψ

$$\psi = 0.0137/(E+0.11) - 0.022 \quad \text{(semicircles)} \qquad (6.10.1)$$

2) Compute the subionospheric latitude, Φ_I

$$\Phi_I = \Phi_u + \psi \cos A \quad \text{(semicircles)} \qquad (6.10.2)$$

If $\Phi_I > +0.416$, then $\Phi_I = +0.416$. If $\Phi_I < -0.416$, then $\Phi_I = -0.416$

3) Compute the subionospheric longitude, λ_I

$$\lambda_I = \lambda_u + (\psi \sin a / \cos \Phi_I) \quad \text{(semicircles)} \qquad (6.10.3)$$

4) Find the geomagnetic latitude, Φ_m, of the subionosphere location looking toward each GPS satellite. It is found by

$$\Phi_m = \Phi_I + 0.064 \cos(\lambda_I - 1.617) \quad \text{(semicircles)} \qquad (6.10.4)$$

5) Find the local time, t at the subionosphere point

$$t = 4.32 \times 10^4 \lambda_I + GPS \quad time \quad \text{(seconds)} \qquad (6.10.5)$$

If t>86,400, use t=t-86,400; if t<0, add 86,400.

6) To convert to slant time delay, compute the slant factor F

$$F = 1.0 + 16.0 \times (0.53 - E)^3 \qquad (6.10.6)$$

7) Then compute the ionosphere time delay T_{iono} by first computing x

$$x = \frac{2\pi(t - 50400)}{\sum_{n=0}^{3} \beta_n \Phi_m^n} \qquad (6.10.7)$$

If $|x|>1.57$, $T_{iono} = F \times (5 \times 10^{-9})\,(\sec ond)$ (6.10.8)

Otherwise

$$T_{iono} = F \times [5 \times 10^{-9} + \sum_{n=0}^{3} \alpha_n \Phi_m^n \times (1 - \frac{x^2}{2} + \frac{x^4}{24})]\,(\sec ond)$$

8) Ionosphere delay can be estimated:

$$Iono\_delay = Cs \times T_{iono}\ (meter) \qquad (6.10.9)$$

where, Cs is light velocity

The Klobuchar Model will be used in our triple simulation to generate the ionosphere delay.

Apparent zenith	Station Height above Sea Level							
Angle(Deg)	0km	0.5km	1km	1.5km	2km	3km	4km	5km
	δ_R (m)							
60	0.003	0.003	0.002	0.002	0.002	0.002	0.001	0.001
66	0.006	0.006	0.005	0.005	0.004	0.003	0.003	0.002
70	0.012	0.011	0.010	0.009	0.008	0.006	0.005	0.004
73	0.020	0.018	0.017	0.015	0.013	0.011	0.009	0.007
75	0.031	0.028	0.025	0.023	0.021	0.017	0.014	0.011
76	0.039	0.035	0.032	0.029	0.026	0.021	0.017	0.014
77	0.050	0.045	0.041	0.037	0.033	0.027	0.022	0.018
78	0.065	0.059	0.054	0.049	0.044	0.036	0.030	0.024
78.5	0.075	0.068	0.062	0.056	0.051	0.042	0.034	0.028
79	0.087	0.079	0.072	0.065	0.059	0.049	0.040	0.033
79.5	0.102	0.093	0.085	0.077	0.070	0.058	0.047	0.039
79.75	0.111	0.101	0.092	0.083	0.076	0.063	0.052	0.043
80	0.121	0.110	0.100	0.091	0.083	0.068	0.056	0.047
	B (mb)							
	1.156	1.079	1.006	0.938	0.874	0.757	0.654	0.563

Table 6.1: Correction terms for Saastamoinen's standard model

6.3 TROPOSPHERE DELAY (Saastamoinen Model)

Caused by the signal refraction in the electrically neutral (or non-ionized) atmospheric layer called the troposphere, extending from the earth's surface to about 8km (though approximately twice as thick at the equator). Another component of the neutral atmosphere is the **stratosphere**, extending up to an altitude of about 50km, to the base of the ionospheric layer. For the purposes of discussing neutral atmospheric delay, under the term "tropospheric delay" will be included both the components due to the troposphere and the stratosphere because the troposphere, although being relatively thin, contains most of the mass of the neutral atmosphere and practically all of the water vapor.

The Saastamoinen model was derived using gas laws and simplifying assumptions regarding changes in pressure, temperature, and humidity with altitude. The zenith dry and wet delays $\tilde{T}_Z$ are given as [Saastamoinen, 1973]:

$$\tilde{T}_Z = 0.002277(1+D)\sec\psi_0(P_0 + (\frac{1255}{T_0} + 0.005)e_0 - B\tan^2\psi_0] + \delta_R \text{ ……m……..(6.11)}$$

where, $D = 0.0026\cos 2\phi + 0.00028h$,

(ϕ is the local latitude, and h is the station height in km)

$\psi_0 = 90\deg - E$ (E >=10 degree, satellite elevation angles).

P_0 and e_0 are in millibars, and T_0 is in K.

The correction terms B and δ_R are given in Table 6.1 for various user height *h*.

90% of troposphere delay due to dry atmosphere can be modeled very well, however, 10% due to wet component of atmosphere is difficult to account for. The unmodeled error can reach 2-3m at about 5 deg elevations [Parkinson]. The effect of troposphere delay is minimized due to high correlation over short to medium baselines, however, if the reference station and user are at significantly different altitude (several thousand feet), then variations in the index of refraction could be significant. In these cases, the DGPS users should apply a differential tropospheric model that accounts for the altitude difference.

In our triple frequencies simulation, Saastamoinen model will be used to produce the troposphere delay from a satellite to receiver.

6.4 ANTENNA PHASE CENTER OFFSET

All GPS measurements relate to the distance from the electrical center of the satellite's transmitter to the electrical center of the receiving antenna. Ideally the *physical* center should coincide with the *electrical* center; however there may be a *constant offset*. This is an antenna-manufacturing problem, but if the antenna is always oriented in the same direction, the impact on the groundmark-to-groundmark solution will be a systematic shortening or lengthening of the baseline. Because the electrical center varies with the direction and strength of the incoming signal, a variation in the satellite-receiver geometry will cause the position of the electrical center to also vary. Tests have shown that this effect is comparatively insignificant for micro strip. For high precision applications care has to be taken not to mix antenna types, or to swap antennas between sites and receivers during a survey.

In the simulation, the values of the receiver antenna phase center offset will be given from National Geodetic Survey (NGS) (http://www.ngs.noaa.gov/ANTCAL/index.shtml). The sampling of the antenna phase offset is given as figure 6.10, and the phase center offset of antenna NOVATEL 702 are given in table 6.2. The values from table 6.2 are added in the carrier phase noise from the simulation.

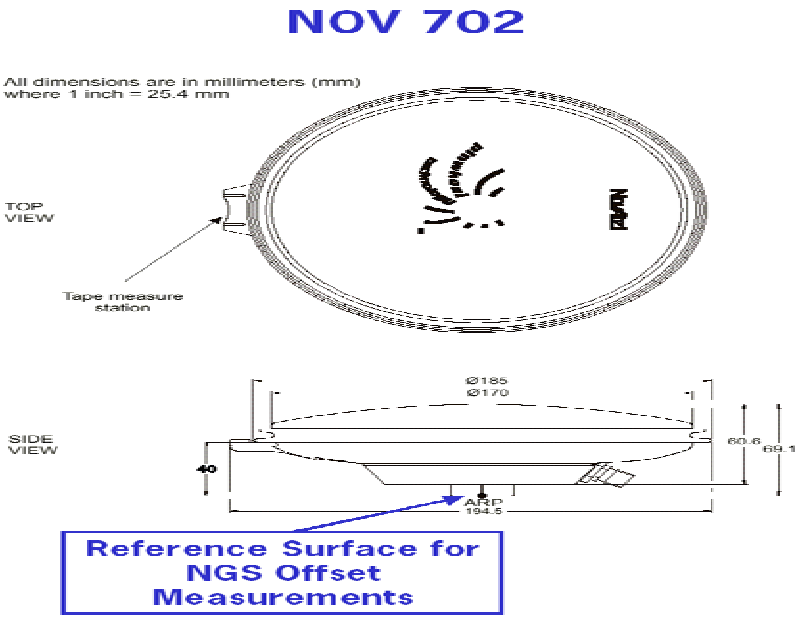

Figure 6.10: Sample of the GPS antenna phase offset for NOVATEL 702

L1 offset (rms): north: 0.2mm; east: 0.2mm; up: 0.3mm

L2 offset (rms): north: 0.1mm; east: 0.0mm; up: 0.5mm

Elevation (degree)	**90**	**85**	**80**	**75**	**70**	**65**	**60**	**55**	**50**
L1 offset RMS (mm)	0.0	0.1	0.2	0.2	0.2	0.2	0.1	0.0	0.0
L2 offset RMS (mm)	0.0	0.0	0.0	0.0	0.1	0.1	0.1	0.1	0.1
Elevation	**45**	**40**	**35**	**30**	**25**	**20**	**15**	**10**	**5**
L1 offset RMS (mm)	0.0	0.0	0.0	0.0	0.0	0.1	0.3	0.0	0.0
L2 offset RMS (mm)	0.2	0.2	0.2	0.3	0.3	0.2	0.3	0.3	0.0

Table 6.2: Sample Values of the GPS antenna phase offset for NOVATEL 702

6.5 MULTIPATH ERROR

The carrier wave propagates along a *straight* line (not quite, there are small bending effects due to the presence of the atmosphere). Multipath is caused by extraneous reflections from nearby metallic objects, ground or water surfaces reaching the antenna. This has a number of effects: it may cause signal interference between the direct and reflected signal leading to *noisier* measurement, or it may confuse the tracking electronics of the hardware resulting in a biased measurement that is the sum of the satellite-to-reflector distance and the reflector-to-antenna distance.

6.5.1 Multipath Reflection Coefficient

Multipath is the unwanted distortion, of the directed line-of-sight satellite signal, by localized reflected and/or diffracted signals. The reflection coefficients for horizontal and vertical polarization are given as following:

$$\Gamma_H = \frac{\sin\theta - \sqrt{\varepsilon - \cos\theta^2}}{\sin\theta + \sqrt{\varepsilon - \cos\theta^2}} \quad \text{.....(6.12)}$$

and

$$\Gamma_V = \frac{\varepsilon\sin\theta - \sqrt{\varepsilon - \cos^2\theta}}{\varepsilon\sin\theta + \sqrt{\varepsilon - \cos^2\theta}} \quad \text{.....(6.13)}$$

$$\Gamma = \eta \times \frac{\Gamma_H + \Gamma_V}{2} \quad \text{.....(6.14)}$$

where η is the diffuse reflection, the diffuse scattering occurs when the electromagnetic wave is reflected by a rough surface. The diffuse reflection is difficult to model due to its random behavior and therefore, is treated like noise in many practical situations.

$$\varepsilon = \varepsilon_r - j\frac{\sigma}{\omega\varepsilon_0} \quad \text{.....(6.15)}$$

j is the complex dielectric constant with time dependent in $e^{-j\omega t}$. Substituting for ω and ε_0 in equation (6.15) gives:

$$\varepsilon = \varepsilon_r - j60\lambda\sigma \quad \text{.....(6.16)}$$

The calculation of each linear reflection coefficient is now straightforward, for a given frequency, grazing angle (θ) (here they are determined as elevation angle of the GPS satellites) λ is the wavelength of the signal (m), dielectric constant (ε_r) and conduction value (σ) for the reflecting surface medium. The linear reflection coefficient for representative materials at 1GHz (man-made and natural) given in Table (6.3) can be plotted

Material	Conductivity	Relative Permissive
Concrete	2×10^{-5}	3
Dry Ground	1×10^{-5}	4
Medium Dry Ground	4×10^{-2}	7
Wet Ground	2×10^{-1}	30
Fresh Water (fresh)	2×10^{-1}	80
Sea Water (sea)	4	20

Table 6.3: Electrical Properties

6.5.2 Effects of Multipath Error on the Code Tracking Loop

The multipath error on Code Tracking Loop Mp_{cm} by narrow correlate technology will be given as following:

In the range of $0 \le \tau_1 < (1 \pm \Gamma_1)T_d$

$$Mp_{cm} = \pm\frac{\Gamma_1\tau_1\cos\Delta\phi}{1+\Gamma_1} \quad \text{.....(6.17)}$$

where $\Delta\phi = 2\pi(\frac{\tau_1}{\lambda} - \text{int}(\frac{\tau_1}{\lambda}))$, λ is the wave length of the signal.

Γ_1 is given from equation (6.15);

τ_1 is the incoming signal code delay, the delay is reflected by the ground and the reflector.

T_d is the early-late correlate spacing (m), $T_d = \frac{T_C \times correlatechip}{2}$

In the range of $(1 \pm \alpha_1)T_d \le \tau_1 < T_C - (1 \mp \alpha_1)T_d$

$$Mp_{cm} = \pm\Gamma_1 T_d\cos\Delta\phi \quad \text{.....(6.18)}$$

where T_C is the chip correlate spacing, is about 293m in L1 code signal.

In the rage of $T_C - (1 \mp \alpha_1)T_d \le \tau_1 < T_C + T_d$

$$Mp_{cm} = \pm\frac{\Gamma_1(T_C + T_d - \tau_1)\cos\Delta\phi}{2 \mp \Gamma_1\cos\Delta\phi} \quad \text{.....(6.19)}$$

It has to be noted that the upper sign of the composite sign (i.e. '+'in'$\pm$', or '-'in '$\mp$') is for the in-phase multipath corresponding to the upper part of the error envelope, and the lower sign of the composite is for the out-of-phase multipath corresponding to the lower part of the error envelop.

6.5.3 Effects of Multipath Error on the Phase Tracking Loop

In a GPS receiver, the carrier phase multipath error (Mp_{rm}) can be given by the difference between the composite signal phases $\Delta\Psi$ (which is tracked by the receiver), which is given as following:

$$\Delta\Psi = \arctan\left(\frac{\Gamma_1 \sin(\frac{2\pi}{\lambda}\times\tau_1)}{1+\Gamma_1\cos(\frac{2\pi}{\lambda}\times\tau_1)}\right) \text{……..rad……(6.20)}$$

$$Mp_{rm} = \frac{\lambda}{2\pi}\Delta\Psi \text{ ……..m……(6.21)}$$

where Γ_1 and τ_1 were shown as in equation (6.17). The details of the multipath error measurement can be referring to [Jayanta, 1999].

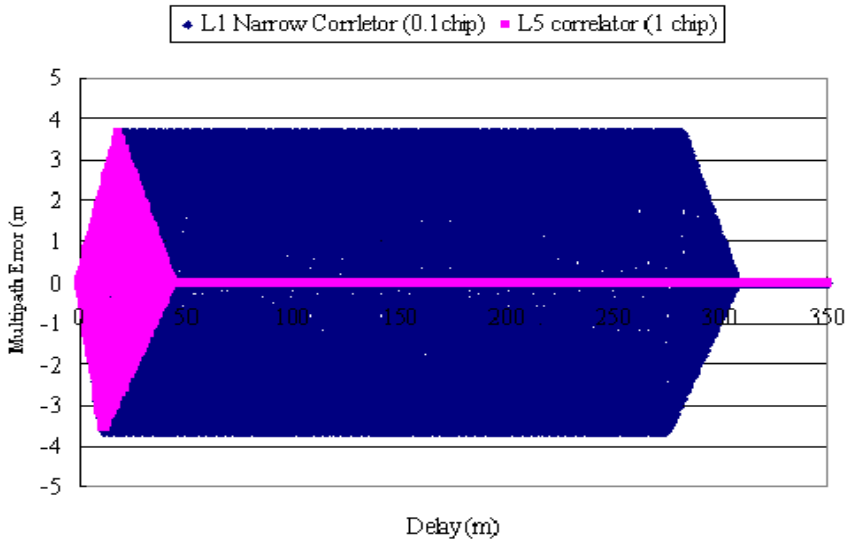

Figure 6.11: Multipath simulation on relative amplitude 0.25

6.5.4 Effects of Multipath Error on the Simulation

From the above discussion, the multipah error reflected by ground on the code and phase observation on L1, and L5 signals can be shown on Figure 6.11. The correlate chip is assumed 0.1 chips on L1 single and 1.0 chip on L5 single. The receiver amplitude between the direct and multipath signals is 0.25 (about 12dB).

6.6 GPS SATELLITE ORBIT

The range from satellite to the receiver will be estimated using the GPS satellite orbit and the position of the receiver. In the simulation, the GPS satellite orbit will be given from YUMA Almanac information. The YUMA Almanac files are generated from US Coast Guard navigation center from

(http://www.navcen.uscg.gov/gps/almanacs.htm). The sample of the YUMA Almanac and definition of the file will be shown as Table 6.4.

Week 175 almanac for PRN-01	
ID:	01
Health:	000
Eccentricity:	0.5404472351E-002
Time of Applicability (s):	589824.0000
Orbital Inclination (rad):	0.9723724451
Rate of Right Ascen (r/s):	-0.7931758961E-008
SQRT (A) (m 1/2):	5153.727539
Right Ascen at Week (rad):	-0.4069756641E+000
Argument of Perigee (rad):	-1.719371504
Mean Anom (rad):	0.6687658141E+000
Af0(s):	0.2651214600E-003
Af1(s/s):	0.0000000000E+000
Week:	175

Table 6.4: The Sample of the YUMA Almanac File for 175 week and PRN01

6.7 SATELLITE EPHEMERIS ERROR

Ephemeris errors results when the GPS message does not transmit the correct satellite location. In the case of the Broadcast Ephemeris within the GPS Navigation Message, these errors can range from (usually) less then typical satellite ephemeris is usually less than 10m. Note that these errors are the same for both P (Y) and C/A code. The effect of the ephemeris error on GPS position is shown as following:

Effect on point position:

Position Error = HDOP*Ephemeris Error……..……..(6.22.1)

Effect on relative position [Parkinson]:

Position Error <= d/r * Ephemeris Error…….(6.22.2)

where, *d* is distance between the receivers, r is the distance between the satellite and receiver (usually as 20,000km). The more details are introduced in [Bradford W. Parkinson, Volume II]. Using equation (6.22.2), for example, a 100-m satellite positioning error at 100-km separation between user and reference produces errors *in the worst case* of less than 1m.

The satellite ephemeris error can be compared with the GPS precise orbit (15 days latency). The GPS precise orbit are derived using 24 hours data segments from the global GPS network coordinated by the International Geodynamics GPS Service (IGS) (from http://www.ngs.noaa.gov/GPS/GPS.html). The accuracy of the orbit can be seen as 5cm [IGS Homepage]. Figure 6.12 shows ephemeris error of navigation message, which is compare with the IGS precise orbit. The calculation time is for 1 hour in 16 July 2003. Left is on the X direction, middle is on the Y direction, and right is on the Z direction. In figure 6.12, it can be seen that the ephemeris errors on X, Y, Z direction is less than 2m.

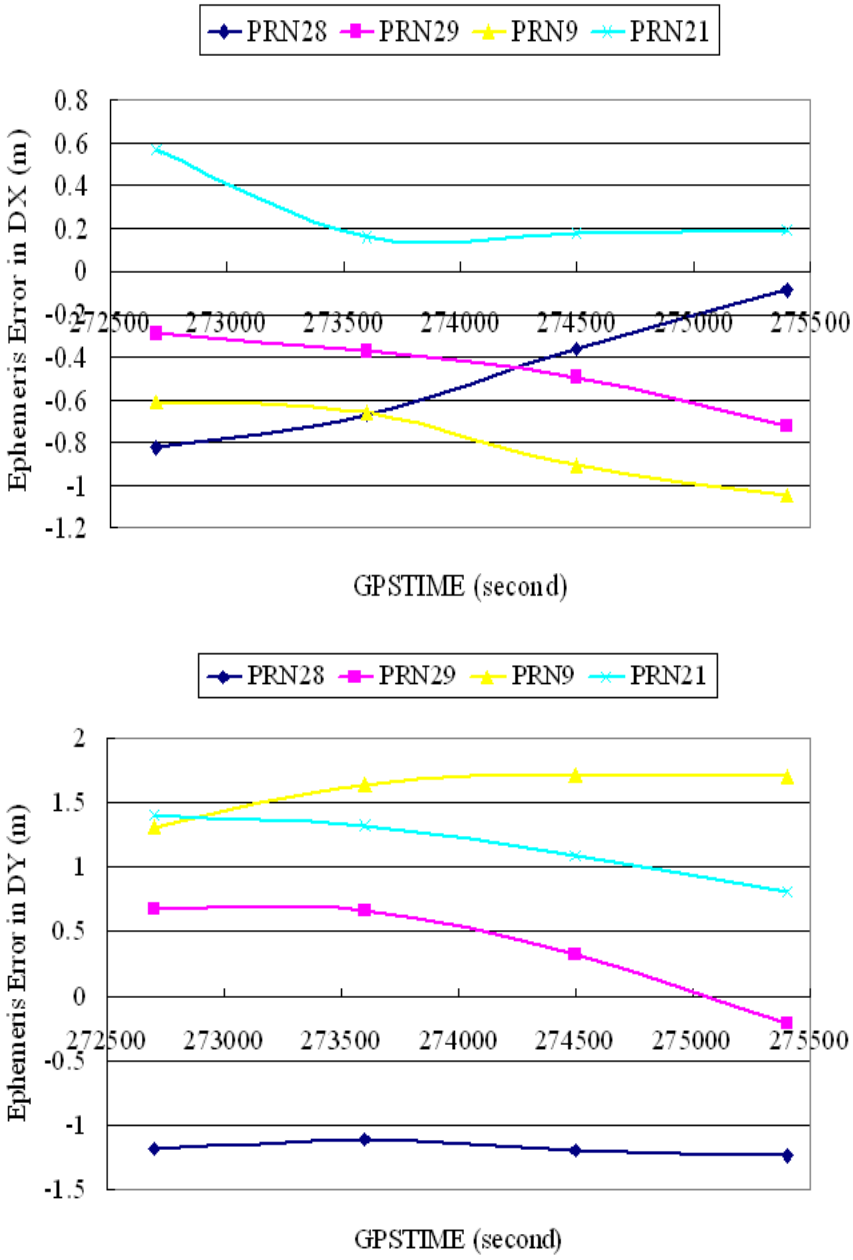

Figure 6.12: Ephemeris error of navigation message

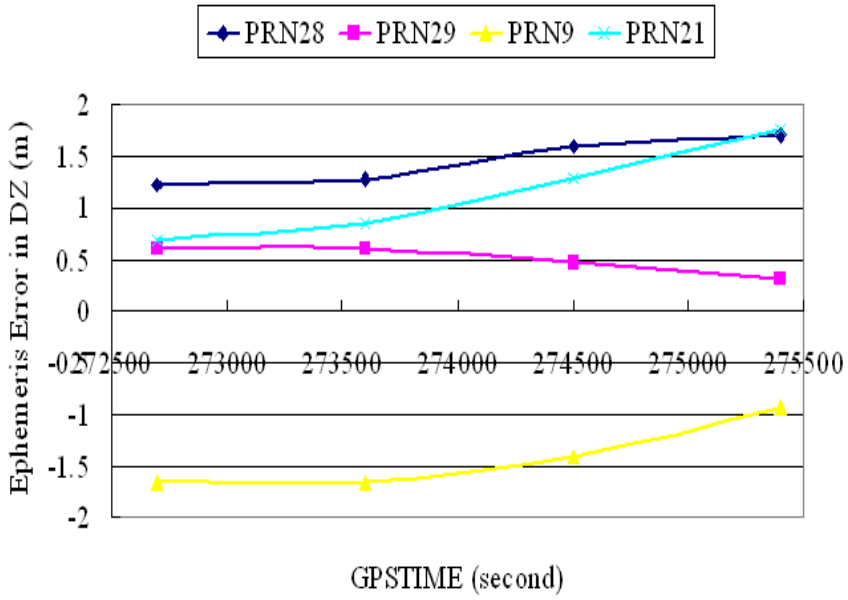

Figure 6.12: Ephemeris error of navigation message

We also tried to estimate the YUMA orbit error with IGS precise orbit. The calculation time is for 24 hours in 20 April 2003. Figure 6.13 shows the PRN1 satellite orbit error of YUMA file for 1 day. Ephemeris error on every direction is about 1000m can be seen.

In the simulation, each satellite ephemeris error is assumed as the error from navigational message, and will be produced as white noise with standard deviation of 2.1m [Lee, 1992].

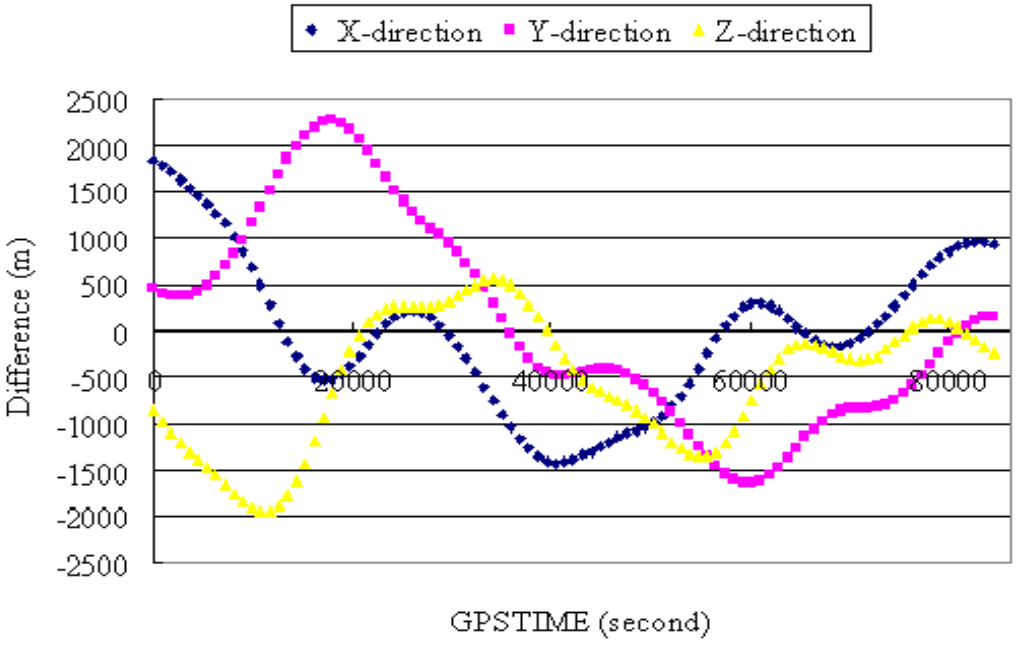

Figure 6.13: PRN1 estimated from YUMA satellite orbit compared with IGS precise orbit

6.8 RESULTS OF TRIPLE SIMULATION

Observation noise, multipath error and code differential positioning from triple frequencies simulation will be estimated in this section. Table 6.5 show that the error parameters in our triple simulation. The calculation time is 20 April 2003.

Error	Reference	Rover
Ionosphere Error	Klobuchar Model	Klobuchar Model
Troposphere Error	Saastamoinen model	Saastamoinen model
Ephemeris Error	Standard deviation 2.1m	Standard deviation 2.1m
Antenna	NOVATEL 702	NOVATEL 702
Code Noise	DLL noise	DLL noise
Phase Noise	PLL noise + antenna phase offset	PLL noise + antenna phase offset
Code Multipath Error	Ground	Ground and Reflector
Phase Multipath Error	Ground	Ground and Reflector

Table 6.5: Error parameters in the triple simulation

6.8.1 Noise in Triple Simulation

Table 6.5 shows the parameters used in our triple frequencies noise simulation. Combining the c/n_0 results of NOVATEL 702 antenna with the values in Table 6.6, the code noise and phase noise of PRN 31 in L1, L2 and L5 can be estimated in figure 6.14. Figure 6.14(1) shows on code observation, and figure 6.14(2) shows on phase observation. In figure 6.14, the elevation is the function of the observation noise can be seen.

	PLL Bandwidth (Hz)	DLL Bandwidth (Hz)	chipping rate	D (chip)	Td (ms)	α
L1	10	0.5	293.05	0.1	20	0.5
L2	10	0.5	293.05	0.1	20	0.5
L5	10	0.5	29.305	1	10	0.5

Table 6.6 The parameter in the triple frequencies noise simulation

6.8.2 Multipath in Triple Simulation

In the simulation, the reference station is only affected by the ground reflect multipath, and the rover station is affected multipath from the ground and the reflector. The reflector building is assumed on the east to the rover station. The distance is 30m, and the observation mask is 30 degree. The calculation time is 20 April 2003. Figure 6.15 shows the multipath error reflected by ground by PRN 31,figure 6.15(1) is on code observation, and figure 6.15(2) is on phase observation. Figure 6.8 shows the multipath reflected by the building by PRN3 satellite, figure 6.16(1) shows on code observation, and figure 6.16(2) shows on phase observation.

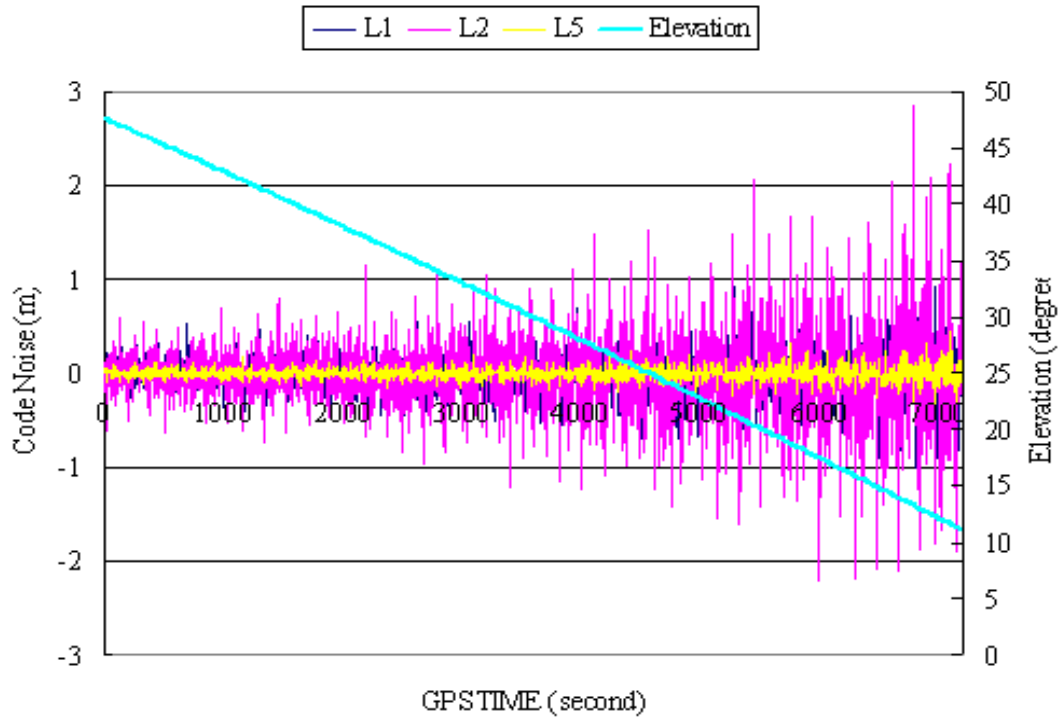

Figure 6.14(1): Code observation noise in the triple simulation by PRN31

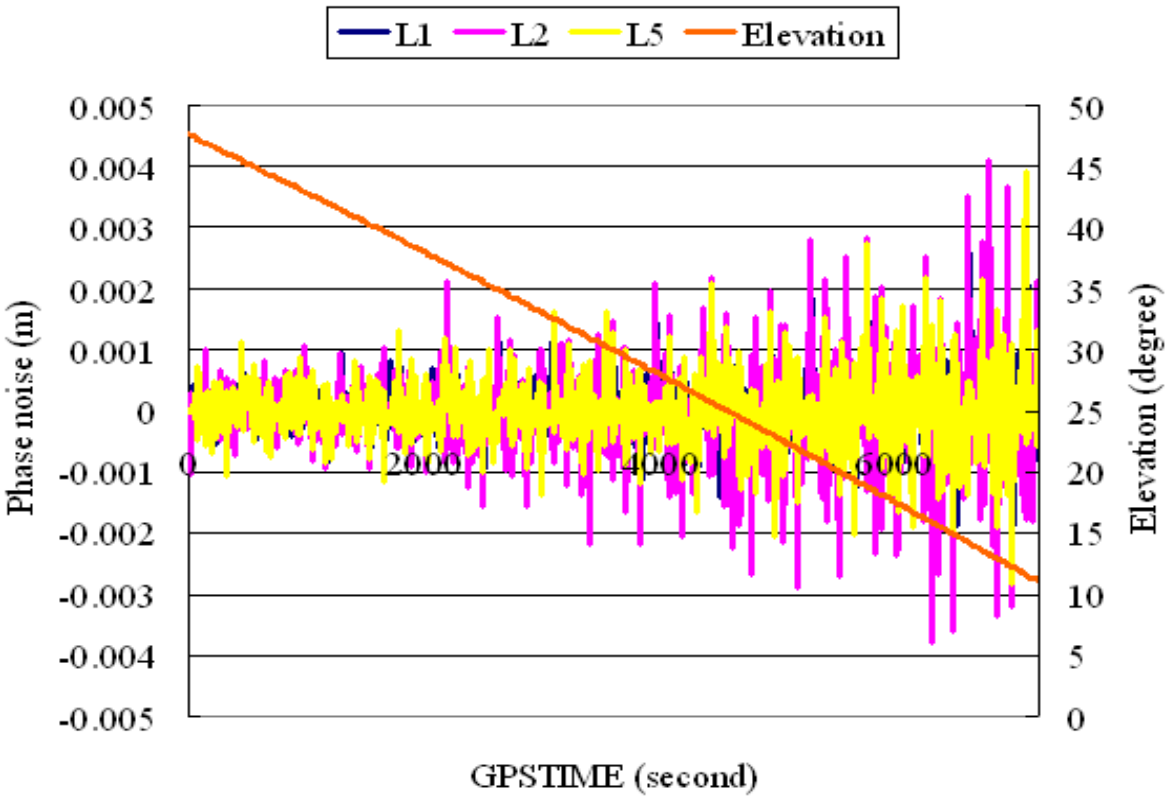

Figure 6.14(2): Phase observation noise in the triple simulation by PRN31

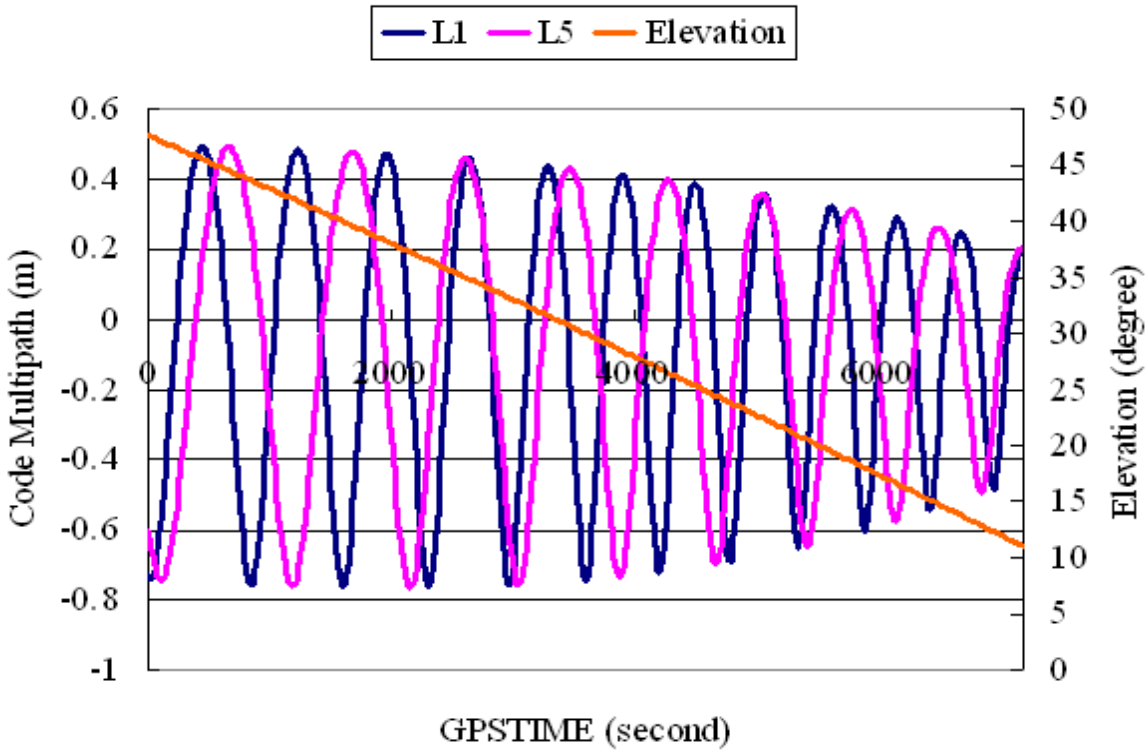

Figure 6.15(1): Multipath error reflected by ground with PRN31 on code observation

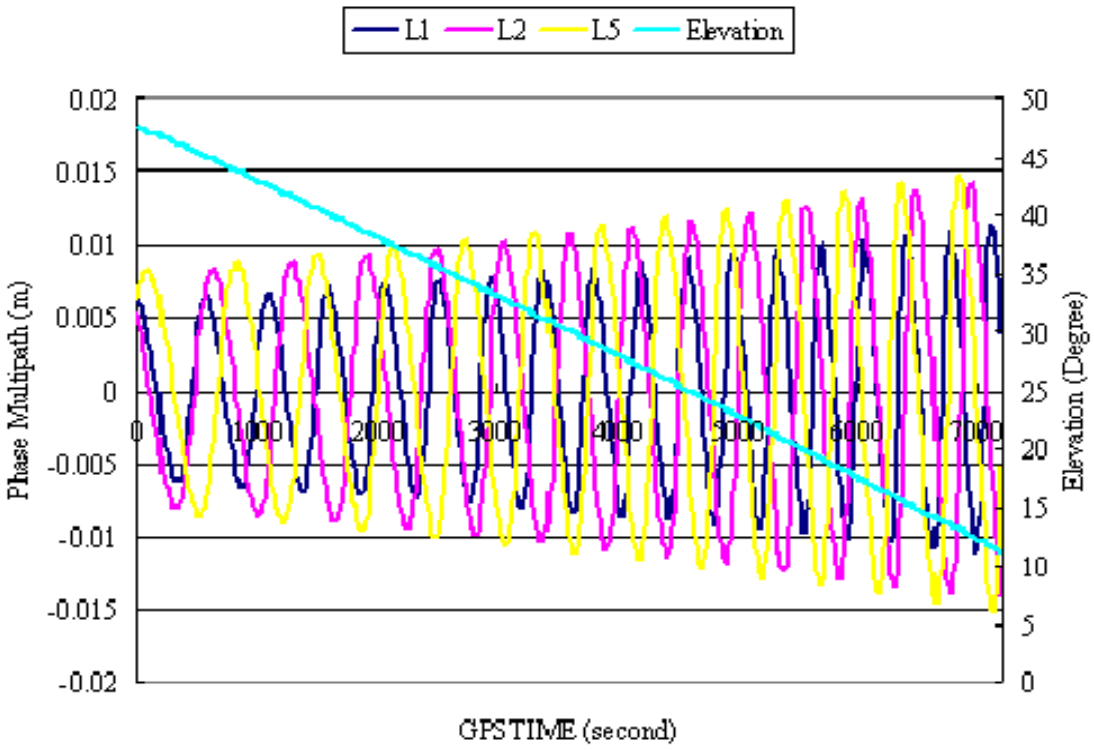

Figure 6.15(2): Multipath error reflected by ground with PRN31 on phase observation

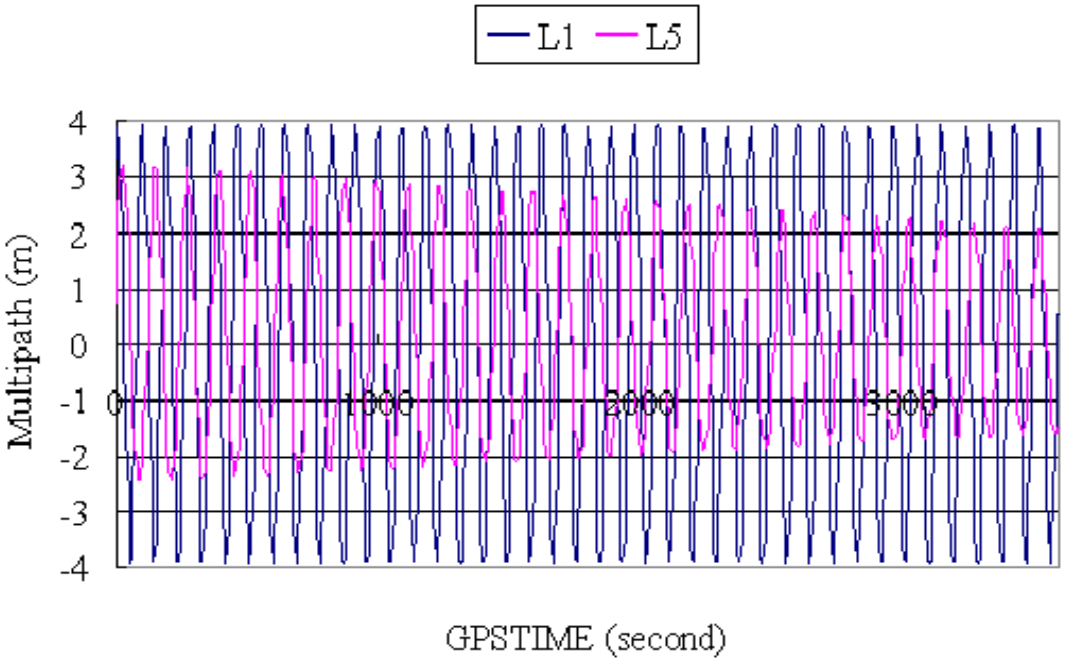

Figure 6.16(1): Multipath error reflected by reflector building with PRN3 on code observation

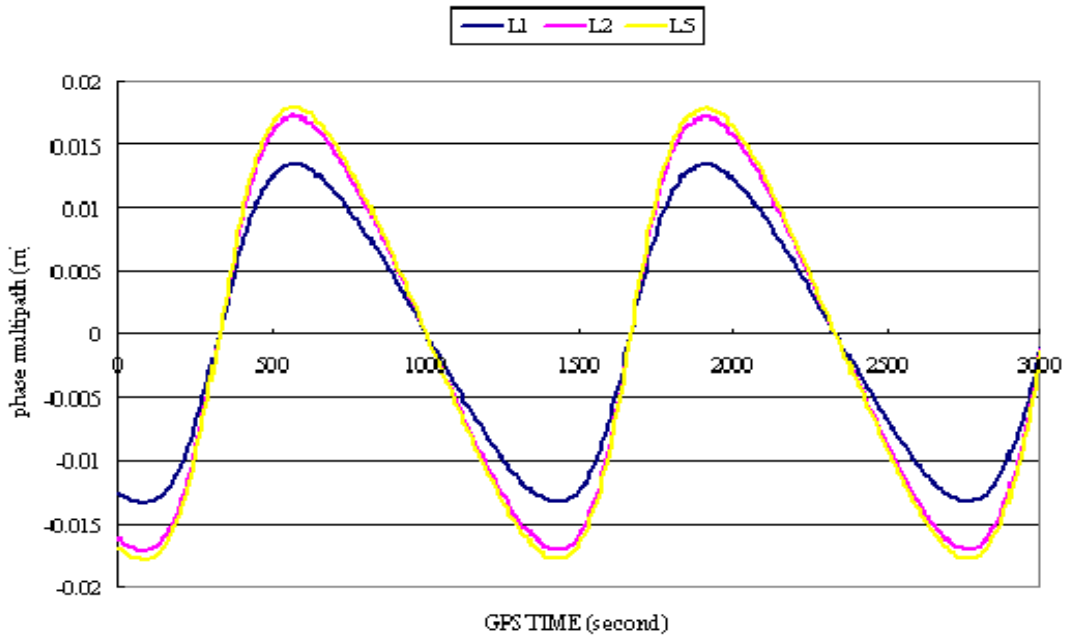

Figure 6.16(2): Multipath error reflected by reflector building with PRN3 on phase observation

6.8.3 L1 Code Differential Positioning Results

The rover station position is estimated by L1 code pseudorange differential measurement. The situation of the reference station is assumed as Table 6.7. The epoch is 1s. The code smoothing time is 20s. The baseline length is about 14km. The distance can be seen as medium baseline. The observation time is for 2 hours.

Name	Lat (degree)	Lon (degree)	Height (m)
Reference station	35.6754640	139.9023540	100
Rover station	35.7802150	139.8128120	100

Table 6.7: The situation of the reference and rover stations in the simulation

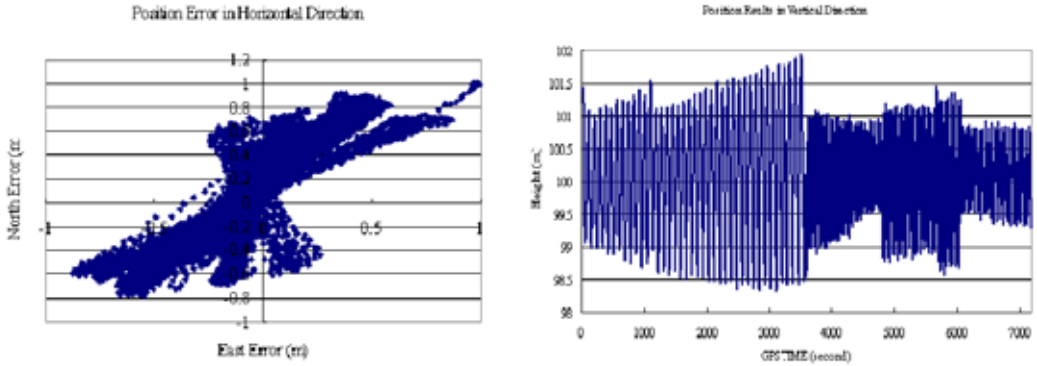

Figure 6.17: Position results under the case of multipath present for 2 hours (baseline about 14km). Left indicates position error in horizontal direction, and right indicates position results in vertical direction

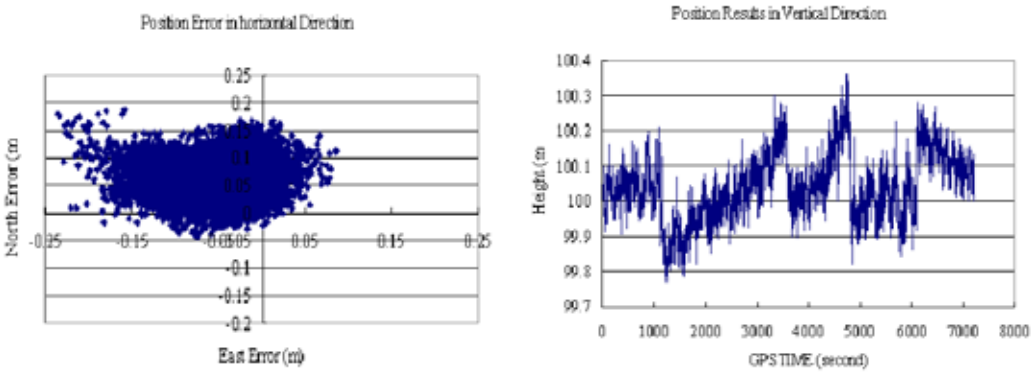

Figure 6.18: Position results under the case of multipath absent for 2 hours (baseline about 14km). Left indicates position error in horizontal direction, and right indicates position results in vertical direction.

	RMS in Lat (m)	RMS in Lon (m)	RMS in Height (m)	Average in Lat (m)	Average in Lon (m)	Average in Height (m)
Multipath Absent	0.0467	0.0345	0.095	0.0617	0.057	0.042
	2drm=0.0949m					
Multipath Present	0.32	0.45	0.84	0.062	0.057	0.04
	2drm=1.10m					

Table 6.8: Position error estimated by L1 pseudorange under the case of multipath absent and present

The positioning results are estimated in Figure 6.17 and Figure 6.18. Figure 6.17 is under the case of multipath error present (multipath from ground in reference station; from ground and reflector in rover station). Figure 6.18 is under case of the multipath error neglected. Table 6.8 shows the position error in L1 code differential measurement. The influence of the multipath in the positioning can be seen here.

6.8.4 Positioning Results in Different Baselines

In order to see the influence from ionosphere error and other errors caused by baseline in the simulation, positioning will be estimated in different baselines by L1 pseudorange differential measurement. Observation time is 0900LT-1100LT on April 20 2003 in Japan. Multipath error is neglected here. The situations of the reference and rover stations are shown in Table 6.9.

Name	Lat (degree)	Lon (degree)	Height (m)	Distance (km)
Reference station	35.6754640	139.9023540	100	
Short baseline	35.670	139.900	100	0.698
Medium baseline	35.7802150	139.8128120	100	14.167
Long baseline	37.0907146	140.9025157	100	180.871
Extra-long baseline	40.1334499	141.7890969	100	521.715

Table 6.9: The situation of the reference and rover stations

Figure 6.19, 6.20 and 6.21 show the position results under the cases of the short baseline, long baseline and extra-long baseline. Table 6.6 shows the position error analysis in different baseline, and the value of the medium baseline is from Table 6.8. The ionosphere error influence in positioning can be seen obviously.

In the next chapter, the ambiguity resolution will be performed with the triple simulation. The baseline influence in AR will be estimated under the case of multipath absent. The multipath influence in AR will be estimated under the case of multipath present in short baseline.

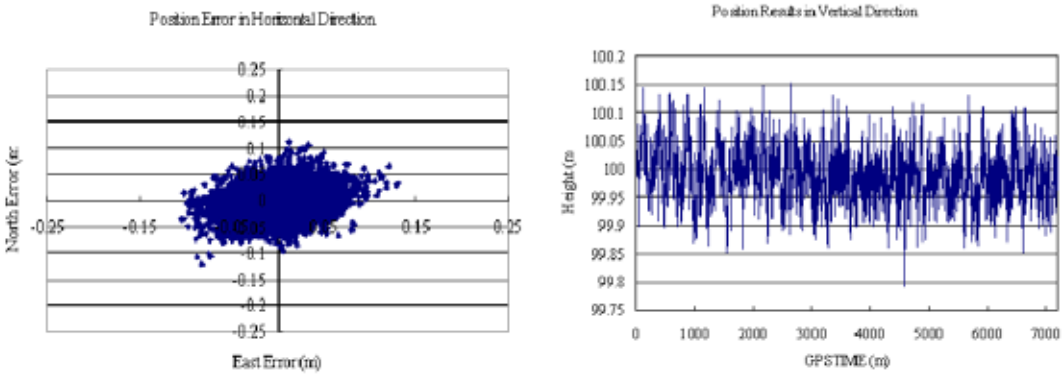

Figure 6.19: Position results in simulation on short baseline (about 700m). Left is Position results on horizontal direction, and right is on vertical direction

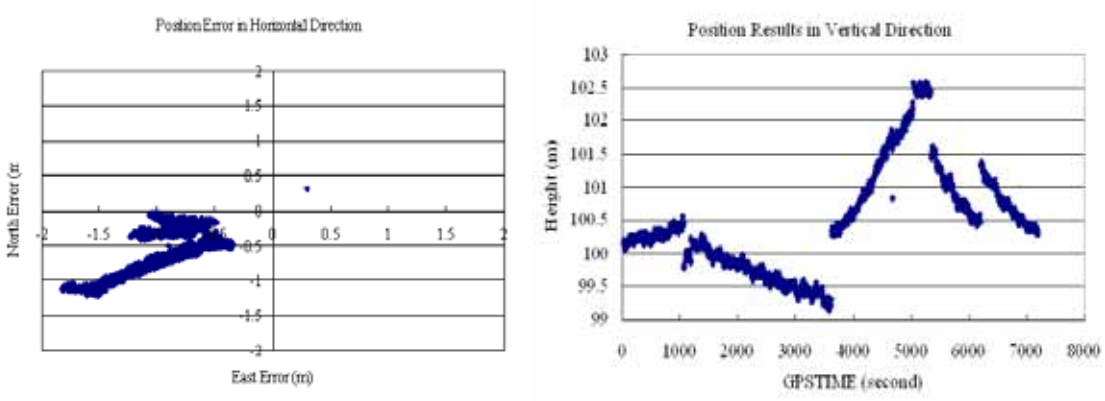

Figure 6.20: Position results in simulation on long baseline (about 180km). Left is Position results on horizontal direction, and right is on vertical direction

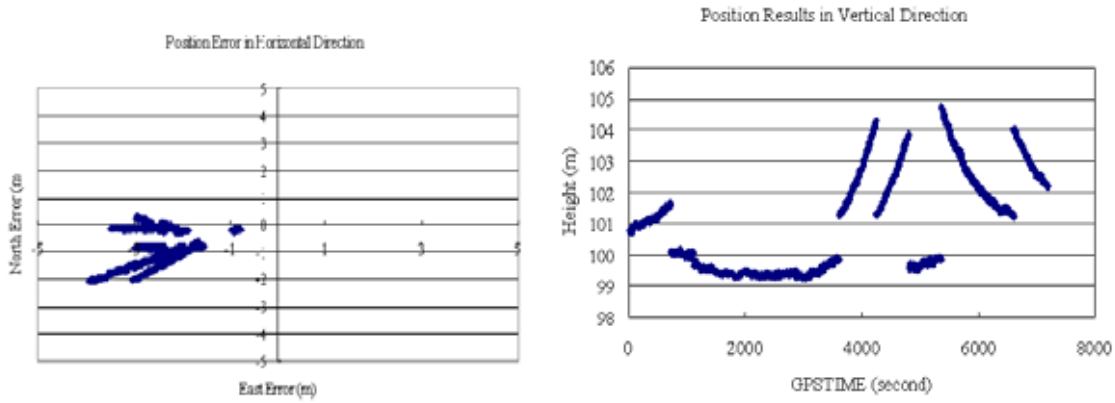

Figure 6.21: Position results in simulation on extra-long baseline (about 540km). Left is Position results on horizontal direction, and right is on vertical direction

	RMS in Lat (m)	RMS in Lon (m)	RMS in Height (m)	Average in Lat (m)	Average in Lon (m)	Average in Height (m)
Short baseline	0.0312	0.0270	0.048	0.0008	0.018	0.0095
	2drm=0.0825m					
Medium baseline	0.0467	0.0345	0.095	0.0617	0.057	0.042
	2drm=0.0949m					
Long baseline	0.295	0.304	0.789	0.899	0.517	0.479
	2drm=0.847m					
Extra-long baseline	0.628	0.575	1.541	2.326	0.782	1.003
	2drms=1.7029m					

Table 6.10: Position Error in the simulation under the cases of different baseline length (multipath absent)

CHAPTER 7
RESULTS & ANALSYS

In this chapter, ambiguity success rate (ASR) will be analyzed for scenarios. From the results of ASR, the performance of AR can be seen. Dual and triple GPS frequencies signals are considered here, and the data is from the triple frequencies simulation that has been introduced in the last chapter.

7.1 ADVANTAGE OF FREQUENCY WITH NEW SIGNAL

Why the frequency of new signal (L5 signal) is 1176.45Mhz? There are many answers for this problem. We are pointing on the advantage on the primary and widelane signal ambiguity absolution by using the signal with this new frequency to answer this question in this section.

In this study we are particularly in the standard error of the estimated ambiguity. Long baseline (ionosphere present) observation algorisms are considered as equation (4.20) and (4.34). Changing the frequency of L5 signal from 1000MHz to 2000MHz. $f_{L1} = 1575.42MHz$ and $f_{L2} = 1227.60MHz$, also the sigma of carrier phase noise is set to 0.01 cycles, and the sigma of code noise is set to 0.3m. For these constants, σ_{N5} can be given in figure 7.1, and σ_{N25} can be given in figure 7.2. Figure 7.1 shows $a = f_{L1} / f_{L5}$ is the function of the primaryL5 signal ambiguity estimation, and figure 7.2 shows $a = f_{L2} / f_{L5}$ is the function of the widelaneL2L5 signal ambiguity estimation. The result estimated by actually L5 signal (1176.45 MHz) is shown as red points in Figure 7.1 and Figure 7.2

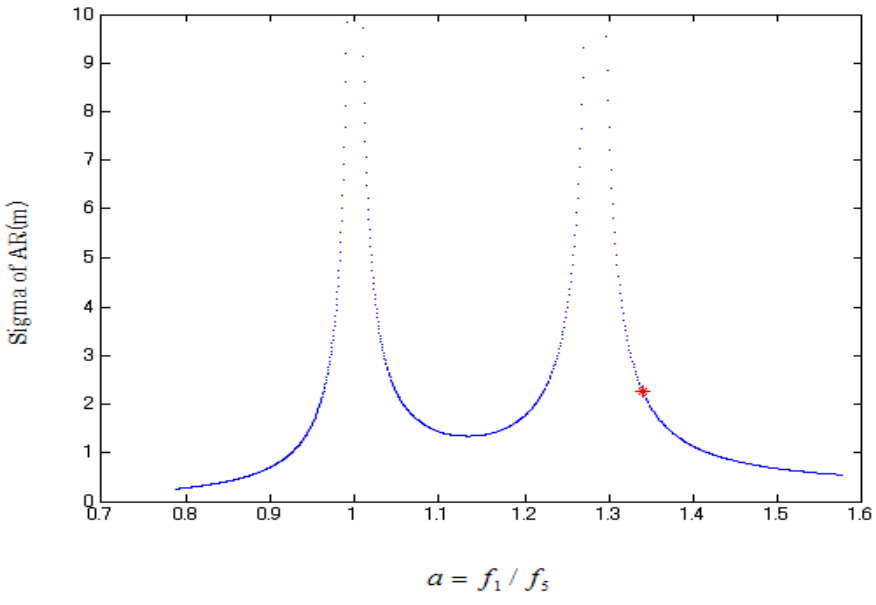

Figure 7.1 Wavelength of L5 is the function of L1 ambiguity resolution

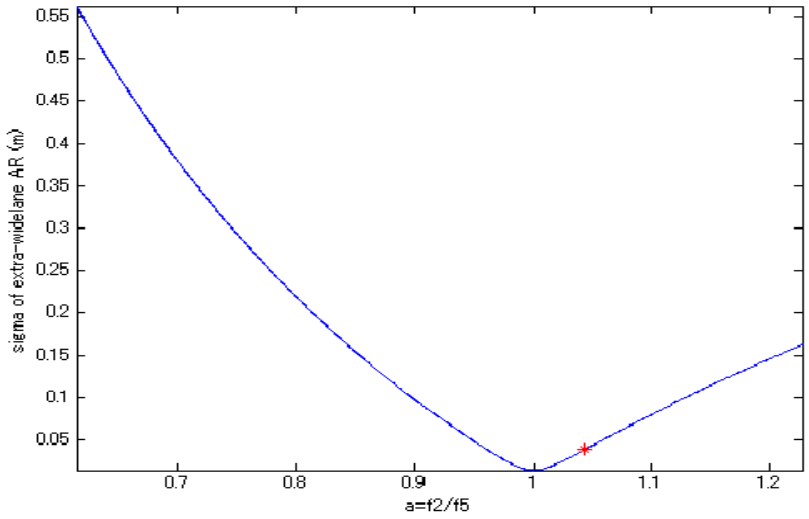

Figure 7.2: Wavelength of L5 is the function of widelaneL2L5 ambiguity resolution

From figure 7.1, the standard deviation increases dramatically for $a=1(f_{L5}=f_{L1})$ and $a=1.28(f_{L5}=f_{L2})$. It means that in dual frequencies, the primary ambiguity is very difficult to be estimated only by carrier phase observations because the numbers of unknowns are more than the numbers of equations. In figure 7.2, the curve has a minimum (0) for $a=1$, and by closing f_{L5} to f_{L2}, σ_{N25} becomes smaller. Combining two figures, the optimum choice of a can be found.

In figure 7.1 and 7.2, red points indicate the results estimated when L5=1176.45GHz, we can see that both of them are in the optimum choice field. Thus the L5 signal (1176.45MHz) will be a good tool in resolving the ambiguity problem.

7.2 SET UP

Using the triple frequencies simulation, four different baseline-lengths will be considered: short baseline (about 0.7 km), medium baseline (about 14 km), long baseline (about 180 km) and extra-long baseline (about 500 km). The computer for calculation is Dell GX270 Celeron 2.40GHz.

A full day for period of 24 hours was considered. Instantaneous positioning is estimated. Thereby no distinction needs to be made between kinematic and static positioning. As a reference location, the city of CHIBA in Japan is used, at latitude 35.67-degree North, longitude 139.90-degree East, and 100m heights. 15-degree satellite elevation cut-off angle is maintained. The ambiguity success rate is computed over 24 hours in April 20-21, 2003. It is noted here that the multipath error is neglected in the baseline analysis. The case of multipath error present will be discussed in the section 7.6.

The ambiguity resolution will be performed under in short, medium, long and extra-long baseline. The situation of the rover receivers has been given as in Table 6.4.

Figure 7.3 shows the sky plot estimated from YUMA files, at 0900LT on April 20 2003, and situation is reference station (CHIBA). The blue “3” means the signal from PRN3 is affected by multipath error from the building reflected that we set.

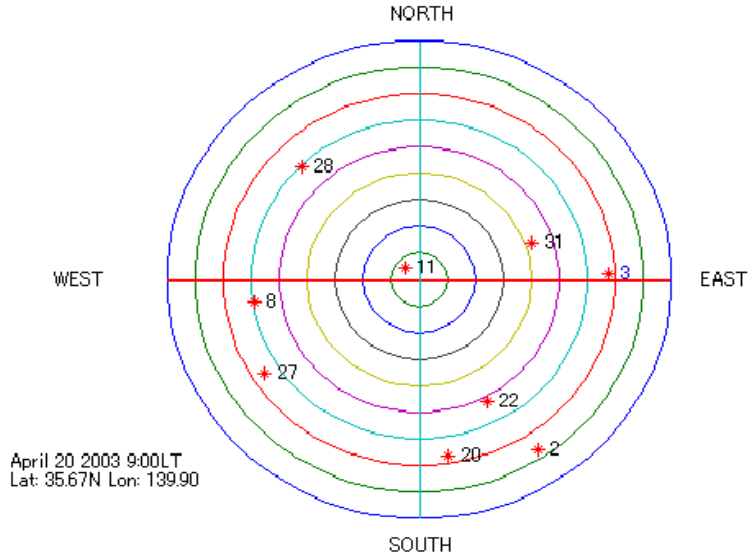

Figure 7.3: Sky plot at the reference receiver on 0900LT April 20 2003

7.3 AR IN DIFFERENT BASELINE

Under the cases of different bases, the integer time of primary signal, widelane (L1L2) signal and extra-widelane (L2L5) signal is estimated in the first, and then, the ambiguity resolution in dual frequencies and in triple frequencies will be compared. In the medium baseline, two methods will be discussed. The geometry-free method will be proposed in the long and extra-long baseline.

7.3.1 Short Baseline

Figure 7.4 shows the ambiguity resolution integration time on the short baseline. Figure 7.4(1) indicates primary signal ambiguity resolution, figure 7.4(2) indicates widelane signal ambiguity estimation, and figure 7.4(3) indicates extra-widelane signal ambiguity estimation.

From figure 7.4, we can see that extra-widelane signal ambiguity can be fixed the most fast, the second is widelane signal ambiguity, and the primary signal is the worst. The reason of it has been introduced in chapter 4. Hence, widelane and extra-wide lane signal will be used to do the primary signal ambiguity.

Figure 7.5 shows the ambiguity success-rate of signal epoch by sampling 120 second over the full day on the short baseline. The vertical scale is logarithmic and ranges from 0.88 to 1.0 on the top figure and 0.98 to 1.0 at the bottom figure. From 7.5, on the short baseline, the ambiguity resolution will be fixed more accurate and faster in triple frequencies than in dual frequencies.

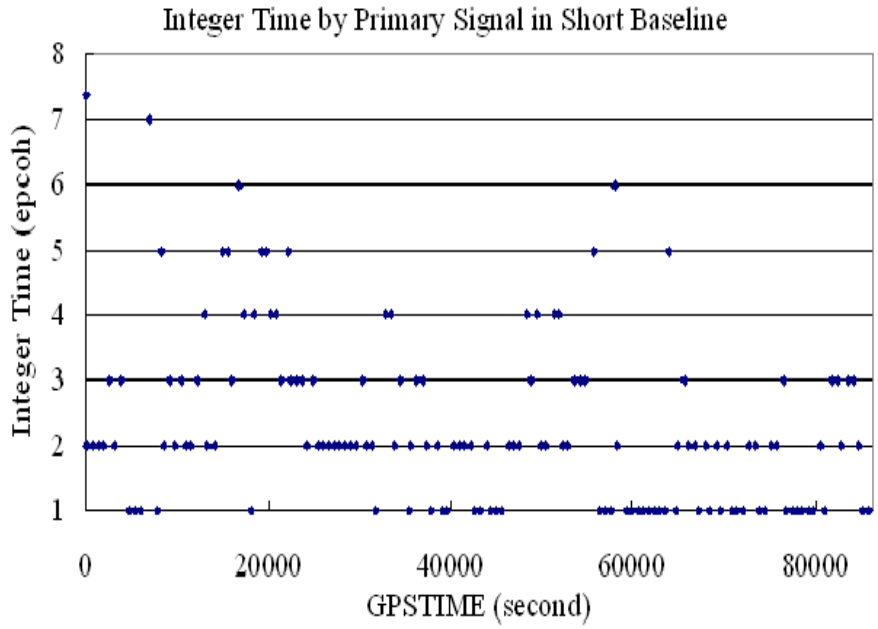

Figure 7.4 (1): Integer time by primary signal in short baseline

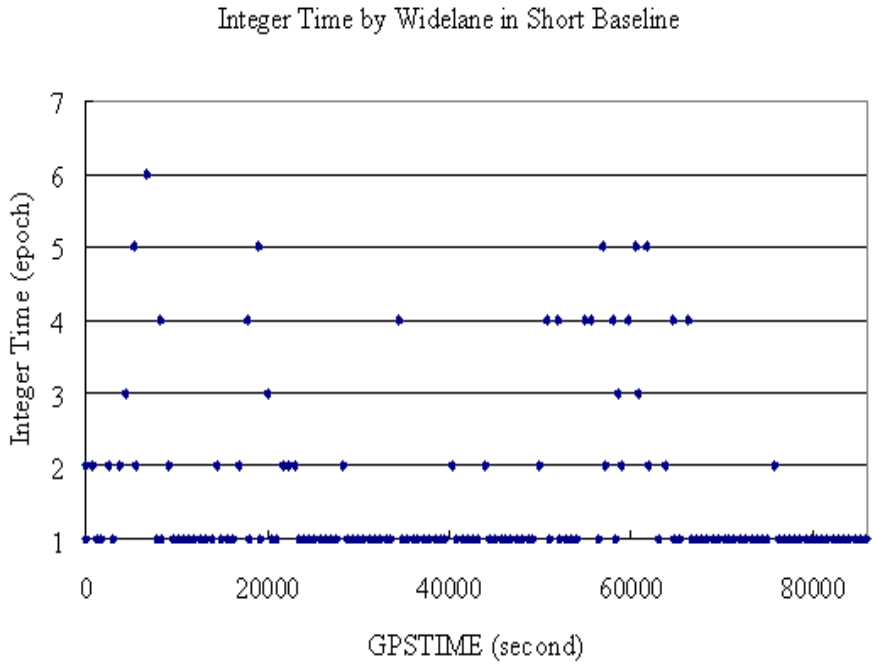

Figure 7.4 (2): Integer time by widelane signal in short baseline

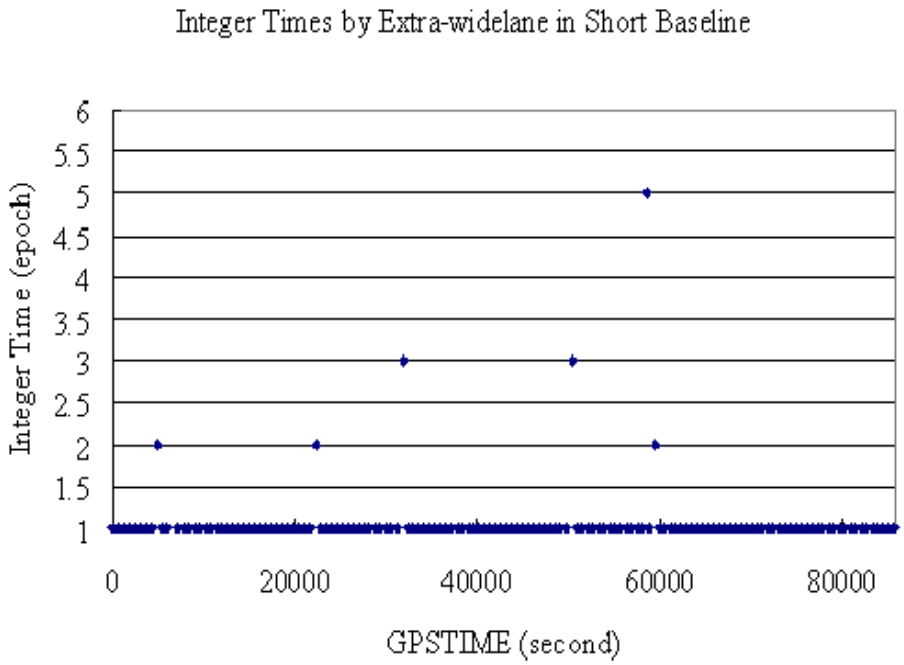

Figure 7.4 (3): Integer time by extra-widelane signal in short baseline

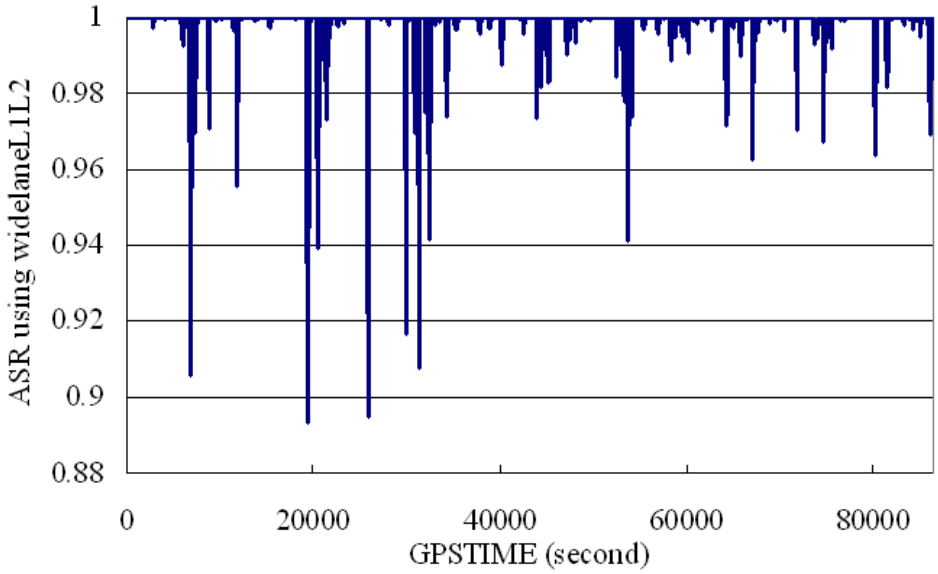

Figure 7.5: ASR of single epoch for dual frequencies on top and triple frequencies at bottom, in a short baseline

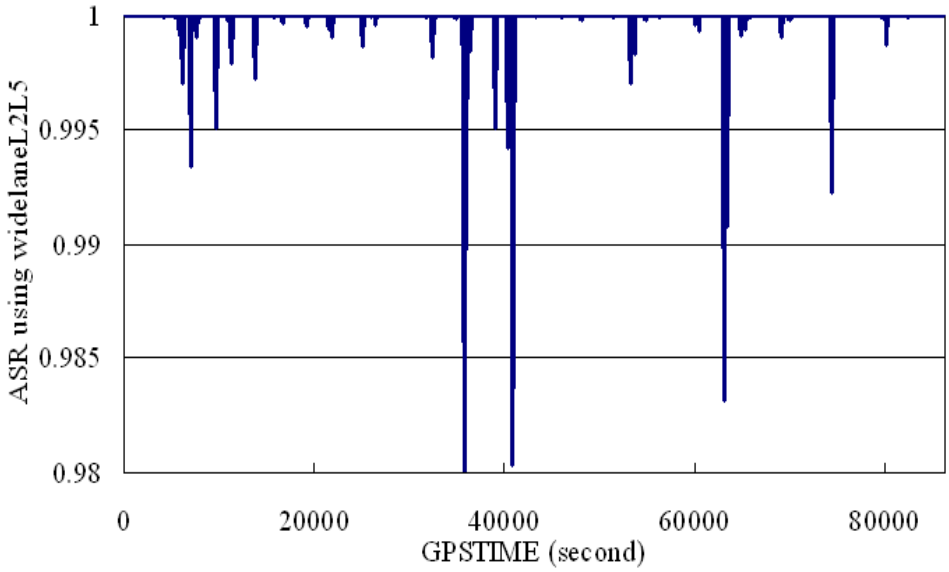

Figure 7.5: ASR of single epoch for dual frequencies on top and triple frequencies at bottom, in a short baseline

7.3.2 Medium Baseline

On the short baseline, differential ionospheric and tropospheric delays are simply absent. However on longer baseline differential atmospheric delays have to be taken into account. The medium baseline case is considered as about 14km. DD ionosphere error of three pairs of primary satellites is presented in figure 7.6 (about primary satellites refers to section 5.1). From figure 7.6, the value of ionosphere error for 24 hours can be seen. The ionosphere error is used Klobuchar model that has been introduced in Chapter 6.

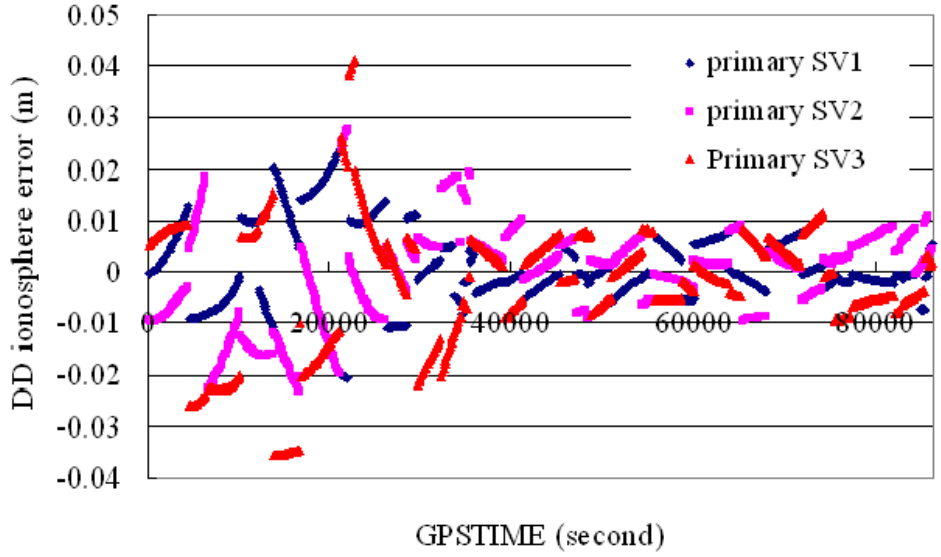

Figure 7.6: DD ionosphere error in medium baseline (about 14km)

As the same as the case of short baseline, the integration time on medium bases is shown in Figure 7.7 Figure 7.71) indicates primary signal ambiguity resolution, figure 7.72) indicates widelane signal ambiguity estimation, and figure 7.7(3) indicates extra-widelane signal ambiguity estimation. Similar to the case of short baseline, extra-widelane signal can be estimated the fastest, the second is widelane signal, and the third is primary signal.

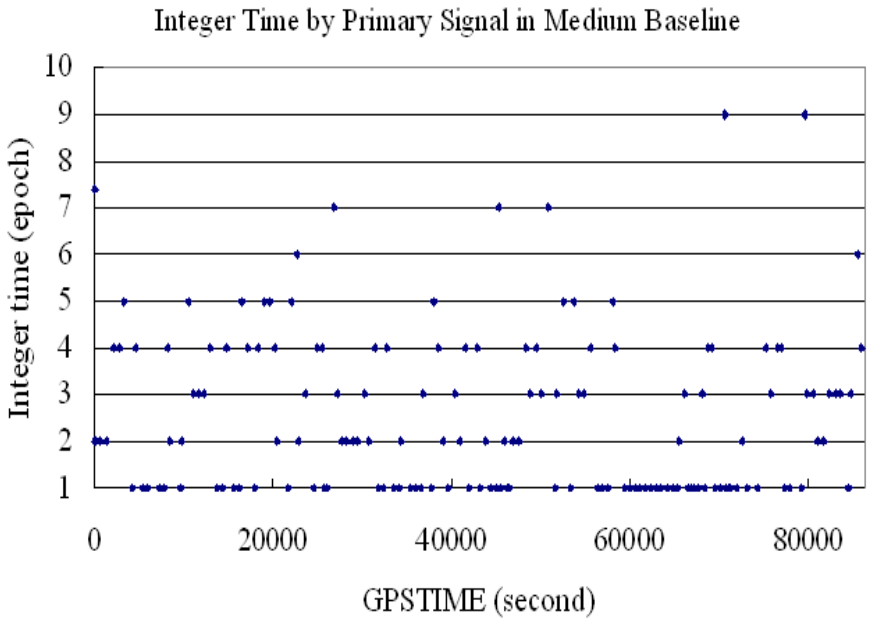

Figure 7.7 (1): Integer time by primary signal in medium baseline

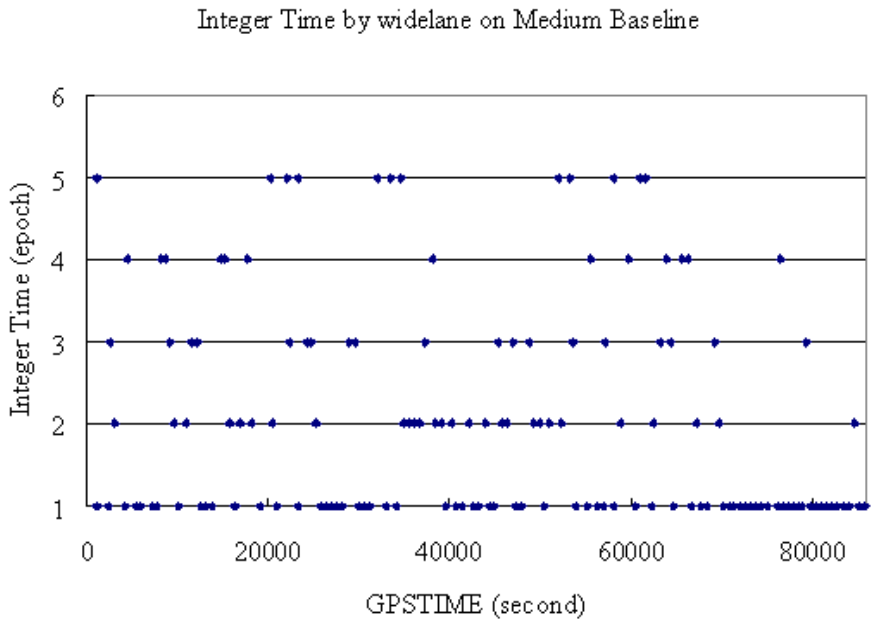

Figure 7.7 (2): Integer time by widelane signal in medium baseline

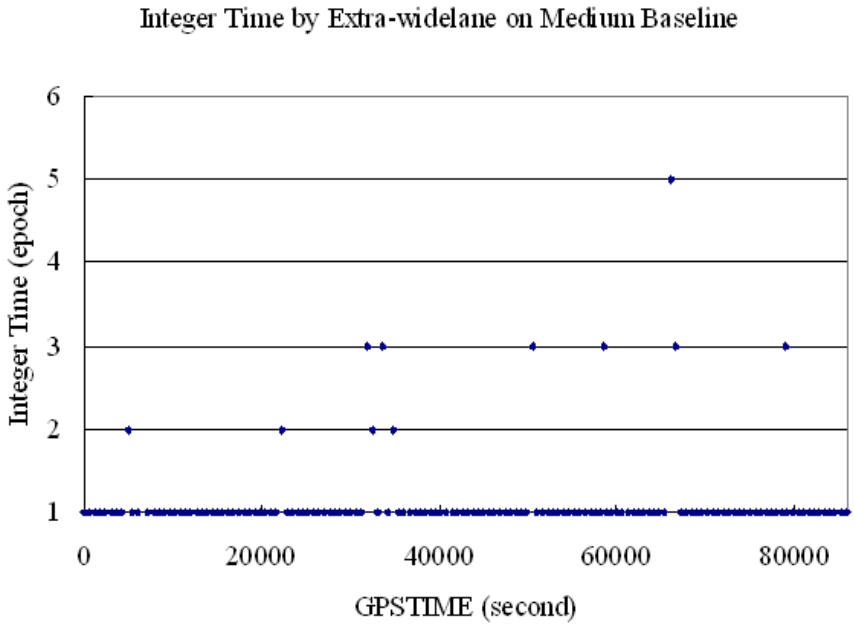

Figure 7.7 (3): Integer Time by extra-widelane signal in medium baseline

In this thesis, two attempts are made to increase ASR on the medium length baseline. The details of two methods have been introduced in the Chapter 5. These two methods are compared with present dual frequencies GPS in Figure7.8. Figure 7.8 shows ASR over the full day on the medium baseline. The vertical scale is logarithmic and ranges from 0.6 to 1.0. From figure 7.8, ASR is obviously lower from 10000 to 30000 (GPSTIME) than the other time of the day. DD ionosphere is the most serious in almost same time can be found in figure 7.6. Ionosphere influence in the ambiguity resolution can be seen. However, similar to the case of short baseline, ambiguity can be resolved more accurate and fast by widelane and extra-widelane signal.

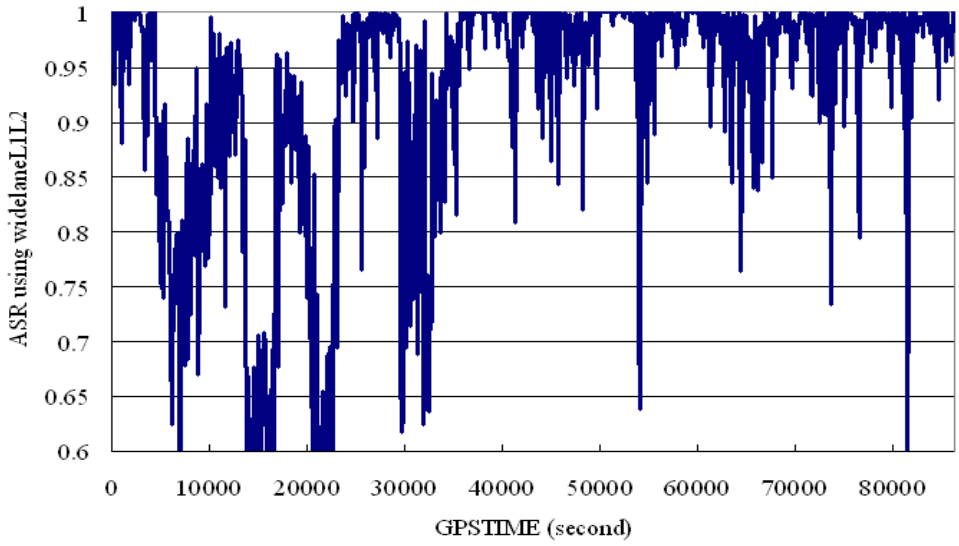

Figure 7.8: ASR of single epoch by widelaneL1L2 on top and widelaneL1L5 in the middle and extra-widelaneL2L5 at bottom, in a medium baseline

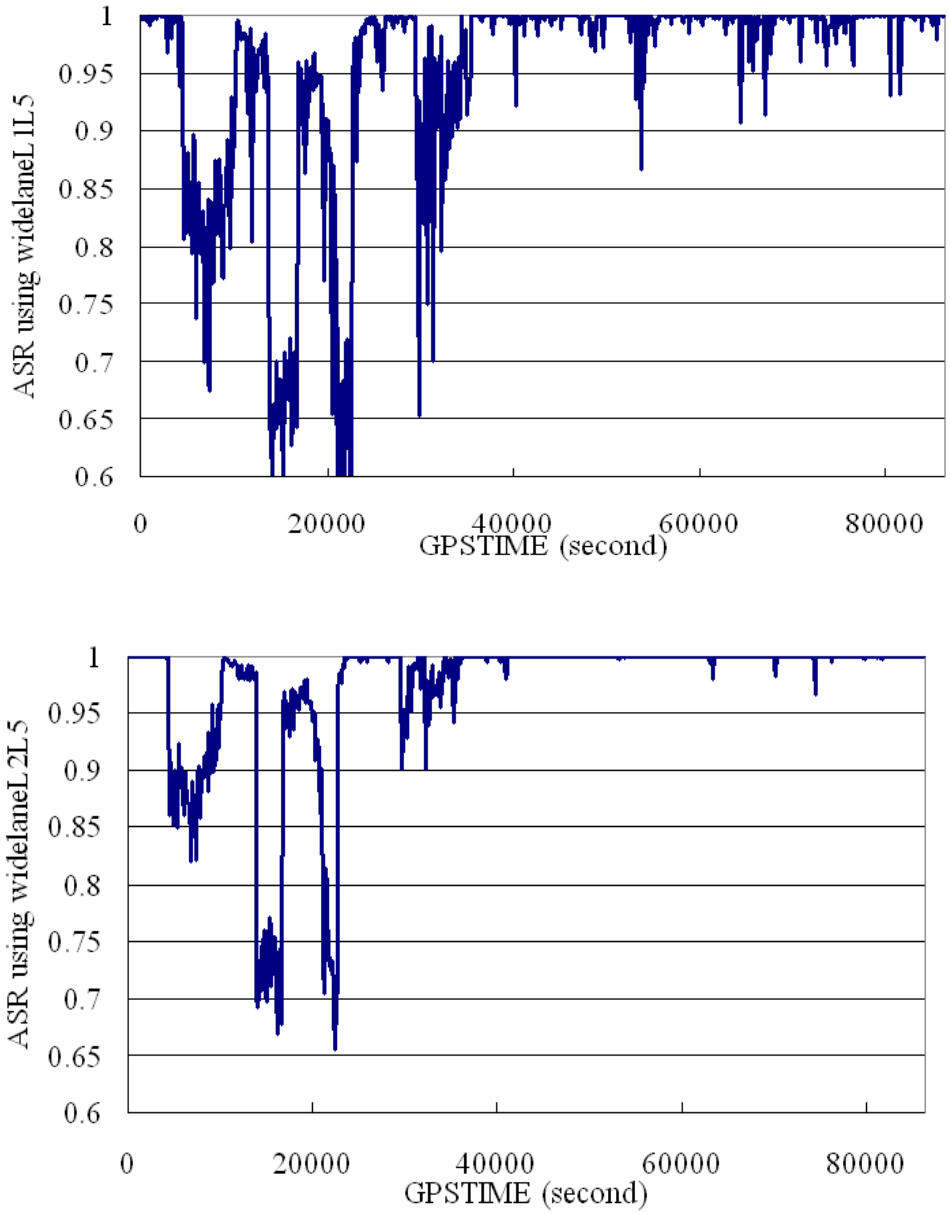

Figure 7.8: ASR of single epoch by widelaneL1L2 on top and widelaneL1L5 in the middle and extra-widelaneL2L5 at bottom, in a medium baseline

7.3.3 Long Baseline

The long baseline case is considered as about 180km. Figure 7.9 shows DD ionosphere error of three pairs of primary satellites for 24 hours. Figure 7.10 shows the ambiguity resolution integer time on the long baseline. Figure 7.10(1) indicates primary signal ambiguity resolution, figure 7.10(2) indicates widelane signal ambiguity estimation, and figure 7.10(3) indicates extra-widelane signal ambiguity estimation. The results of ambiguity resolution are as same as short and medium baseline, the best is extra-widelane signal, the second is widelane signal, and the worst is primary signal.

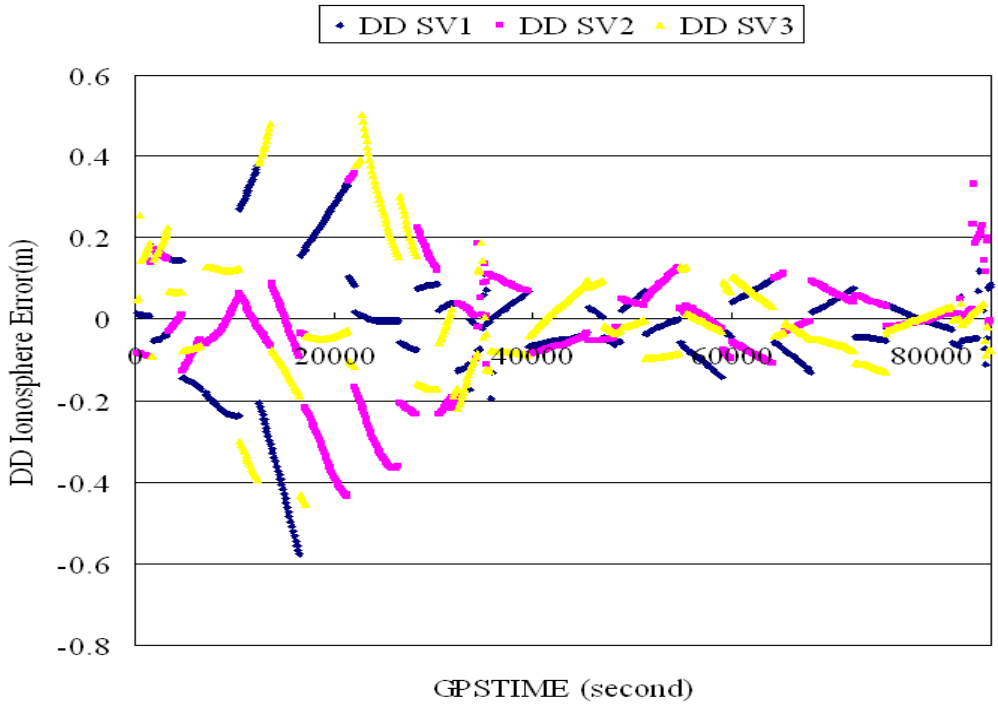

Figure 7.9: DD ionosphere error in long baseline (about 180km)

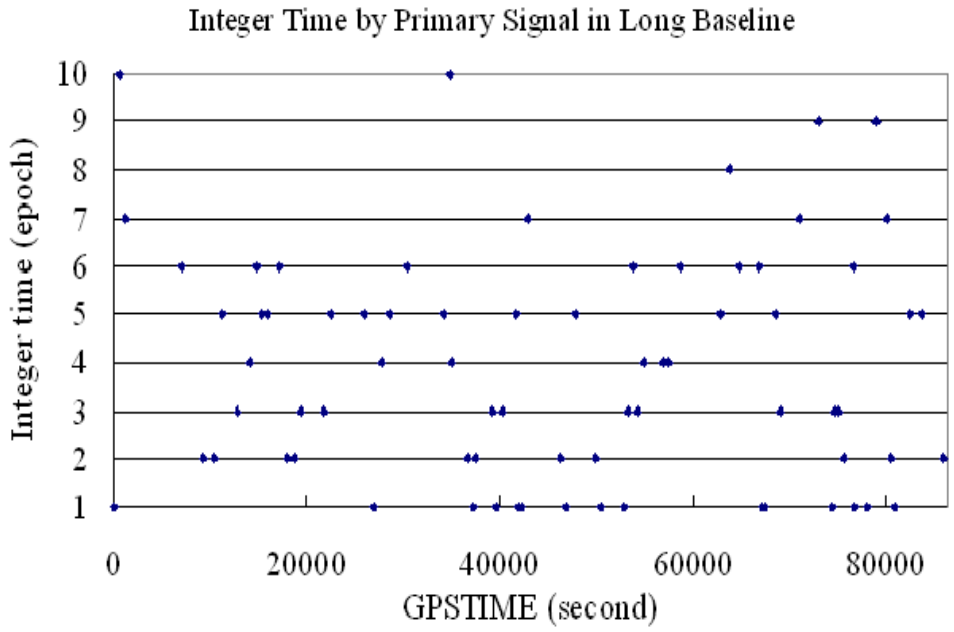

Figure 7.10 (1): Integer time by primary signal in long baseline

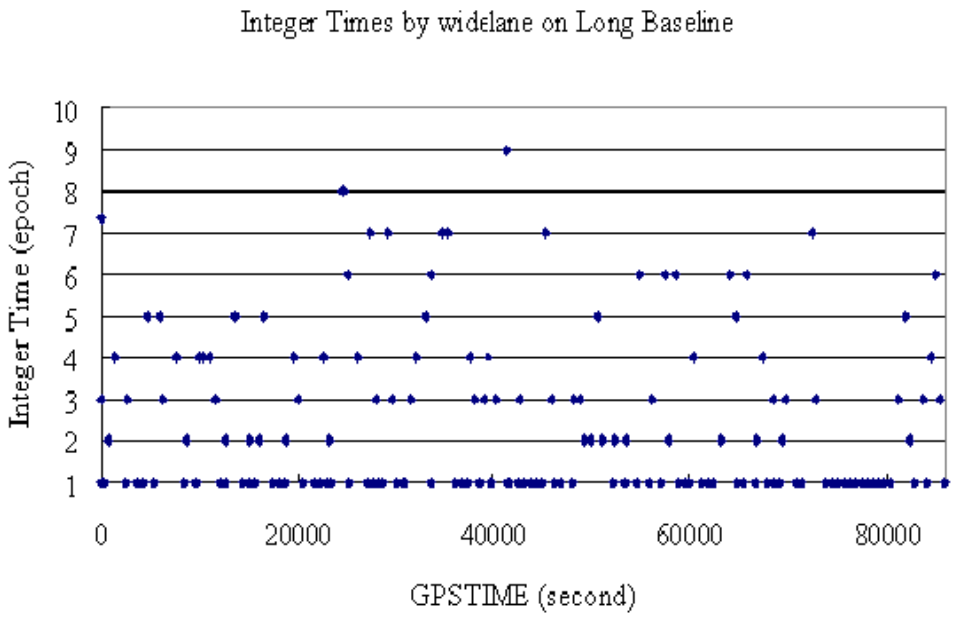

Figure 7.10 (2): Integer time by widelane signal in long baseline

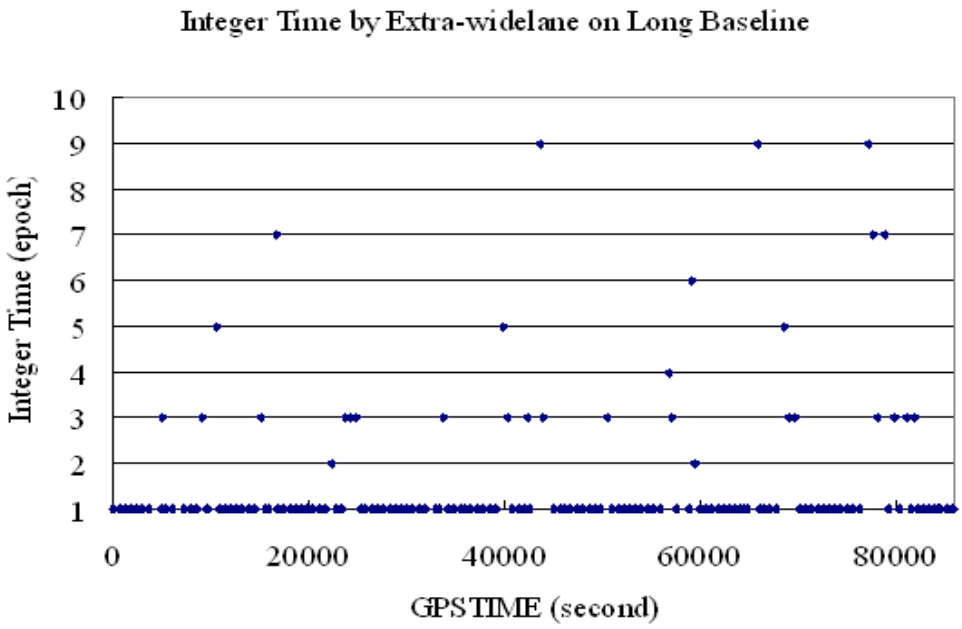

Figure 7.10 (3): Integer time by extra-widelane signal in long baseline

Figure 7.11 shows ASR over the full day on the long baseline. The vertical scale is logarithmic and ranges from 0.0 to 1.0. From figure 7.11, we can see the ambiguity resolution is no obvious change between two figures. It means that in long baseline, the ambiguity by triple frequencies is no improved. This is the most difference from short and medium baseline. It can be seen that the ASR is close to 99% at about 80000 (GPSTIME) when DD ionosphere error is very small, the ionosphere influence in the ambiguity resolution can be known.

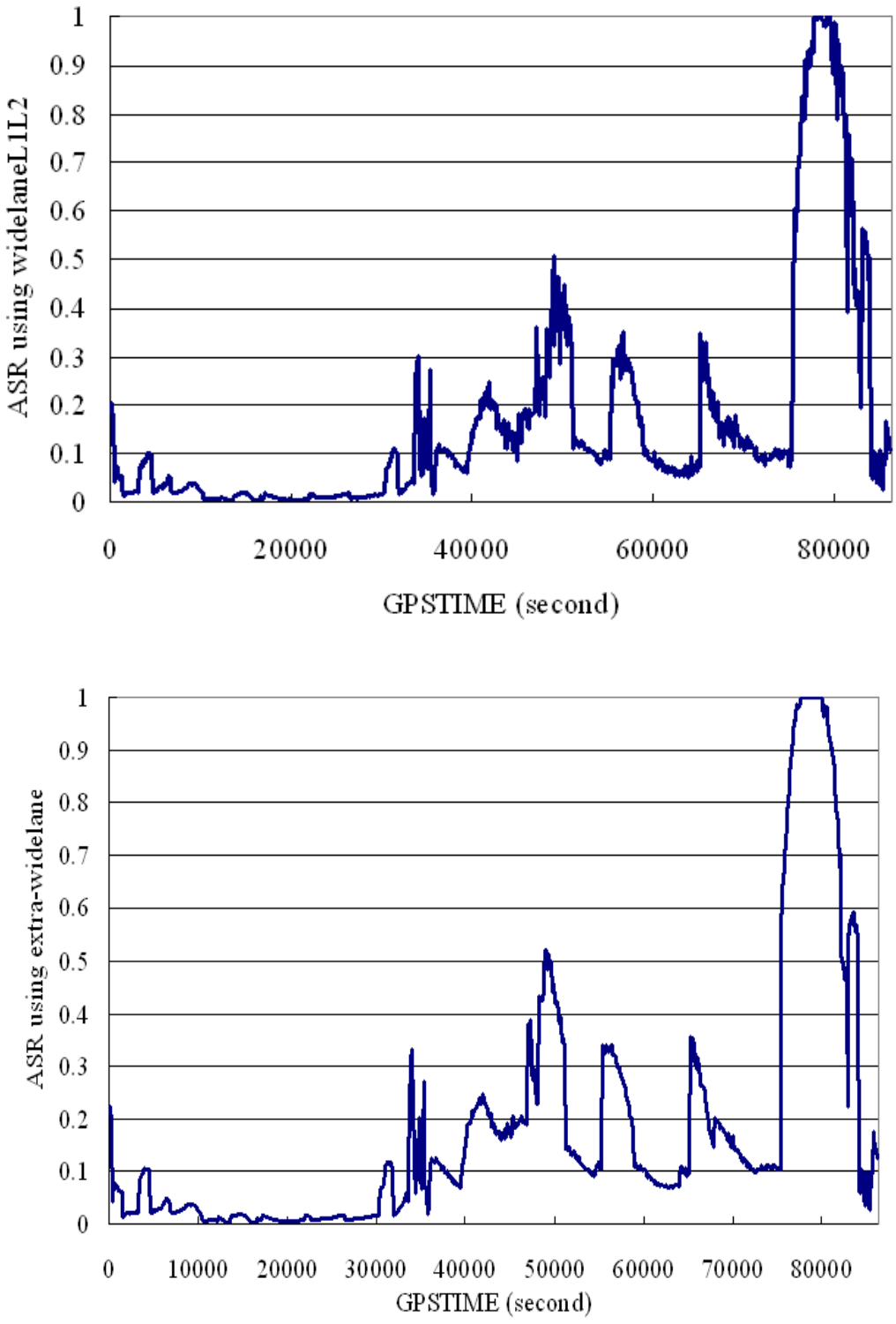

Figure 7.11: ASR of single epoch by widelaneL1L2 on top and extra-widelaneL2L5 at bottom, in long baseline

7.3.4 Extra-Long Baseline

The extra-long baseline case is considered as about 500km. Figure 7.12 shows DD ionosphere error of three pairs of primary satellites for 24 hours.

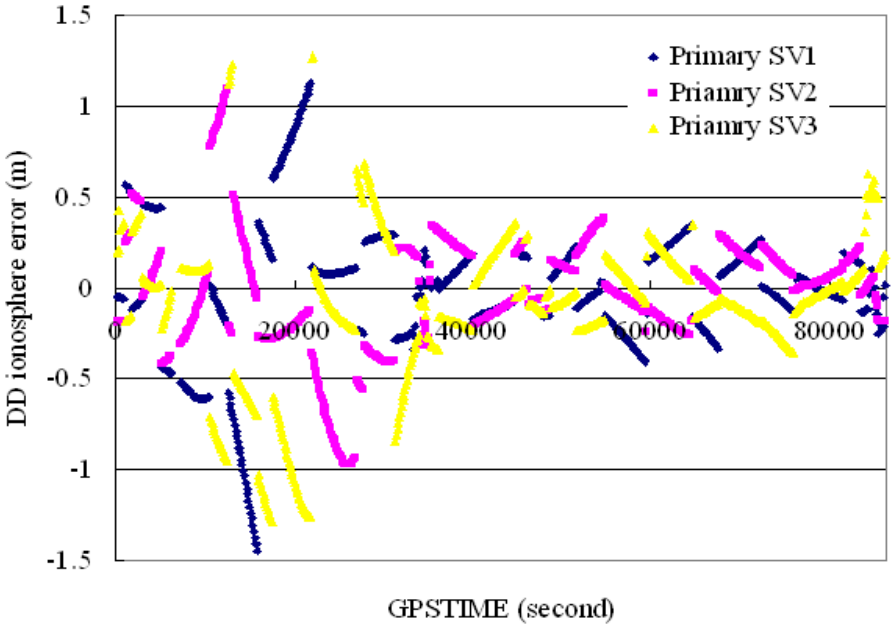

Figure 7.12: DD ionosphere error in extra-long baseline (about 500km)

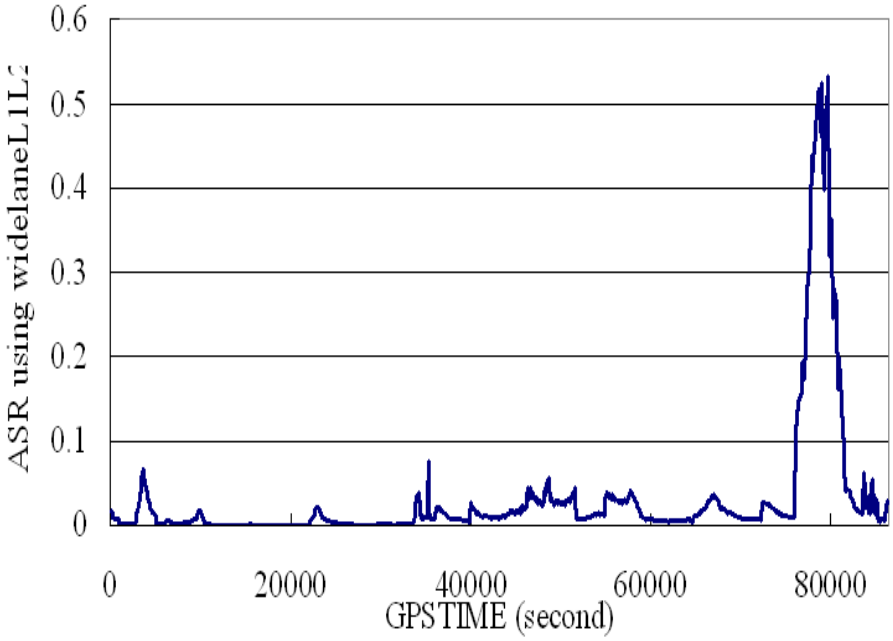

Figure 7.13: ASR of single epoch by widelaneL1L2 on top and extra-widelaneL2L5 at bottom in extra-long baseline

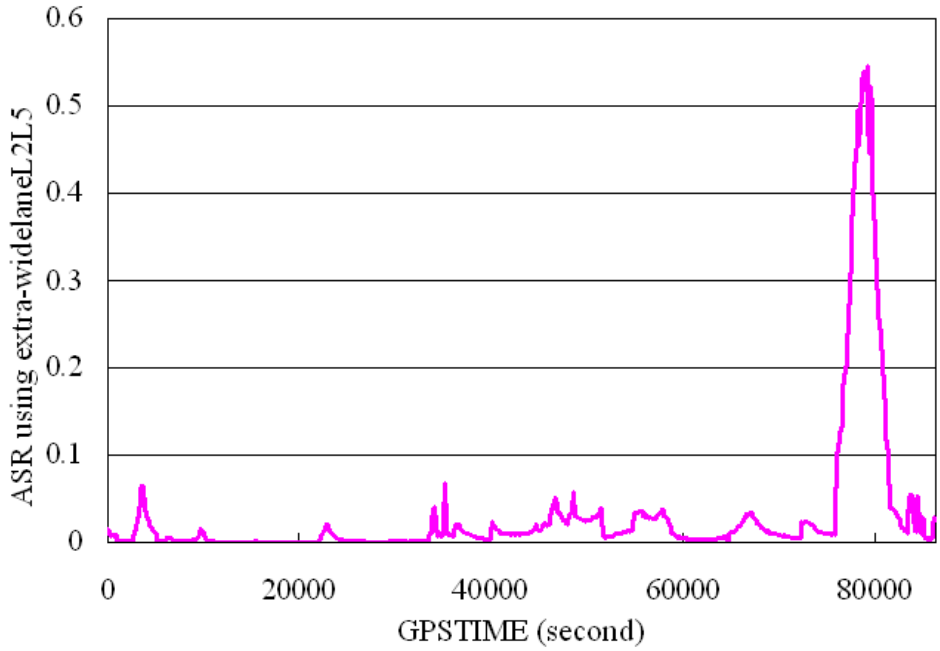

Figure 7.13: ASR of single epoch by widelaneL1L2 on top and extra-widelaneL2L5 at bottom in extra-long baseline

Figure 7.13 shows ASR over the full day on the extra-long baseline. The vertical scale is logarithmic and ranges from 0.0 to 0.6. Similar the case of long baseline, it is no improved by triple frequencies in ambiguity resolution. By the ionosphere becoming stronger, ASR for 24 hours in extra-long baseline becomes lower than in long-baseline. However, at about GPSTIME 80000, ASR is the highest in the all day.

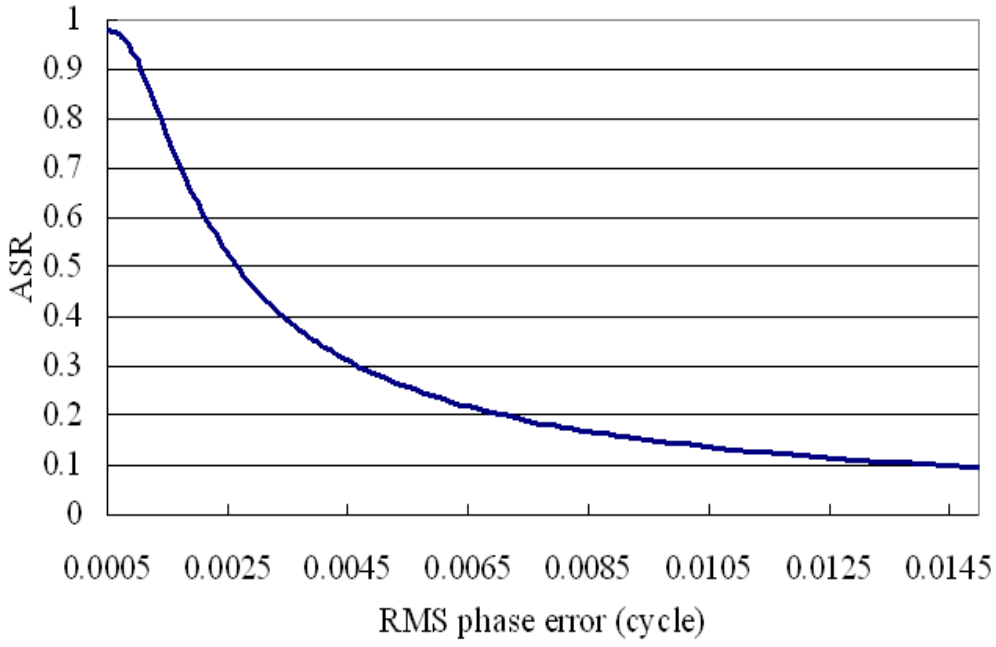

Figure 7.14: Relation between ASR and RMS phase error in geometry-free method

7.3.5 Geometry-Free Method in Extra-Long Baseline

In long and extra-long widelane, ambiguity resolution is affected by the ionosphere error. Geometry-free method is proposed here. The details of the geometry-free method have been discussed in Chapter 5. The advantage of geometry-free method is no affected by baseline. However, it is influenced by carrier phase noise. Using time averaging method for relative long time (about hundreds of seconds), the carrier phase noise can be reduced. Relation between ASR and RMS phase error reduced by time averaging is presented in figure 7.14. The satellite constellation is assumed in short baseline. The horizontal scale ranges from 0.0005 to 0.015 cycles. From the figure 7.14, ASR will be estimated more than 95% when sigma of carrier phase is less than 0.0005 cycles.

7.4 IONOSPHERE INFLUENCE

The ambiguity success-rate is likely to degrade with increasing baseline length, because of the ionosphere effect. This behavior is shown explicitly in Figure 7.15. The tropospheric delay uncertainty was assumed as Saastamoinen Model and the ionospheric delay uncertainty, expressed by standard deviation σ_I. Multipath error is neglected here. For illustrative purpose, the horizontal axis indicates the standard deviation of DD ionosphere error ranges from 0.001m to 0.2m, and assumed as 3ppm. The vertical axis ranges from 0.0 to 1.0. From figure 7.15, we can see that the distance will extend to about 30 km when ASR in triple frequencies will be more than 90%. The improvement from triple frequencies in medium baseline will be seen here.

7.5 OBSERVATION NOISE INFLUENCE

7.5.1 Accurate Code Measurement

Referring to Table 5.2 we conclude that code observations with 5-30 cm accuracy are virtually achievable with present and new signals. The possibilities to reduce the code measurement error due to noise are carrier

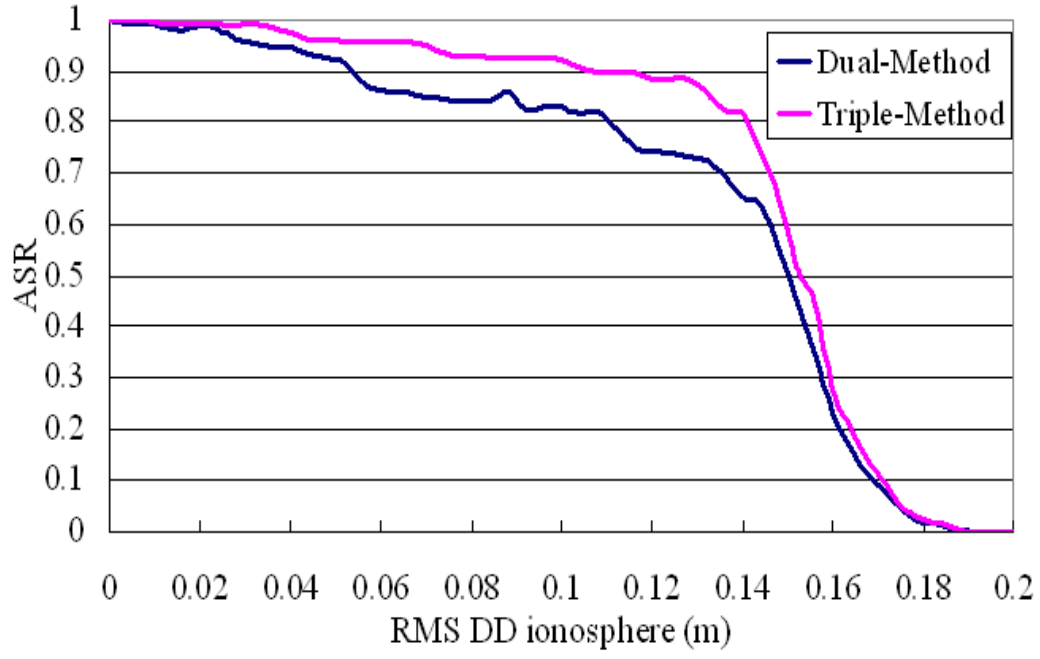

Figure 7.15: Ionosphere error effect in ambiguity resolution

smoothing or the time average. Figure 7.16 shows the RMS code error as a function of ASR. The vertical axis indicates the ASR (logarithmic) of single epoch from 0.75 to 1.0; the horizontal axis indicates the RMS code error from 0.1m to 0.5m. Figure 7.17 indicates the RMS code noise is the function in ambiguity resolution using extra-widelane signal. The vertical axis indicates the ASR (logarithmic) of single epoch from 0.99 to 1.0; the horizontal axis indicates the RMS code error from 0.1m to 2.0m.

The measurement is under the short baseline case, and the phase standard error is assumed in Table 5.2. From two figures, we can see that different from dual frequencies, ambiguity resolution using extra-widelane signal is nearly no affected by code noise. If RMS code noise is smaller than 0.1m, ambiguity can be estimated fast both in dual and triple frequencies.

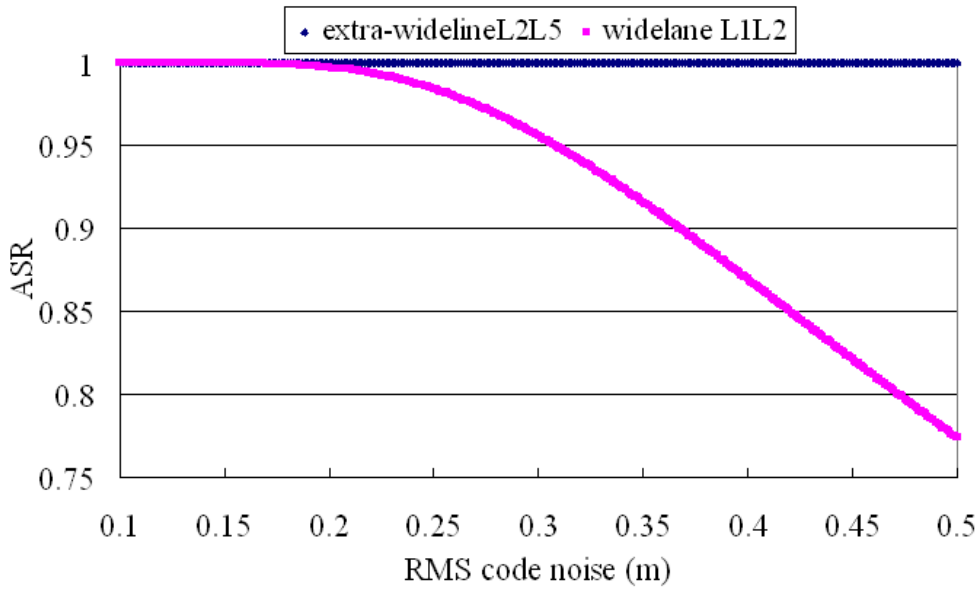

Figure 7.16: Code noise effect in ambiguity resolution

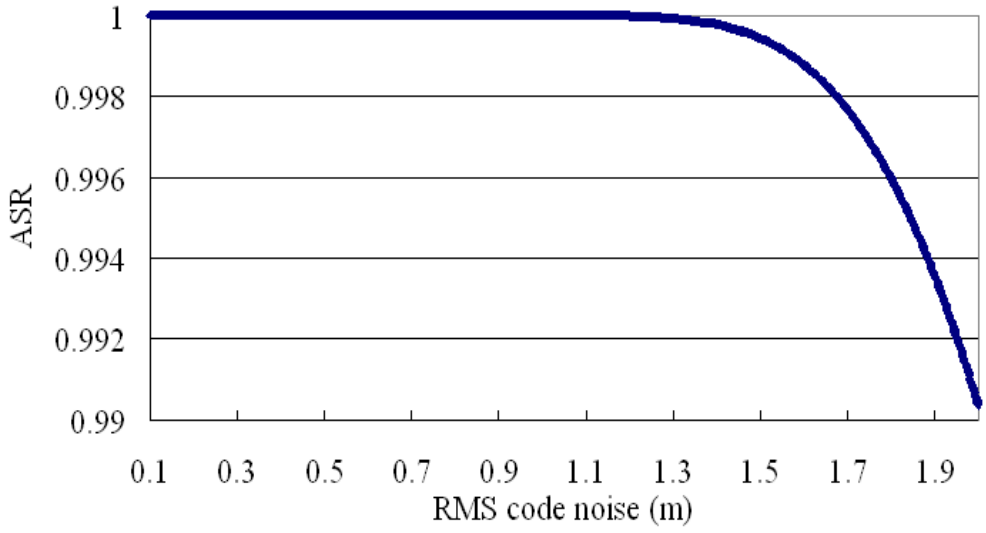

Figure 7.17: Code noise effect in ambiguity resolution using extra-widelaneL2L5 signal

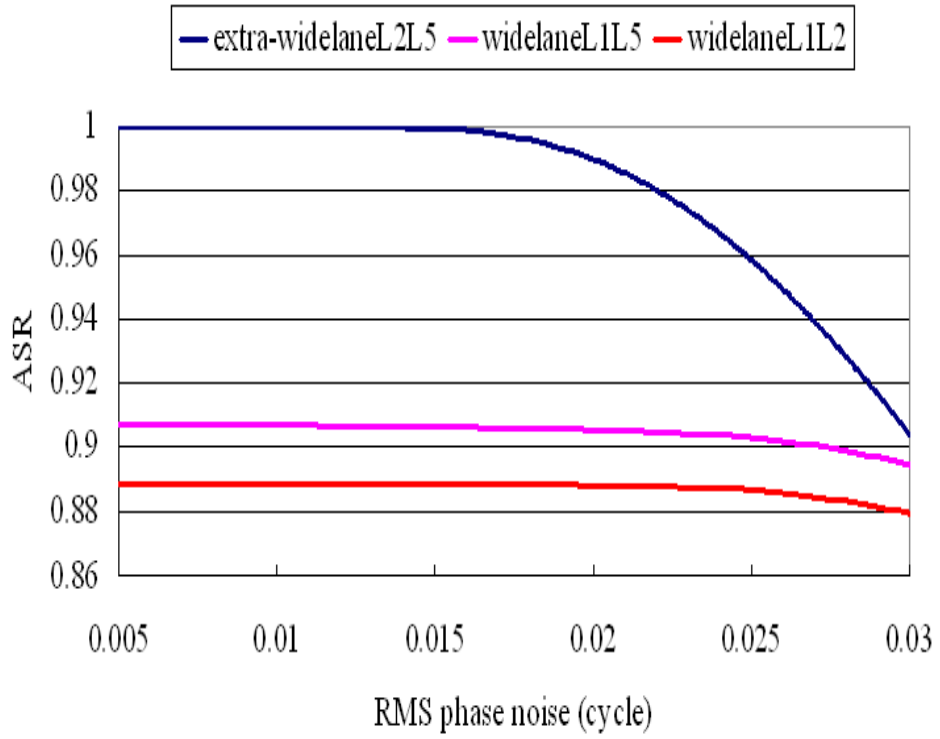

Figure 7.18: Carrier Phase noise effect in ambiguity resolution

7.5.2 Accurate Phase Measurement

Figure 7.18 shows the RMS phase error as a function of ASR. The vertical axis indicates the ASR of single epoch (logarithmic) from 0.86 to 1.0; the horizontal axis indicates the RMS L1 phase error ranges from 0.005cycle to 0.015cycle. The measurement is under the short baseline case, and the code standard error is assumed in Table 5.2. From figure 7.18, if no ionosphere influence, in ambiguity resolution, extra-widelane is the most fast, the widelaneL1L5 is the second, and widelaneL1L2 is the last. When L1 phase noise is more than 0.02 cycles, ASR using extra-widelane signal reduced dramatically.

7.6 MULTIPATH ERROR INFLUENCE

In the above different baseline analysis, the multipath error was all neglected. But the multipath is the important error source in the ambiguity resolution in the actually. Using our multipath generation simulation (introduced in Chapter 6), ASR will be estimated in the case of the multipath present and the case of the multipath absent. Figure 7.19 shows integer time for dual frequencies (top) and triple frequencies (bottom) in short baseline for 24 hours. We can see obviously that the ambiguity using extra-widelaneL2L5 can be estimated faster than using widelane L1L2 from figure 7.19.

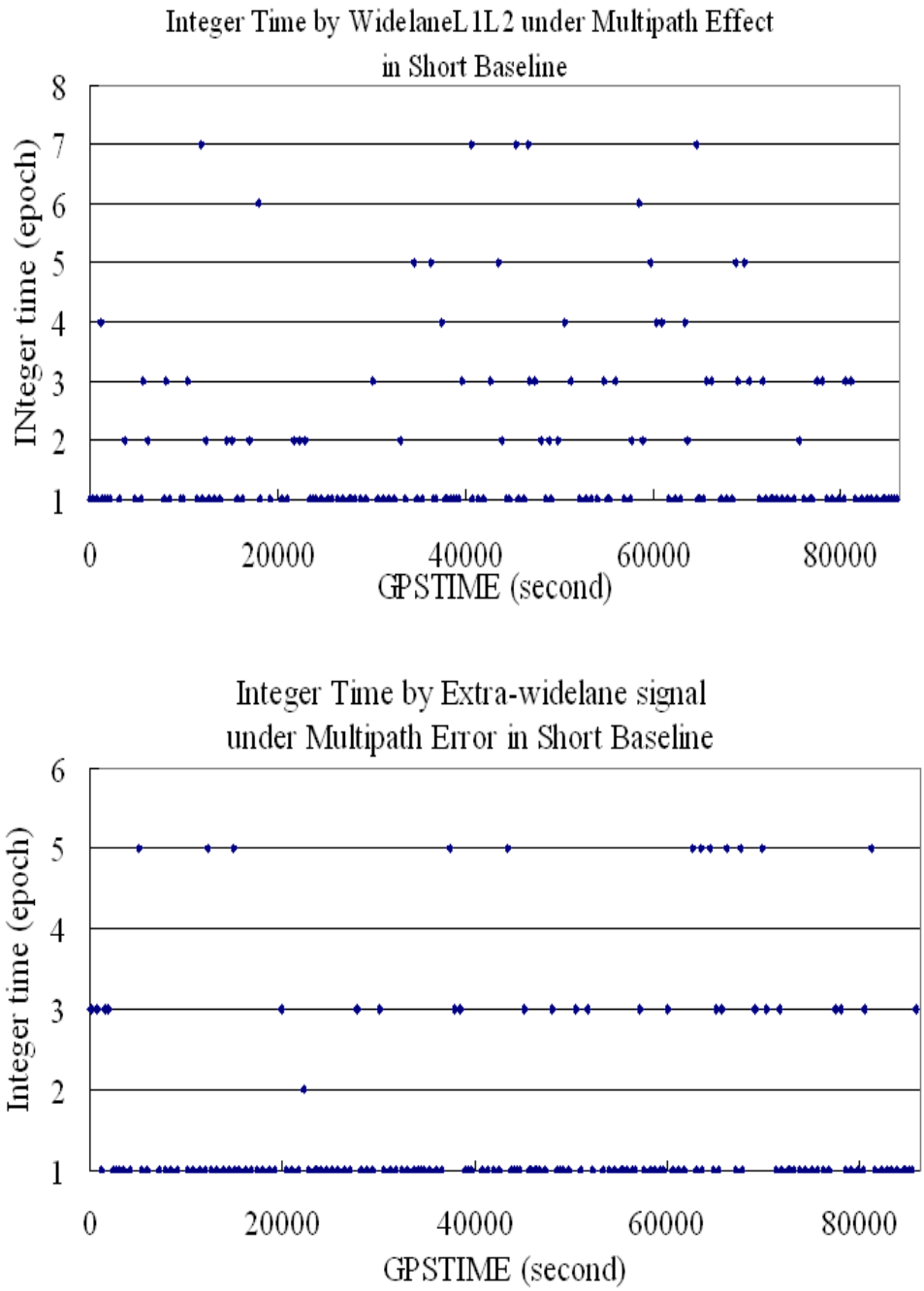

Figure 7.19: Multipath error effect for widelane L1L2 on top and for extra-widelane L2L5 at bottom in ambiguity resolution

7.7 NUMBERS OF VISIBLE SATELLITES

As we known that ambiguity resolution is base on the GPS satellite constellation. Figure 7.20 shows numbers of the visible satellites is the function in ambiguity resolution for 24 hours in medium baseline. The left of vertical axis indicates the ASR of single epoch (logarithmic) from 0.6 to 1.0; the right of vertical axis indicates numbers of visible satellites; the horizontal axis indicates GPSTIME. The influence of visible satellites' numbers can be seen in figure 7.20. From figure 7.20, we can see that numbers of visible satellites is a function in the both in dual and triple frequencies.

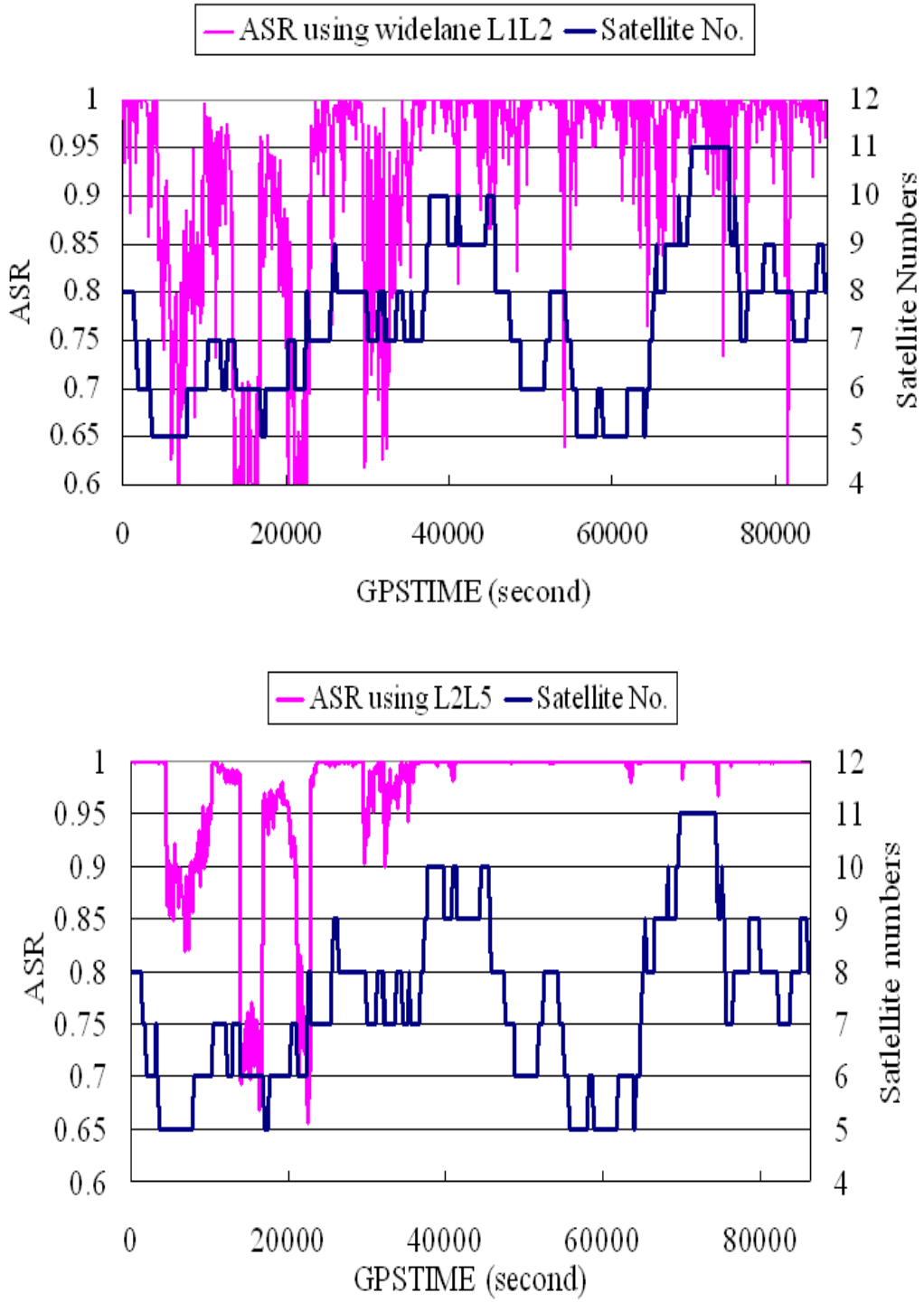

Figure 7.20: Numbers of visible satellites is a function in ambiguity resolution in medium baseline. The case of dual frequencies is on the top and the case of triple frequencies is at the bottom

7.8 SUMMARY

Based on the theory and numerical calculation using triple frequencies simulation, the benefit from triple frequencies is discussed, and the comparison of ASR for various scenarios for 24 hours (about 720 times in one day) is shown in table 7.1.

1. In short baseline, ambiguity resolution can be faster and more accurate by triple frequencies than by dual frequencies, especially in single epoch resolution.
2. In medium baseline, similar to short baseline, ambiguity resolution can be faster and more accurate than by dual frequencies. Two methods, using widelane L1L5 signal method and using extra-widelane L2L5 signal method, can be used in triple frequencies. However, ambiguity resolution will be influenced by ionosphere error.
3. In long and extra-long baseline, different from short and medium baseline, ambiguity resolution is not improved by the triple frequencies because of ionosphere error. As the length of baseline becomes longer, ambiguity resolution becomes worse.
4. In long and extra-long baseline, geometry-free method is proposed. Geometry-free method is not affected by the baseline length. However, it is affected by the carrier phase noise. With reducing the carrier phase noise by long session time averaging, ambiguity resolution can be improved.
5. If more useful ambiguity resolution methods are proposed in triple frequencies, user will have more choice to select the optimum method.
6. Ionosphere error can affect the ambiguity resolution both in dual and triple frequencies.
7. Code noise has nearly no influence in the ambiguity resolution using extra-widelane method.
8. Phase noise can affect ambiguity resolution both in dual and triple frequencies. The best results of ambiguity resolution are obtained by using extra-widelane L2L5 signal, the second by using widelaneL1L5, and the last by using widelaneL1L2. ASR using extra-widelane signal will reduce dramatically when the standard deviation of L1 carrier phase noise is bigger than 0.02 cycles.
9. When multipath is present, ambiguity resolution can be faster in triple frequencies than in dual frequencies.
10. Ambiguity resolution is a function of numbers of visible satellites in the both in dual and triple frequencies.

	Multipath Absent				Multipath Present
	Short Baseline	Medium Baseline	Long Baseline	Extra-long Baseline	Short Baseline
Dual	99.06%	90.85%	5.61%	0.2%	83.56%
Triple	99.98%	95.83%	8.23%	0.6%	93.32%

Table 7.1 Comparison of ASR for dual and triple frequencies for various scenarios

CHAPTER 8
CONCLUSION AND RECOMMENDATION

The major of this thesis is to show the benefit from the triple frequencies in ambiguity resolution for RTK positioning. The thesis is composed two parts. The theory of ambiguity resolution, widelane combination and geometry-free combination and other combinations are introduced in the first part. The second part consists the details of triple frequencies simulation, which focuses on the error model analysis, and numerical calculation by the triple simulation.

8.1 CONCLUSION

1. There are two obvious advantage of the new signal (L5 signal) in ambiguity estimation: one is that code noise and multipath noise of L5 signal will be smaller than present signal (L1, L2), it can improve the code positioning accuracy; the other is that the frequency of L5 signal is close to the frequency of L2 signal, so we can create extra-widelane L2L5 signal with wavelength 5.86m.
2. Using the extra-widelane method and widelane methods to resolve the primary ambiguity, in short baseline and medium baseline, ambiguity can be determined more fast and accurate in triple than in dual frequencies. But in long baseline, there is no obvious improvement in the triple frequencies.
3. Using the geometry-free method to resolve the primary ambiguity, the method is not affected baseline length and only use carrier phase observations, but it is affected by the carrier noise in the widelane signal and extra-widelane signal.
4. Different combination methods can be used in the triple frequencies, including extra-widelane combination, widelane combination and geometry-free methods. The results show that in short and medium baseline, extra-widelane combination method can estimate ambiguity the most fast in the most time.
5. In short baseline, code noise can affect ambiguity resolution both in dual and triple frequencies, however, carrier phase noise nearly cannot affect ambiguity resolution in extra-widelane combination method when RMS phase noise is smaller than 0.02 cycles.
6. When multipath is present, ambiguity can also be determined faster in triple frequencies than in dual frequencies.
7. Numbers of visible satellites can affect the ambiguity resolution both in dual and triple frequencies.

8.2 RECOMMENDATION

1. In this thesis, the widelane method was used to resolve the primary ambiguity. In our recently research, the LAMBDA (standing for Least-squares AMBiguity decorrelation Adjustment) method is used to estimate the ambiguity. This method can reduce the ambiguity searching space to improve the speed of the ambiguity resolution.
2. Since the ionosphere error cannot be neglected in the long distance RTK positioning in triple frequencies, in order to improve the accuracy of ambiguity estimation in Japan, the more accurate ionosphere model of local area in Japan has to be created in the future, for example creating high accuracy real-time local TEC map of Japan.

3. Galileo system in Europe and Quasi-Zenith satellite system in Japan will be performed in the future. Two systems are both triple frequencies systems, the numbers of visible satellites will be increased, and using high elevation satellite will reduce multipath error. Combining with these two systems, ambiguity resolution in Japan can be more accurate and faster than present GNSS system.

REFERENCE

Bernd Eissfeller, Christian Tiberius (2002). "*Real-Time Kinematic in the Light of GPS Modernization and Galileo*" ION GPS, Salt Lake City.

BESER, J. & PARKINSON, B.W. (1982). "*The application of NAVSTAR differential GPS in the civilian community*." Navigation, 29(2), 107-136.

B.Horfmann-Wellenhof, H. Lichtenegger, and J. Collins "*GPS Theory and Practice*" fourth, revised edition Novographic, Ing. Wolfgang Schmid, A-1230 Wien Australian

Bradford W. Parkinson. "*Global Positioning System: Theory and Applications*" publisehed by the American Institute of Aeronautics and Astronautics, Inc. Washington, DC 20024-2518

Brunner, F, K., and Gu, M. (1991). "*An Improved Model for the Dual frequencies Ionospheric Correction of GPS Observations*" Manuscripta Geodaetica, Vol. 16, pp. 280-289.

Bugoslavskaya, N.Y., (1962). "*Solar activity and ionosphere, for radio communication specialists*", Pergamon Press Ltd. New York

Chris Rizos, Shaowei Han (1995) "*A New Method for Constructing Multi-satellite Ambiguity Combinations for improved Ambiguity Resolution. "* Proceedings of ION GPS-95, Palm Springs, 12-15 pp. 1145-1153.

Davies, K. (1989) Ionospheric Radio, Peter Peregrinus, Ltd., London.

Elliot D. Kaplan (1996). "*Understanding GPS Principles and Applications*" Artech House Boston London

Hatch, Ronald R. (2000). "*Promise of a Third Frequency*", GPS World, vol.7, no.5 pp55-58

Jayanta Kumar Ray (1999). "*Mitigation of GPS Code and Carrier Phase Multipath Effects Using a Multi-Antenna System*" UCGE Reports Number 20136

Klobuchar, John (1996). "*A. Ionospheric Effects on GPS, in global positioning system: Eheory and Applications*", Vol. I, B. Parkinson, J Spilker, P. Axelrad, and P. Enge. American Insitute of Aeronautics and Astronautics, pp.485-515

Lee, Y.C. (1992). "*Receiver Autonomous Integrity Monitoring (RAIM) Capability for Sole-Means GPS Navigation in Oceanic Phase of Flight*" IEEE 1992 Position Location and Navigation Symposium (PLANS) Record, Monterey, CA,1992, pp.464-472

Lioneal Ries, C. Macabiau, V.Calmettes (2003). "*A software Receiver for GPS-IIF L5 Signal*" ION GPS 2003, 24-27 September 2002, Portland, OR

Melbourne, W.G. (1985). "*The Case for Ranging in GPS Based Geodetic System, Processing 1st International Symposium on Precise Position with Global Position System*" edited by Clyde Goad, pp 403-412, U.S. Department of Commerce, Rockville, Maryland.

Mohinder S. Grewal, Lawrence R. Weill Angus P. Andrews. "*Global Positioning System, Inertial Navigation, and Intergration*"

Odijk, D. (2000). "*Weighting ionospheric corrections to improve fast GPS positioning over medium distances.*" Proceeding of ION GPS-2000. Salt Lake City, Utah, September 19-22. pp. 1113-1123.

Pany, T., M. Irsigler, B. Eissfeller and J. Winkel (2002). "*Code and carrier phase tracking performance of a future Galieo RTK receiver.*" Paper presented at GNSS 2002, Copenhagen, Denmark, May 27-30

Pratap Misra, Per Enge, Per Enge. (2001) "*Global Position System*" courtesy of the Boeing Company, United States of America

RIZOS, C.GRANT, D.B. (1990). "*Contributions to GPS Studies*", C. Rizos (ed.), PP204.

RTCA C-159. "*NAVTAR GPS L5 Signal Specification*"

Saastamoinen, J. (1973). "*Contribution to Theory of Atmospheric Refraction*", Bulletin Geodesique, Vol. 105, Sep. 1972, Vol. 106, Dec. 1972, Vol.107, March

Tenuissen P.J.G (1995), "*The least-squares ambiguity decorrelation adjustment: a method for fast GPS integer ambiguity estimation*", Journal of Geodesy, 70(1/2), pp.65-82

Tenuissen P.J.G (1999). "*An optimality property of the integer least-squares estimator.*" Journal of Geodesy, 73,587-593

Teunissen, P.J.G (2001). "*GNSS ambiguity bootstrapping: theory and application*". In: Proc. KIS2001, International Symposium on Kinematic System in Geodesy, Geometric and Navigation, Banff, Canada, pp.246-254

Tenuissen P.J.G (2003) "*An Invariant Upperbound for the GNSS Bootstrappend Ambiguity Success-rate*" Journal of Global Positioning Systems

Toshiaki Tsujii, Masaaki Murata, Masatishi Harigae, Takatsugu Ono and Toshiharu Inagaki (1998). "*Devlopment of Kinematic Gps Software, KINGS, and Flight Test Evaluation*" March, 1998

Yun Zhang, Falin W. Kubo, Yasuda (2003). "*TEC measurement by single dual frequencies receiver*" GPS/GNSS International Symposium, pp 351-358 Tokyo, Japan